Wavelet Transform based Atmospheric Radar Signal Processing

A Thesis submitted in partial fulfillment of
The requirements for the Degree of

DOCTOR OF PHILOSOPHY
In
Electronics Science

By
K. Sreedevi

School of Physics
University of Hyderabad
Hyderabad-500 046
India

March-2009

DECLARATION

I hereby declare that the work embodied in this thesis entitled ***"Atmospheric Radar signal Processing Employing Wavelet Transforms"*** is the result of investigations carried out by me under the supervision of **Prof. K.Venu** and **Dr. S.L. Sabat**, School of Physics, University of Hyderabad, India, and same hasn't been submitted for the award of the degree or diploma of any other University or Institution.

Place: Hyderabad

Date: (K. Sreedevi)

UNIVERSITY OF HYDERABAD
Hyderabad-500 046
INDIA

CERTIFICATE

This is to certify that the work described in this thesis entitled "***Wavelet Transform based Atmospheric Radar Signal Processing***" has been carried out by **K. Sreedevi** under our direct supervision for the full period prescribed under PhD ordinances of the University and the same has not been submitted for any other degree or diploma at this or any other University.

Dean **Prof. K. Venu** **Dr. S.L. Sabat**

Place: Hyderabad
Date:

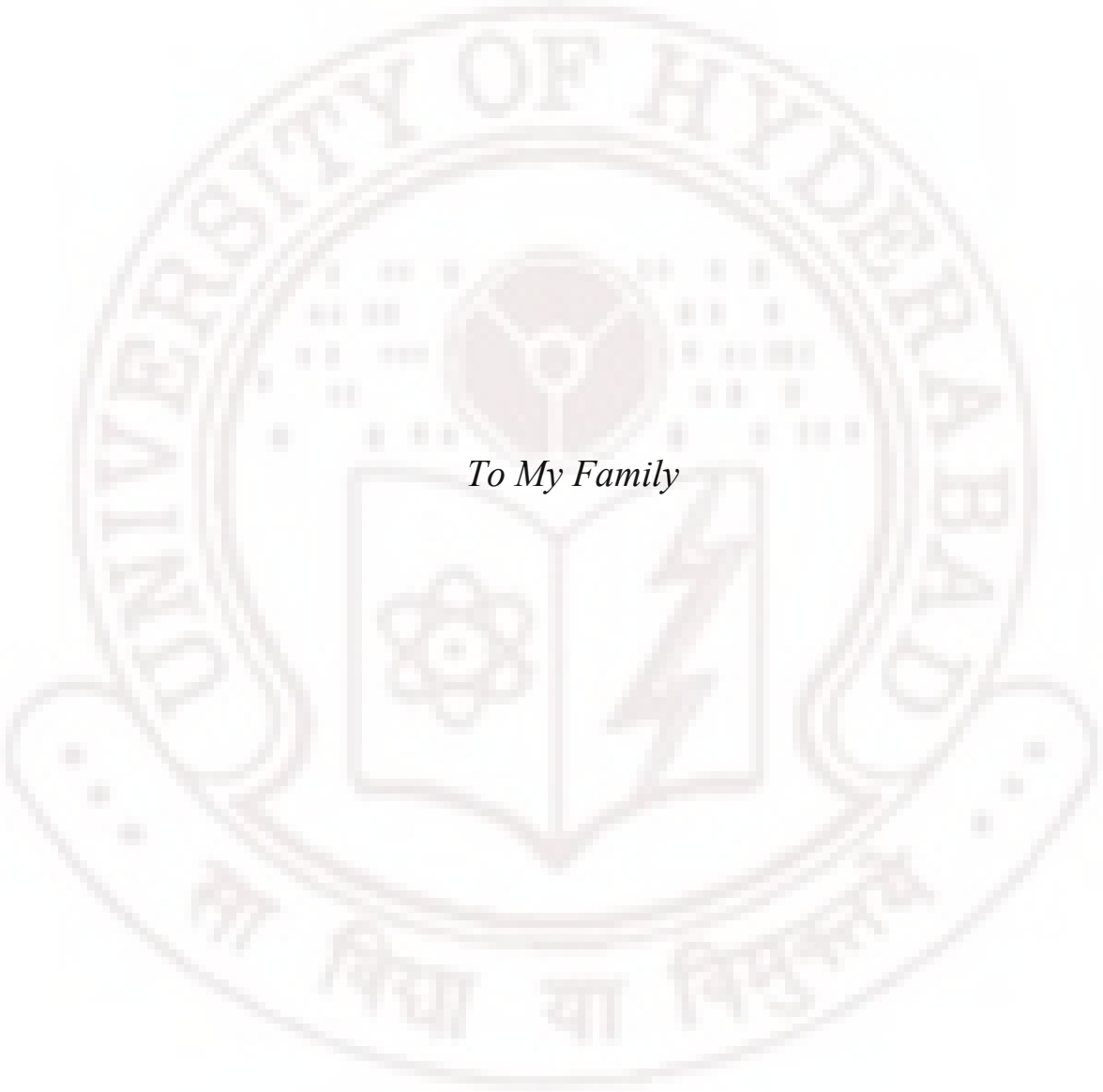

To My Family

Acknowledgements

I would like to express my gratitude to those who have helped me in pursuing this work and, particularly made this thesis possible.

First and fore most, I thank my supervisor **Prof. K.Venu** for giving me the opportunity to work under him and introducing me to the Wavelets. Teaching many principles and techniques, patience in his guidance and his esteemed guidance throughout my research is unforgettable. I thank for his availability for timely discussion and his help in entire research work.

I express my sincere thanks to **Dr. Samrat Sabat**, for all his support, help in my entire research work, and the helpful comments on my thesis draft.

I thank **Prof. Vipin Srivastava**, Dean, and **Prof. V.S.S. Sastry**, former Dean for providing all the necessary facilities to carry out my work. I would also thank **Prof. T. Somayajulu, Prof. G. Rajaram**, and other faculty members of School of Physics for their suggestions, help and guidance in various occasions.

I would acknowledge with thanks **Prof. Arun Agarwal**, Computer Science Department, who taught me Image Processing as part of PhD course work.

I would like to express my sincere gratitude to **Prof P.B Rao**, National Remote Sensing Agency (NRSA), for his valuable suggestions, teaching principles and encouragement in my research.

Financial assistance from the Indian Space Research Organization **(ISRO)**, India is gratefully acknowledged. I am also deeply indebted to the other authorities of National Atmospheric Research Laboratory (NARL) **Prof D. Narayana Rao**, **T.V.C. Sarma**, **Dr. Anandan**, Engineers, Scientists, research scholars, and technicians and other employs of NARL for their suggestions, help in various aspects during visit to NARL.

I wish to thank **Abraham** for his help in all my administration works. I would like to thank all technical and non-teaching staff members of the School of Physics for their help and co-operation, during my research tenure. I wish to extend my sincere thanks to the University authorities for providing all the necessary facilities for this work.

My special thanks to my friend **G. Lakshmi Narayana** for all his support, encouragement, and help in completing this thesis. I also thank my lab mate **Ranga Babu** for all his help during my research work.

I wish to thank my friends **Shanthi**, **Prema**, **Padma**, **Usha**, **Saritha**, **Sailaja**, **Bharghavi**, **Santoshi** , research scholars of School of Physics and hostel mates, for their help, whose company made my stay here a memorable one. I thank my friends from CBIT, GIOE, Andhra University and SV University for their company during my study.

There are no words to express my gratitude towards **my parents and my sister** for their care. My deepest gratitude is expressed to all my relatives for their selfless support, encouragement and also presence in times of need. Last but not least my special thanks go to my life partner, **Sunil Kumar Reddy** for his caring, love, consistence encouragements and patience.

Contents

Abbreviations

ADC	:	Analog-to-Digital converter
ATM	:	Adaptive Tracking Algorithm
CAT	:	Clear Air Turbulence
CQF	:	Constant Q filters
CWT	:	Continuous Wavelet Transform
DBS	:	Doppler Beam Swinging
DFT	:	Discrete Fourier Transform
DVW	:	Doppler velocity window
DWT	:	Discrete Wavelet Transform
FFT	:	Fast Fourier Transform
FIR	:	Finite Impulse Response
FT	:	Fourier Transform
IF	:	Intermediate Frequency
IPP	:	Inter Pulse Period
LM	:	Levenberg-Marquardt's
MRA	:	Multiresolution analysis
MST	:	Mesosphere-Stratosphere-Troposphere
NCAR	:	National center for Atmospheric Research
NIMA	:	NCAR Improved Moments algorithm
NWCA	:	NCAR Wind and Confidence Algorithm
PRF	:	Pulse Repetition Frequency
QMF	:	Quadrature mirror filtering
RF	:	Radio Frequency
SAD	:	Spaced Antenna Drifts
SNR	:	Signal to Noise Ratio
STFT	:	Short Term Fourier Transform
UVW	:	Zonal, Meridonal and Wind velocities
WSD	:	Wavelet Shrinkage Denoising

List of Symbols

$\downarrow 2$	:	Down sampling/ Decimation
$\uparrow 2$	:	Up sampling/ Interpolation
$*$	:	Convolution
$<f, g>$	:	Inner product of f and g
$\psi(t)$	:	Mother wavelet
$\psi^*(t)$	:	Complex conjugate of $\psi(t)$
$\psi_{a,b}(t)$	:	Baby wavelets
$\varphi(t)$	:	Scaling function
$\varphi_{j,k}(t)$	:	Family of scaling functions
$\delta(n)$	:	Delta function
ρ	:	Atmospheric pressure (in Mb)
η	:	Volume reflectivity coefficient
λ	:	Carrier wavelength
θ	:	Beam tilt angle
a	:	Scale parameter
A_e	:	Effective antenna area
b	:	Translation/ localization
c	:	Velocity of light i.e. 3×10^8 m/s.
$c_j(k)$	:	Scaling coefficients
$d_j(k)$	:	Wavelet coefficients
e	:	Partial pressure of water vapor (in Mb)
f	:	Frequency
f_C	:	Carrier frequency
f_D	:	Doppler frequency
$\overline{f_D}$	:	Mean Doppler frequency
f_w^2	:	Spectral width
$g(t)$	:	Input signal
H	:	Vertical height
$h_0(n)$	:	FIR low pass filter
$h_1(n)$	:	FIR high pass filter

$h_{0A}(k)$	:	Analysis low pass filter
$h_{0S}(k)$	:	Synthesis low pass filter
$h_{1A}(k)$	:	Analysis low pass filter
$h_{1S}(k)$	:	Synthesis low pass filter
i	:	Unit vector
L^2	:	Finite energy functions $\int_{-\infty}^{\infty} \lvert f(x)\rvert^2 dx < \infty$
m_0, m_1 and m_2	:	Zeroth, first and second order moments
n	:	Refractive index
N	:	Noise power
N_e	:	Critical electron density
N_c	:	Number density of electrons
$\overline{\mathrm{N}}$	:	Average noise level
P_n	:	Power spectrum of received signal of MST radar
P_r	:	Total signal power
$\mathrm{P_r}$	:	Received power
P_t	:	Transmitted power
Q	:	Quality factor
r	:	Range resolution
R	:	Set of real numbers
R	:	Range of reflecting volume
$R_{xy}(\tau)$	:	cross correlation of $x(t)$ and $y(t)$
$\mathrm{STFT_x^w}$	:	STFT of signal $x(t)$
t	:	Time
T	:	Absolute temperature (^0K)
	:	Threshold level
τ	:	Time parameter
T	:	Inter-pulse-period
t_R	:	Range time delay
v_j	:	Vector space spanned by scaling functions
$w(t)$	:	Window function
w_j	:	Vector space spanned by wavelets
$x(t)$	:	Time domain signal

$X(f)$	:	Frequency domain signal
$W_x(a, b)$	:	Continuous Wavelet Transform
Z	:	Set of integer numbers
Z_k	:	Complex time series data of MST radar

List of Figures

List of Tables

PREFACE

Wavelet transform has many recent applications in variety of fields in science and technology. The applications are wide ranging including signal and image processing, denoising, data compression and adaptive signal processing. The ability to provide time frequency localization of non-stationary signals, multi resolution analysis and the flexibility in the choice of basis functions make the wavelet based techniques very versatile and powerful tool for signal processing. However the application of wavelet transforms for radar signal processing has hitherto been rather limited. This thesis aims to use wavelet transform based signal processing to improve the range and accuracy of atmospheric radar data.

Mesosphere-Stratosphere-Troposphere (MST) radar is used to measure wind velocities, temperature pressure and humidity of an atmosphere. The target in this case, unlike radars used to detect objects such as aircrafts etc., is soft target i.e. variation in the air refractive index due to the variations in the air pressure. MST Radar is high power coherent pulse Doppler radar operating typically around 50 - 200 MHz. When RF pulse is fired into the atmosphere, small part of its energy is scattered and reflected back due to the variation in radio refractive index of neutral atmosphere. Therefore MST radar signal is extremely weak. It is estimated that the signal strength drops typically by about 2 dB per km and the signal is obscured by the noise beyond a range when the SNR drops below -10 dB despite considerable improvements in radar design and transmitted power. The range up to which discernable signal can be observed in MST radar data is limited to typically 12-14 km, when only standard signal averaging and filtering techniques are used. So far different averaging techniques, such as consensus average and median estimator, were employed to improve SNR. Certain adaptive techniques were proposed to trace the signals from noisy data at higher ranges (up to 16-22 km). Similarly higher order spectral estimation technique was used to account for non-Gaussian nature of the Doppler echoes. All these methods have yielded reliable detection of the Doppler echoes to a maximum range of about 22 km under favorable conditions. The work reported here deals with application of discrete time wavelet transform for denoising and analysis of MST radar data with a view to increasing the height coverage and improve the accuracy of the parameters extracted from the spectra. The Experimental data used in this work was

collected using the MST radar facility at the National Atmospheric research laboratory at Gadanki, India (13.5^0N, 79^0E).

Wavelet transform is a mathematical technique that can be used to split a signal into different frequency bands with a time resolution matched to its frequency scale, thus providing excellent time and frequency representation. Further the basis function in Wavelet transform is not completely fixed as in the case of other transforms such as Fourier and Laplace Transform etc. Thus the form of the basis function can be chosen, of course while satisfying the requirements of a basis function of wavelet, in such a fashion that it resembles the functional form of the signal of interest. Then it provides a sparse representation of the signal, wherein the entire energy in the signal is with in few wavelet coefficients, providing good signal to noise separation. Therefore the first phase of the work reported in this thesis pertains to designing a basis function suitable for the MST radar clear-air echo.

As the spectrum of the MST radar clear-air Doppler echo is predominantly of Gaussian in nature in the off-vertical direction, it was assumed that the wavelet basis function is a shifted Gaussian in frequency domain. A wavelet function should exhibit normalization, orthogonality properties and it should have one zero at π in the frequency response. It should be ensured that the chosen wavelet basic function and the corresponding MRA filter coefficients should satisfy these properties. The corresponding MRA filter coefficients in this work were calculated by rewriting the low pass filter coefficients in terms of trigonometric functions of Sine and Cosine represented by parametric angles, such that the above conditions are satisfied. Then these parametric angle values were obtained by LEVENBERG-MARQUARDT optimization method. It was found that eight filter coefficients represent chosen wavelet. Then high pass filter coefficients were calculated using the recursion relation between low pass and high pass filter coefficients. Frequency response of these filter coefficients were found to be as desired i.e. say, as in the case of a standard wavelet like Daubechies wavelet (db10). The ability of this wavelet to reconstruct MST radar signal perfectly with minimal artifacts is verified in the following way. Towards this first an MST radar signal was decomposed using this wavelet and then reconstructed back by performing inverse wavelet transform and it was found that the signal is reconstructed without any observable artifacts. The analysis of the MST radar data performed using this wavelet, as described below, provided better results *viz*. compared to next best standard wavelet Daubechies (db10).

First it is necessary to find out the required levels of decomposition for the designed wavelet for MST radar data before applying denoising technique and it was found that three-level wavelet decomposition is sufficient in the present case. Then proper thresholding method and threshold values were selected in order to get best level of denoising. Different standard threshold selection techniques such as Adaptive threshold, Universal threshold, a Heuristic threshold and Minimax (minimum of maximum) threshold selection method were examined and hard and soft thresholding techniques were considered. These techniques were tested by denoising both reasonably strong and reasonably weak signals. After extensive study it is found that Adaptive threshold selection technique provides suitable thresholds for both strong and weak signals, the threshold values are slightly adjusted manually in order to have single set of thresholds for all the ranges. It was found that hard thresholding method is suitable for MST radar data. This denoising technique was applied on all range bins of experimental MST radar profile. This procedure is first applied on simulated data as Doppler echo position is known in that case. The Doppler echo in these simulated spectra was chosen to have Gaussian distribution with width typical of observed Doppler echoes, with a chosen shift and unit peak value for the lowest range bin. Random Gaussian noise was added to this spectrum to obtain a noisy signal by using standard noise generator. Then the data for higher range bins were generated by reducing the Doppler echo strength by 2 dB per every kilometer keeping the noise power constant as in the case of a realistic MST radar data. Different experimental situations were simulated by generating the profiles for different seed values of the noise generator. Wavelet based denoising technique is applied on these profiles to verify denoising performance.

Adaptive tracking methods were employed earlier to track the MST radar signals in the higher range bins, where the signal strength becomes comparable or even less than the noise level based on the knowledge of the position and other details of the Doppler echoes at lower bins. An adaptive tracking method is developed in this work on the same lines of one of the earlier methods with suitable modifications. This method works based on SNR, permissible wind shear and Doppler velocity window (DVW). An SNR threshold is chosen (after several trails) to be 15 dB below the SNR of the highest range bin. The tracking started from the first bin whose highest peak was selected as Doppler echo as in almost all cases the Doppler echo is quite prominent and easily detectable in several smaller range bins. From the next bin onwards, the Doppler peak in a range bin (say i^{th} bin) is chosen in the following way. First a Doppler window (DVW) was fixed

based on the position of the detected Doppler echo of the previous (i-1) bin. Doppler velocity window limits are set at ± 10% of the coherent integration filter band width on either side of the mean Doppler shift of the previous range bin since the signal is not to expect to change by more than 10% of the coherent filter bandwidth from one range bin to the next. Then five most prominent peaks are chosen within this window as candidate signals. Starting from the peak having highest total power, the peak satisfying the SNR criterion was chosen as the Doppler echo. If none of the peaks satisfy the SNR criterion, the strongest peak which falls within the permissible wind shear is chosen as Doppler echo. The wind shear threshold was selected based on earlier two range bins. The wind shear threshold for present bin (say i^{th} bin) is set by adding the full width of the Doppler velocity peak in present bin to the difference in mean Doppler velocity between present bin (say i^{th} bin) and previous bin (i-1). The wind shear threshold set for present bin is used for next range bin to identify prominent peak.

If no Doppler echo was detected based on the above two criteria in a given range bin that bin was skipped and DVW and wind shear threshold for the next bin were computed from the earlier bins. This adaptive tracking method had improved ability to detect the Doppler echoes at higher ranges. This adaptive tracking algorithm combined with wavelet denoising using the wavelets designed here was used in this work for the processing of the MST radar data as described below.

The methodology developed in this work, for the wavelet denoising of the MST radar data was first tested using the simulated data, generated as described the above, as the details of the signal are known in simulated data. Different types of variations in the Doppler shifts were considered. The analysis of the data using the procedure as described the above resulted in an increase in the range, on the average, by about 60%. That is, when the data were denoised using the wavelet designed in this work and the Doppler echo was tracked using the adaptive tracking method described the above, the range up to which the signal was correctly detected was typically about 60% higher compared to tracking the raw data itself. Further if the denoising is performed using the next best suited wavelet, *viz*., Daubechies wavelet and then the same adaptive tracking method was applied, the improvement in the range compared to raw signal was only about 30%. This clearly demonstrates the suitability of the designed wavelet to the clear air echo signals of the MST radar.

Then the efficacy of this methodology in improving the range was verified using the experimental data. The data was collected using the MST radar facility at Gadanki,

India (13.5^0N, 79^0E). The data from the beams in all four directions (making angle of 10° with the vertical beam) were collected, denoised using the currently designed wavelet and tracked using the adaptive tracking method described the above. The correctness of the detected Doppler echoes using this method was ascertained by comparing the North and South beams, as the profiles of the Doppler echoes in these two directions should show mirror symmetry within the normal ranges. The results show that the detected echoes show mirror symmetry to much higher ranges when they were denoised using the designed wavelets compared to the Daubechies wavelet or the raw data. Similar results were obtained when East and West beams were compared. There seems to be the consistent result on a large collection of the data giving about 80% improvement in the range compared to the raw data. That is, while the standard wavelet (db10) based denoising improves the ability to detect Doppler echoes reliably by about 40% (improvement in the range), employing the wavelet designed in this work provides almost 80% improvement.

These studies show that, this method of denoising the MST radar data using wavelet analysis not only improves the range over which the Doppler echoes are reliably detected, it also improves the accuracy of the parameters derived from such data. This is demonstrated by collecting 10 sets of the MST radar data with a time span of about half an hour on a day when the weather was steady. It was assumed that the weather conditions, such as wind velocities and directions did not change within this short period. The data was denoised using the designed wavelet and Doppler echoes were detected using the adaptive tracking method described the above for each of these sets of the data. The first three moments (m_0, m_1 and m_2) of the Doppler echoes of each range in each of these profiles were computed for those detected echoes. Now the data for a given range in all the sets were averaged and corresponding standard deviations were computed. These results were compared with the raw data. The results show that, the denoising using the designed wavelet not only improves the ranges, but also the standard deviations in the computed physical parameters improve substantially even in the lower ranges. The results also show that the accuracy of the derived parameters improve due to this analysis even in ranges where other methods can also detect the Doppler echo. This aspect was further verified by considering simulated data where the expected values of all the parameters are known. Several simulated profiles (about 10) correspond to different seed values of the noise generator are considered. These sets have different noise values

though echo positions and other parameters remain the same. This situation is equivalent to several sets of experimental data collected in a short span under steady weather conditions. The first three moments corresponding to the Doppler power spectra (m_0, m_1 and m_2) were computed for some chosen ranges by using the adaptive tracking method described the above and standard deviations of these parameters over all the sets of data (about 10) were computed. Similar computations were performed after denoising these signals using the designed wavelet. It was again observed that the wavelet based denoising technique, besides increasing the detectable range, improves the accuracy of estimated parameters even at lower altitudes where correct Doppler echo were detected even otherwise.

The work embodied in this thesis is divided into nine chapters. Brief, chapter-wise details are presented below.

Chapter 1 presents an introduction to and theoretical background of wavelet transforms. It also deals with typical applications of wavelet transforms in different areas.

Chapter 2 details some of the background of MST radar necessary for understanding the remainder of this document. It includes an introduction to MST radar data, information this data contains and applications of MST radar. SNR issues in MST radar signal processing, present detection capabilities need for improvement are discussed. An adaptive tracking method of identifying signals in a noisy background is presented here. This chapter also provides technical details of the MST radar facility using which the experimental data reported in this thesis were collected.

Chapter 3 presents the details of the wavelet designing methodologies and denoising techniques. First part of this chapter deals with criteria for selection of wavelet for an application, design aspects and reviews existing wavelet designing methods, where as second part introduces the denoising technique based on wavelet thresholding. It also introduces the threshold selection rules such as Adaptive, Universal, Heuristic and Minimax threshold selection rules and thresholding methods (hard and soft).

Chapter 4 presents the details of wavelet designed for MST radar clear-air-echoes in this work. It starts with criteria for selection of wavelet for an application. Wavelet designing methodology, suitable to MST radar, adopted in this work is presented. Then procedure based on which MRA filter coefficients were computed is described. The results of different tests on this designed wavelet are also presented in this chapter.

Chapter 5 provides the details of development of suitable denoising methodology for the MST radar data. It starts with determining required wavelet decomposition level,

threshold levels and thresholding method to MST radar data. The results of this denoising technique based on these threshold levels on different signals and its ability to improve SNR and detectability of weak signals are also reported in this chapter.

Chapter 6 describes the adaptive tracking algorithm developed in this work and the results of verification of the same on the simulated data.

Chapter 7 deals with results of the analysis of the simulated data using the methods developed the above. The results on the simulated data generated using different Doppler shift variations and different noise profiles are summarized. Comparisons with the standard wavelets are also presented.

Chapter 8 deals with results of the analysis of the experimental data using this designed wavelet. The results of the analysis on a large number of experimental data collected under different circumstances and the details of the improvement achieved both in the range of reliable detection of Doppler echoes as well as in the accuracies of the derived parameters are provided in detail.

Chapter 9 presents overall conclusions based on the investigations carried out in this work and possible extensions of this work.

Chapter 1

Wavelet Transforms and Applications

This chapter reviews some of the background related to wavelet concepts, which will be used extensively in the following chapters. This can be found in many books and papers at many different levels of exposition. Some of the standard books are [Chui, 1992, Daubechies, 1992, Mallat, 1998, Meyer, 1993 and Vetterli M and Kova˘cevi´c, 1995]. Introductory papers include [Graps, 1995, Strang, 1994 and Vidakovic, 1994], and more technical ones are [Cohen and Kovacevic, 1996, Mallat, 1996 and Strang and Strela, 1995]. Different applications of wavelets in a wide variety of fields are also discussed in this chapter.

1.1 What makes wavelets useful in signal processing?

In signal processing, the representation of signals plays a fundamental role. David Marr elaborated in [Marr, 1982] on this topic. Most of the signals in practice are time domain signals in their raw format. This representation is not always the best representation of the signal for most of the signal processing related applications. In many cases, the useful information is hidden in the frequency content (spectral components) of the signal. Few of the frequency transforms are Fourier transform, Hilbert transform, Short time Fourier transform (STFT), Wigner distributions and Wavelet Transform.

1.1.1 Fourier Transform: Fourier transform (FT) of a given time domain signal $x(t)$ is given below

$$X_{FT}(\omega) = \int_{-\infty}^{\infty} x(t) \cdot e^{-j\omega t} \cdot dt \tag{1.1}$$

Where ω and t stands for angular frequency and time respectively and exponential term $e^{-j\omega t}$ is a basis function. This exponential term can be written as

$$e^{-j\omega t} = \cos(\omega t) + j \cdot \sin(\omega t) \tag{1.2}$$

Hence in FT basis functions are Sine and Cosine functions, which are having infinite support (length). FT gives the frequency information of the signal, which means that it tells us about the different frequency component present in the signal, but it fails to give information regarding where in time those spectral components appear because FT is computed by multiplying the signal $x(t)$ with an exponential term with infinite support, at some frequency f, and then integrated over all times (Eq.1.1). In FT there is no frequency resolution problem in the frequency domain, i.e. we know exactly what frequencies exist; similarly there is no time resolution problem in time domain, since we know the value of the signal at every instant of time. Conversely, the time resolution in the frequency domain, and the frequency resolution in time domain are zero, since there is no information about them.

This makes Fourier representation is suitable for analyzing *stationary* signals where spectral components do not change with time but, inadequate when it comes to analyzing *transient* or *non-stationary* signals i.e. signals with time varying spectra. In signal and image processing, concentrating on transients (like, e.g., image discontinuities) is a strategy for selecting the most essential information from often an overwhelming amount of data. In order to facilitate the analysis of transient signals, i.e., to localize both the frequency and the time information in a signal, numerous transforms and bases have been proposed (see e.g., [Mallat, 1998 and Vetterli M and Kova˘cevi´c, 1995]). Among those, in signal processing the Wavelet and the Short Term Fourier Transform (STFT) or windowed Fourier transform or Gabor transform are quite standard. Let us briefly discuss about these two transforms.

1.1.2 Short Term Fourier Transform: This transform is similar to Fourier transform. In STFT, the signal is divided into small portions, where these portions of the signal are assumed to be stationary. For this purpose a smooth window function $w(t)$ (typically Gaussian) is chosen. The signal is multiplied by a window function and the Fourier integral is applied to the windowed signal. For a signal $x(t)$, the STFT is [Mallat, 1998].

$$X_{STFT}(\tau, \omega) = \int_{-\infty}^{\infty} [x(t) \cdot w(t-\tau)] \cdot e^{-j\omega t} dt \tag{1.3}$$

Where, $e^{-j\omega t}$ is Fourier transform basis function, τ and ω are time and frequency parameters respectively. Note that the basis functions of a STFT expansion are $w(t)$ modulated by a sinusoidal wave and shifted in time; the modulation frequency changes while the *window remains fixed*. Here window is of finite length, which may not be suitable to all frequencies. If the chosen window is narrow it results in good time resolution but poor frequency resolution. Conversely, a wide window causes good frequency resolution but poor time resolution. Furthermore wide windows violate the condition of stationary.

To analyze transient signal of various supports and amplitudes in time, it is necessary to use time-frequency elements with different sizes for different time locations. For example, in the case of high frequency structures, which vary rapidly in time, we need higher time resolution to accurately trace the trajectory of the changes; on the other hand, for lower frequency, we will need a relatively higher absolute frequency to give a better measurement on the value of frequency. The next section shows that wavelet transform provide a natural representation which satisfies these requirements as illustrated in Fig (1.1).

1.1.3 Wavelet Transform: The wavelet transform (WT) is developed as an alternative approach to the STFT to overcome the resolution problem. Wavelet analysis is done in a similar way to the STFT analysis, in the sense that the signal is multiplied with a function (wavelet), similar to window function in the STFT, and the transform is computed separately for different portions of the time domain signal. However main difference between STFT and the WT is the width of the window is changed while computing transform based on signal spectral components. Hence WT results in varying resolution, i.e. higher frequencies are better resolved in time and lower frequencies are better resolved in frequency as explained below, which is probably the most significant characteristic of the wavelet transform. In addition, basis function is not completely fixed as in the case of other transforms such as Fourier and Laplace Transform etc.

1.1.4 Comparison of Time- Frequency resolutions: Figure (1.1) compares the frequency resolutions of Fourier transform, the windowed Fourier transform (STFT) and the wavelet transform. In a time series with a high resolution in the time domain each point contains information about all frequencies. Due to the convolution properties the opposite is true for the FT of the time series. In this case every point in the frequency

domain contains information from all points in the time domain. The windowed (Short Term) Fourier transform divides the time-frequency plane in rectangular boxes [Nielsen and Wickerhauser, 1996]. The resolution in time is increased at the expense of the frequency resolution. The wavelet transform overcomes this problem by scaling the basis functions relative to their support. The WT needs more time for the detection of low frequencies than for the detection of high frequencies. Using these properties of the WT, it is possible to describe an experimental signal on different frequency levels which leads to Mallat's Multiresolution Analysis (MRA).

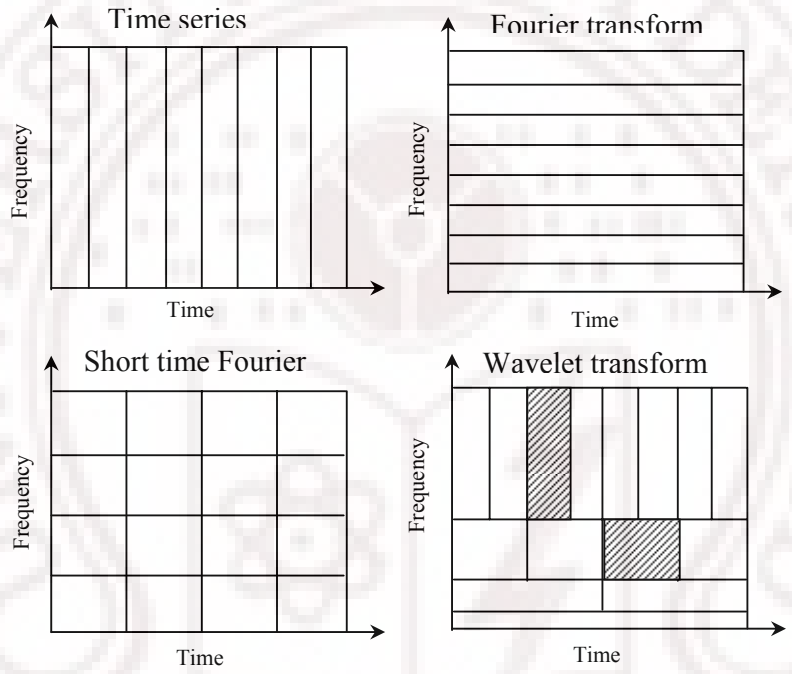

Figure 1. 1: Comparison of time-frequency properties for a time series, its Fourier transform, short-time Fourier transform and wavelet transform

1.2 Historical perspective of wavelet transforms

In the history of mathematics, wavelet analysis shows many different origins [Meyer, 1993]. Much of the work was performed in the 1930s, and, at the time, the separate efforts did not appear to be parts of a coherent theory.

1.2.1 PRE-1930: Before 1930, the main branch of mathematics leading to wavelets began with Joseph Fourier with his theories of frequency analysis. Fourier's assertion played an essential role in the evolution of the ideas mathematicians had about the functions. He

opened up the door to a new functional universe. After 1807, by exploring the meaning of functions, Fourier series convergence, and orthogonal systems, mathematician gradually were led from their previous notation of *frequency analysis* to the notion of *scale analysis.*

The first recorded mention of what we now call as "wavelet" seems to be in 1909, in a thesis by Alfred Haar. Haar wavelet is compact support wavelet (vanishes outside of a finite interval). Unfortunately, Haar wavelets are not continuously differentiable which some what limits their applications.

1.2.2 THE 1930: In the 1930s, several groups working independently researched the representation of functions using *scale-varying basis functions*. The researchers discovered a function that can vary in scale and can conserve energy when computing energy of a function. Their work provided David Mar with an effective algorithm for numerical image processing using wavelets in the early 1980s.

1.2.3 THE 1980: In 1980, Grossman and Morlet, a physicist and an engineer, broadly defined wavelets in the context of quantum physics. These two researchers provided a way of thinking for wavelets based on physics intuition.

1.2.4 POST 1980: In 1985, Stephane Mallat gave wavelets an additional jump start through his work in digital signal processing. He discovered some relationships between quadrature mirror filters, pyramid algorithms, and orthogonal wavelet bases. Inspired in part by these results, Meyer Y constructed the first non-trivial wavelets. Unlike Haar wavelets, Meyer wavelets are continuously differentiable; however they don't have compact support. A couple of years later, Ingrid Daubechies used Mallat's work to construct a set of wavelet orthonormal basis functions that are perhaps the most elegant, and have become the cornerstone of wavelet application.

1.3 Wavelet Representation

Unlike the Fourier transform, whose basis functions are sinusoids, wavelet transforms are based on small waves i.e. wavelets, which are small, localized waves of a particular shape having an average value of zero as shown in Fig (1.2). Note the support of wavelet basis is finite in time whereas the Fourier basis oscillates forever. This allows

wavelets to provide both spatial/time and frequency information (hence time frequency analysis); where as the non-local Fourier transform gives only frequency information.

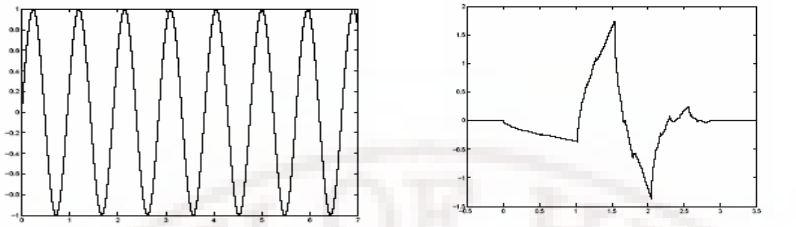

(a) A Fourier basis function (b) A wavelet basis function

Figure 1. 2 : An example of the basis functions of Fourier transforms and Wavelet transforms.

The central idea in wavelet transform is to analyze a signal according to scale. Wavelet analysis means breaking up a signal into scaled and translated versions of wavelet (mother wavelet). One chooses a particular wavelet, stretches it (to meet a given scale) and shifts it, while computing wavelet transform. The Fig (1.3) below shows a signal $x(t)$ along with the Morlet wavelet at thee scales and shifts.

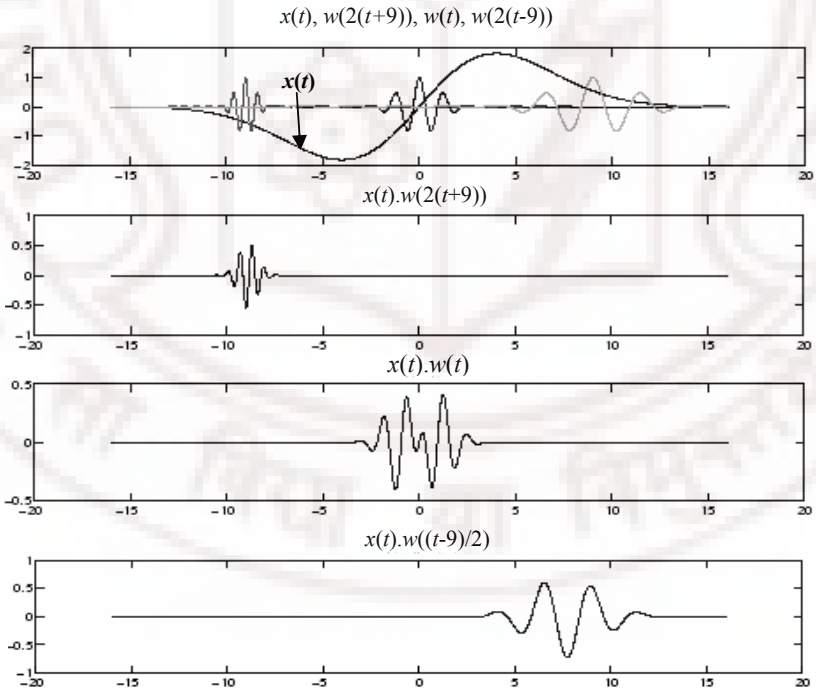

Figure 1. 3: An example of wavelet representation. A signal x(t) along with the Morlet wavelet at thee scales and shifts (w(2(t+9)), w(t), and w((t-9)/2)). [Rao and Bopadikar, 1998].

Mallat [1989] first showed that the wavelet transform provides the foundation of a powerful new approach to signal processing and analysis, called multiresolution analysis (MRA). MRA theory unifies techniques from several fields, including sub-band coding from signal processing [Woods and O'Neil, 1986], Quadrature mirror filtering (QMF) from speech recognition [Vaidyanathan and Hoang, 1988], and pyramidal image processing [Burt and Adelson, 1983]. Due to the close links to these techniques, the wavelet transform has found many applications [Basseville el al., 1992, Brailean and Katsaggelos, 1995, Chang et al., 2000 and Shapiro, 1993].

1.4 Continuous Wavelet Transform

The continuous wavelet transform (CWT) of a signal $x(t) \in L^2$ (space of all square integrable functions) is defined as

$$W_x(a,b) = \frac{1}{\sqrt{a}} \int_{-\infty}^{\infty} x(t)\, \psi^* \left(\frac{t-b}{a} \right) dt \quad = \int_{-\infty}^{\infty} x(t)\, \psi^* (a,b)\, dt \tag{1.4}$$

Where, $\psi^*(t)$ denotes the complex conjugate of $\psi(t)$. As seen in the above Eq. (1.4), the transformed signal is a function of two variables, b and a, the *translation/ localization* and *scale* parameters, respectively. $\psi(t)$ is the transforming function, and it is called the *mother wavelet* which is prototype for generating the other window functions (baby *wavelets*) [Rao and Bopadikar, 1998].

$$\psi_{a,b}(t) = \frac{1}{\sqrt{a}} \psi \left(\frac{t-b}{a} \right) \tag{1.5}$$

Here, $1/\sqrt{a}$ is the normalization factor to ensure that all wavelets have the same energy. The term translation is related to the location of a wavelet, as the wavelet is shifted through the signal, which corresponds to the time information in the transform domain. The variation of a has a dilation effect (when $a>1$) and a contraction effect (when $a<1$) of the mother wavelet. Therefore, it is possible to analyze the long and short period features of the signal or the low and high frequency aspects of the signal.

This transform is called as continuous wavelet transform (CWT), because the scale and localization parameters assume continuous values.

1.4.1 CWT as a correlation: Given two finite signals $f(t)$ and $g(t) \in L^2$, their inner product is given by

$$\langle f(t),\ g(t) \rangle = \int f(t) g^*(t)\, dt \tag{1.6}$$

Equation (1.6) leads to

$$W_x(a,b) = \langle x(t),\ \psi_{a,b}(t) \rangle \tag{1.7}$$

The cross correlation $R_{x,y}$ of the two functions $x(t)$ and $y(t)$ is defined as:

$$R_{xy}(\tau) = \int x(t) y^*(t-\tau) dt = \langle x(t), y(t-\tau) \rangle \tag{1.8}$$

Then
$$W_x(a,b) = \langle x(t), \psi_{a,0}(t-b) \rangle = R_{x,\psi_{a,0}}(b) \tag{1.9}$$

Thus $W_x(a, b)$ is the cross correlation of the signal $x(t)$ with the mother wavelet at scale a and translation b**.** If $x(t)$ is similar to the mother wavelet at this scale and translation, then $W_x(a, b)$ will be large.

1.4.2 Filtering Interpretation: The CWT offers both the time and frequency selectivity. The translating effect will result the time selectivity of the CWT and frequency selectivity is achieved with collection of linear, time variant filters with impulse responses that are dilations of the mother wavelet reflected about the time-axis. This can be explained from the convolution, which is given as:

$$h(t) * x(t) = \int h(t-\tau) x(\tau) d\tau \tag{1.10}$$

Then
$$W_x(a,b) = x(b) * \psi_{a,0}{}^*(-b) \tag{1.11}$$

For any given scale a (frequency ~$1/a$), the CWT $W_x(a, b)$ is the output of the filter with the impulse response $\psi_{a,0}{}^*(-b)$ to the input $x(b)$, and i.e. we have a continuum of filters, parameterized by the scale factor a. These filters defined by the mother wavelet are of constant Q**,** which is the ratio of center frequency to the bandwidth. The Fig (1.4) shows the filters defined by the CWT for different values of a**.**

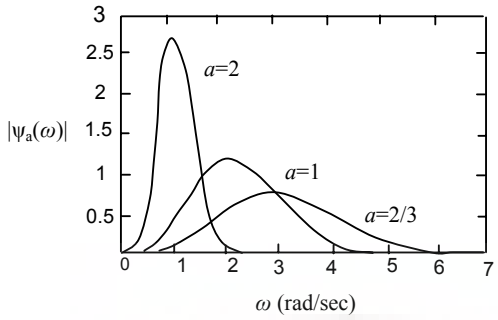

Figure 1. 4: Squared magnitude response of a Mexican hat wavelet as a function of a. Here $\psi_a(\omega) = F(\psi_{a,0}(-t))$

The inverse CWT is defined as

$$x(t) = \frac{1}{C_\psi}\left(\int_{-\infty}^{\infty}\int_{-\infty}^{\infty} W_\psi(a,b)\,\psi_{a,b}(t)\,dadb/a^2 \right) \tag{1.12}$$

When using a transform in order to get better insight into the properties of a signal, it should be ensured that the signal can be perfectly reconstructed from its representation. Otherwise the representation may be completely or partly meaningless. For the wavelet transform the condition that must be met in order to ensure perfect reconstruction is [Rao and Bopadikar, 1998]

$$C_\psi = \int_{-\infty}^{\infty} \frac{|\psi(\omega)|^2}{|\omega|} d\omega < +\infty \tag{1.13}$$

Where, $\psi(\omega)$ denotes the Fourier transform of the wavelet. This condition is known as the *admissibility condition* for the wavelet $\psi(t)$. Obviously, in order to satisfy (1.13) the wavelet must satisfy

$$\psi(0) = \int_{-\infty}^{\infty} \psi(t)\,dt = 0 \tag{1.14}$$

Moreover, $|\psi(\omega)|$ must decrease rapidly for $|\psi(\omega)| \rightarrow 0$ and for $|\omega| \rightarrow \pi$. That is, $\psi(t)$ must be a band pass impulse response. Since a band pass impulse response looks like a small wave, the transform is named wavelet transform.

The CWT is highly *redundant*, and is *shift invariant.* It is extensively used for the characterization of signals [Mallat and Hwang, 1992]: the evolution of the CWT magnitude across scales provides information about the local *regularity* of a signal. [Burrus and Gopinath, 1998]

1.5 Discrete wavelets transform

The CWT provides a redundant representation of the signal in the sense that the entire information of $W_x(a, b)$ need not be used to recover the input signal $x(t)$. This redundancy, on the other hand, requires a significant amount of computation time and resources. By sampling a and b on a dyadic grid, a type of non-redundant wavelet representation is developed which is called as Discrete Wavelet Transform. This type of representation is also arises in the context of Multiresolution Resolution Analysis (MRA). DWT is considerably easier to implement when compared to the CWT. The basic concepts of the DWT will be introduced in the following sections along with its properties and algorithms used to implement it.

1.6 Scaling Functions

In order to understand MRA we start by defining the scaling function and then define wavelet in terms of it. Set of scaling functions in terms of integer translates of the basic scaling function is defined as

$$\varphi_k(t) = \varphi(t-k) \qquad k \in Z \quad \varphi \in L^2 \tag{1.15}$$

The subspace of $L^2(R)$ spanned by these functions is defined as

$$v_0 = \overline{\underset{k}{span}\{\varphi_k(t)\}} \qquad \text{for all integers } k \text{ from } -\infty \text{ to } +\infty \tag{1.16}$$

This means that

$$f(t) = \sum_k a_k \varphi_k(t) \quad \text{for any} \quad f(t) \in v_0 \tag{1.17}$$

A two-dimensional family of functions is generated from the basic scaling function by scaling and translation as

$$\varphi_{j,k}(t) = 2^{j/2} \varphi(2^j t - k) \tag{1.18}$$

Whose span over k is,

$$v_j = \overline{\underset{k}{span}\{\varphi_k(2^j t)\}} = \overline{\underset{k}{span}\{\varphi_{j,k}(t)\}} \quad \text{for all integers } k \in Z \tag{1.19}$$

This means that if $f(t) \in v_j$ then it can be expressed as

$$f(t) = \sum_k a_k \varphi(2^j t + k) \tag{1.20}$$

For $j>0$, the span can be larger since $\varphi_{j.k}(t)$ is narrow and is translated in smaller steps, therefore can represent finer detail. For $j<0$, $\varphi_{j.k}(t)$ is wider and translated in large steps. So these wider scaling functions can represent only coarse information, and the space they span is smaller.

1.7 Multiresolution Analysis (MRA)

MRA, as implied by its name, analyzes the signal at different frequencies with different resolutions. MRA is designed to give good time resolution at high frequencies and good frequency resolution at low frequencies. This approach makes sense especially when the signal at hand has high frequency components for short duration and low frequency components for long duration. Fortunately, the signals that are encountered in practical applications are often of this type.

An MRA consists of the nested linear vector spaces with

$$v_j \in v_{j+1} \quad for all\ j \in Z \tag{1.21}$$

Or

$$\{0\} \subset .... \subset v_{-2} \subset v_{-1} \subset v_0 \subset v_1 \subset v_2 \subset ..... \subset L^2 \tag{1.22}$$

$$v_{-\infty} = \{0\}, \quad v_{\infty} = L^2 \tag{1.23}$$

The space that contains high resolution signals will contain those of lower resolution also.

$$f(t) \in v_j \quad \Leftrightarrow \quad f(2t) \in v_{j+1} \tag{1.24}$$

Above Eq. (1.24) indicates elements in a space are simply scaled versions of the elements in the next space. The relation ship of the spanned spaces is illustrated in Fig (1.5)

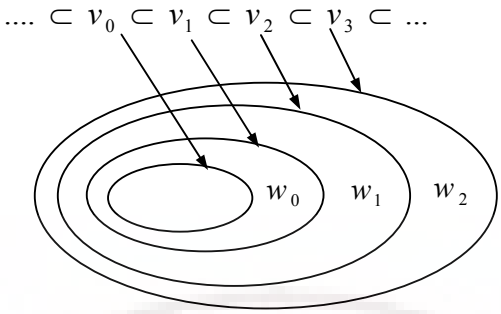

Figure 1. 5: Nested Vector Spaces Spanned by the scaling functions and wavelet functions

If $\varphi(t)$ is in v_0, it is also in v_1, the space spanned by $\varphi(2t)$.This means $\varphi(t)$ can be expressed in terms of a weighted sum of shifted $\varphi(2t)$ as [Burrus et al., 1998]

$$\varphi(t) = \sum_n h_0(n)\sqrt{2}\varphi(2t-n), \qquad n \in Z \tag{1.25}$$

Where, the coefficients $h_0(n)$ are a sequence of real/complex numbers called the scaling filter coefficients (or scaling filter) and √2 maintains the norm of the scaling function with the scale of two. It is called *the refinement equation, the MRA equation, recursion equation* and *dilation equation.*

1.8 The Wavelet functions

The important features of signal can be described by a set of wavelet functions $\psi_{j,k}(t)$, which spans the *difference* between the spaces spanned by the various scales of the scaling functions.

There are several advantages to requiring that the scaling functions and wavelets be orthogonal, orthogonal basis allow simple calculation of expansion coefficients. The orthogonal component of v_j in v_{j+1} is w_j. This means that all members of v_j are orthogonal to all members of w_j.

$$\left\langle \varphi_{j,k}(t), \psi_{j,l}(t) \right\rangle = \int \varphi_{j,k}(t)\,\psi_{j,l}(t)dt = 0 \quad \text{for} \quad j,k,l \in Z \tag{1.26}$$

The relationship of the various subspaces can be seen from the following expressions. We start with j=0, (1.17) becomes

$$v_0 \subset v_1 \subset v_2 \subset ..... \subset L^2 \tag{1.27}$$

Wavelet spanned subspace w_0 can be defined as

$$v_1 = v_0 \oplus w_0 \tag{1.28}$$

This extends to

$$v_2 = v_0 \oplus w_0 \oplus w_1 \tag{1.29}$$

In general this gives

$$L^2 = v_0 \oplus w_0 \oplus w_1 \oplus ..... \tag{1.30}$$

When v_0 is the initial space spanned by the scaling function $\varphi(t-k)$.

Figure (1.5) pictorially shows relationship of scaling functions and wavelet functions for different scales j. The scale of the initial space is arbitrary and could be chosen at a higher resolution (say, j =10) or at a lower resolution (say, j =-10).
At j=-∞ Eq. (1.30) becomes

$$L^2 = ... \oplus w_{-2} \oplus w_{-1} \oplus w_0 \oplus w_1 \oplus w_2 \oplus ..... \tag{1.31}$$

Above Eq. (1.31) shows that wavelet functions completely describe the original signal i.e.

$$g(t) = \sum_{j,k} C_{j,k} \psi_{j,k}(t) \tag{1.32}$$

Another way to describe the relation of v_0 to the wavelet space is

$$w_{-\infty} \oplus ... \oplus w_{-1} = v_0 \tag{1.33}$$

This again shows that the scale of scaling space is arbitrarily. In practice, it is usually chosen to represent the coarsest detail of interest in a signal.

Since these wavelets reside in the space spanned by the next narrower scaling function, i.e.$w_0 \subset v_1$, they can be represented by a weighted sum of scaling function $\varphi(2t)$

$$\psi(t) = \sum_n h_1(n) \sqrt{2} \varphi(2t - n), \qquad n \in Z \tag{1.34}$$

Where, the coefficients $h_1(n)$ are a sequence of real/complex numbers called the wavelet filter coefficients (or wavelet filter). The wavelet coefficients are required by Orthogonality to be related to the scaling function coefficients $h_0(n)$ by

$$h_1(n) = (-1)^n h_0(1-n) \tag{1.35}$$

For finite even length-N $h_0(n)$ Eq. (1.35) becomes

$$h_1(n) = (-1)^n h_0(N-1-n) \tag{1.36}$$

The function generated by Eq. (1.34) gives the prototype or mother wavelet $\psi(t)$ for a class of expansion functions of the form

$$\psi_{j,k}(t) = 2^{j/2}\psi(2^j t - k) \tag{1.37}$$

Where, 2^j is the scaling of t (j is $\log_2$ of the scale), $2^{-j}k$ is the translation in t, and $2^{j/2}$ maintains the L^2 norm of the wavelet at different scales.

According to Eq. (1.30) any function $g(t) \in L^2(R)$ *could* be written as a series expansion in terms of the scaling function and wavelets.

$$g(t) = \sum_{-\infty}^{\infty} c(k)\varphi_k(t) + \sum_{j=0}^{\infty}\sum_{k=-\infty}^{\infty} d(j,k)\psi_{j,k}(t) \tag{1.38}$$

In this expansion, the first summation in Eq. (1.38) gives a function that is a low resolution or coarse approximation of $g(t)$ where as second summation adds higher or finer resolution as index $g(t)$ increases, which adds increasing detail. This is analogous to Fourier series where the higher frequency terms contain the detail of the signal. [Burrus et al., 1998]

1.9 Signal Representation in DWT

The discrete wavelet transform (DWT) is the signal expansion into (bi)-orthogonal wavelet basis. In this transform scale is sampled at dyadic steps $a \in \{2^j : j \in Z\}$, and the position is sampled proportionally to the scale $b \in \{k2^j : (j, k) \in Z^2\}$. Since

$$L^2 = v_{j_0} \oplus w_{j_0} \oplus w_{j_0+1} \oplus \ldots\ldots \tag{1.39}$$

Using equations (1.18) and (1.37), a more general statement of the expansion Eq. (1.38) can be given by

$$g(t) = \sum_k c_{j_0}(k)\varphi_{j_0,k}(k) + \sum_k \sum_{j=j_0}^{\infty} d_j(k)\psi_{j,k}(k) \tag{1.40}$$

Or

$$g(t) = \sum_k c_{j_0}(k)\varphi_{j_0,k}(k) + \sum_k \sum_{j=j_0}^{\infty} d_j(k)\psi_{j,k}(k) \tag{1.41}$$

Where, j_0 could be arbitrarily chosen in between -∞ and ∞, the choice of j_0 sets the coarsest scale whose space is spanned by $\varphi_{j_0,k}(t)$ .The rest of $L^2(R)$ is spanned by the wavelets which provide the high resolution details of the signal.

The set of expansion coefficients $c_{j_0}(k)$ and $d_j(k)$ are called DWT of $g(t)$. If the wavelet system is orthogonal, these coefficients can be calculated by inner products.

$$c_j(k) = \langle g(t), \varphi_{j,k}(t) \rangle = \int g(t)\varphi_{j,k}(t)dt \tag{1.42}$$

And

$$d_j(k) = \langle g(t), \psi_{j,k}(t) \rangle = \int g(t)\psi_{j,k}(t)dt \tag{1.43}$$

Even for the worst case signal, the wavelet expansion coefficients drop off rapidly as j and k increase. This is why the DWT is efficient for signal and image compression. The DWT is similar to a Fourier series but, in much more flexible and informative. It can be made periodic like a Fourier series to present periodic signals efficiently. However, unlike a Fourier series, it can be used directly on non-periodic transient signals with excellent results.

1.10 Parseval's theorem

If the scaling and wavelet functions form an orthogonal basis Parseval's theorem relates the energy of the signal $g(t)$ to the energy in each of the components and wavelet coefficients. This is the one reason why orthogonality is important.

For the general wavelet expansion of (1.38) or (1.41), Parseval's theorem

$$\int |g(t)|^2 dt = \sum_{l=-\infty}^{\infty} |c(l)|^2 + \sum_{j=0}^{\infty} \sum_{k=-\infty}^{\infty} |d_j(k)|^2 \tag{1.44}$$

1.11 Filter banks and the DWT

In practical applications we never deal with scaling functions and wavelets. Only the coefficients $h_0(n)$ and $h_1(n)$ in the dilation equations (1.25) and (1.34) and $c_{j_0}(k)$ and $d_j(k)$ in expansion equations (1.38), (1.42) and (1.43) need to be considered and they can be viewed as digital filters and digital signals respectively [Gopinath and Burrus, 1992 and Vaidyanathan, 1992] While it is possible to develop most of the results of wavelet theory using filter banks only.

1.11.1 Wavelet Analysis by Multirate Filtering: The relationship between the expansion coefficients at a lower scale level in terms of higher scale is given by following equations. [Burrus et al., 1998]

Relationship for scaling coefficients

$$c_j(k) = \sum_m h_0(m-2k)c_{j+1}(m) \tag{1.45}$$

Corresponding relationship for the wavelet coefficients is

$$d_j(k) = \sum_m h_1(m-2k)d_{j+1}(m) \tag{1.46}$$

These equations show that the scaling (Approximation) and wavelet (detail) coefficients at different levels of scale can be obtained by convolving the expansion coefficients at scale j by the time reversed recursion coefficients $h_0(-n)$ and $h_1(-n)$ then down sampling or decimating (taking every other term, the even terms) to give the expansion coefficients at the next level of j-1.These structures implement Mallat's algorithm

The implementation of equations (1.45) and (1.46) is shown in Fig (1.6) Where down pointing arrows is indicate down sampling and left two boxes denote FIR (finite impulse response) filtering or a convolution by $h_0(-n)$ or $h_1(-n)$.

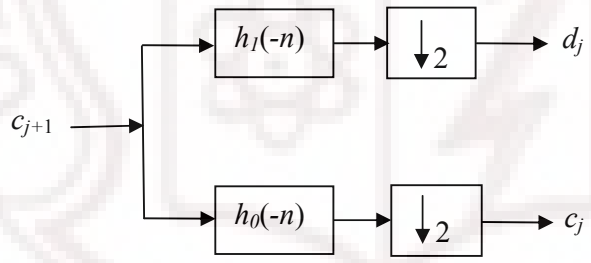

Figure 1. 6: One stage Two-Band Analysis Bank

Here FIR filter implemented by h_0 is a low pass filter and the one implemented by h_1 is a high pass filter. The average number of data points out of this system is the same as the number in. The number is doubled by having two filters, and then it is halved by decimation back to the original number. This means no information has been lost in this system and hence perfect reconstruction is possible. The aliasing occurring in the upper bank can be cancelled by the lower bank. This is the idea behind the perfect reconstruction in filter bank theory [Vaidyanathan, 1992 and Fliege, 1994].

This process (splitting, filtering, and decimation) is called as *wavelet decomposition*. We can repeat this *wavelet decomposition* on scaling coefficients for iterating the filter bank. Figures (1.7 and 1.8) show three stages Two-Band Analysis tree and Frequency Bands for the Analysis tree.

The first stage of two banks divide the spectrum of x[n] into two equal bands (low pass and high pass), resulting in scaling (approximation) coefficients and wavelet (detailed) coefficients at lower scale. The second stage then divides that low pass band into another low pass and high pass bands and so on. This results in a logarithmic set of bandwidths as illustrated in Fig (1.8) These are called "constant-Q" filters (CQF) in filter bank language because the ratio of the band width to the center frequency of the band is constant. . We can observe that down sampling assures that reconstructed signal has the same number of samples as the original one.

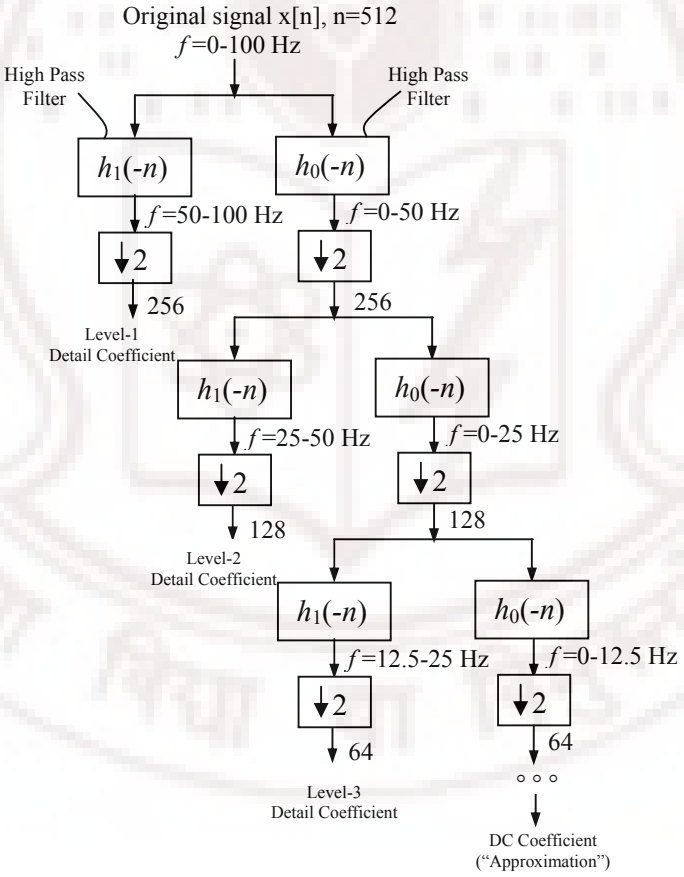

Figure 1. 7: Three stage Two-Band Analysis Tree

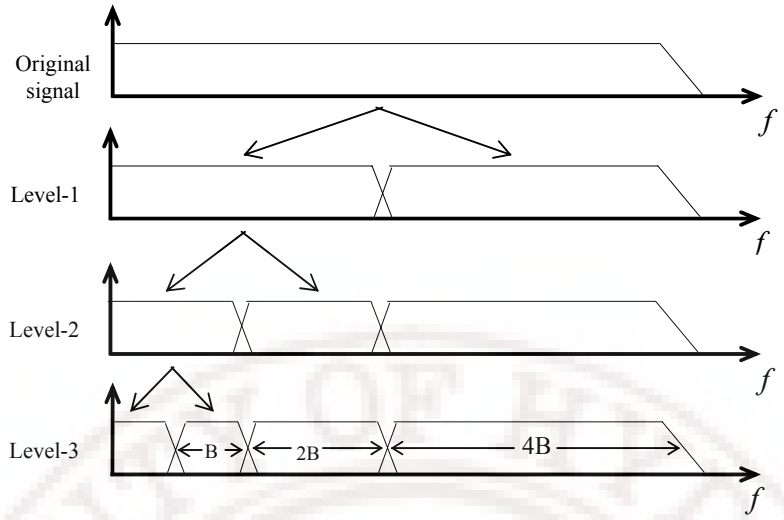

Figure 1. 8: Frequency Bands for the Analysis tree

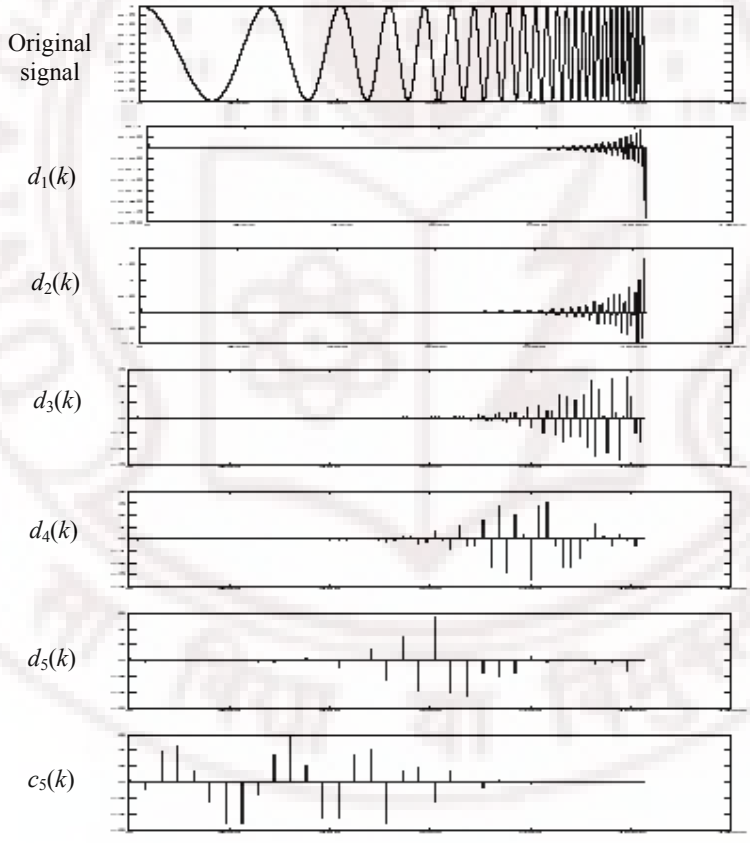

Figure 1. 9: DWT of a chirp signal, notice how location in *k* trances the frequencies in the signal in a way the Fourier transform can not. [Matlab, 2004]

Figure (1.9) shows original signal (chirp signal, which has a time-varying frequency) and corresponding approximation and detailed coefficients. Notice how location in k traces the frequencies in the signal in a way the Fourier transform can not. This suggests that wavelet transform is well suited for time-frequency analysis

1.11.2 Wavelet Synthesis by Multirate Filtering: A reconstruction of the original fine scale coefficients of the original signal can be made from a combination of the scaling function (approximation) and wavelet coefficients (detail) coefficients at a coarse resolution.

We start with two sets of coefficients $c_j(k)$ and $d_j(k)$ at scale index j and produce the coefficients at scale index j+1. We have following relation. [Burrus et al., 1998]

$$c_{j+1}(k) = \sum_m c_j(m)h_0(k-2m) + \sum_m d_j(m)h_1(k-2m) \tag{1.47}$$

This equation can be evaluated by up-sampling the j scale coefficient sequence $c_j(k)$ (which means double its length by inserting zeros between each term), then convolving with the scaling filter coefficients $h_0(n)$.The same is done to the j level wavelet sequence $d_j(k)$ and the results are added to give the j+1 level scaling coefficients. This structure is show in Fig (1.10); this combining process can be extended to any level by combining the appropriate scale wavelet coefficients. The resulting two-scale tree is show in Fig (1.11)

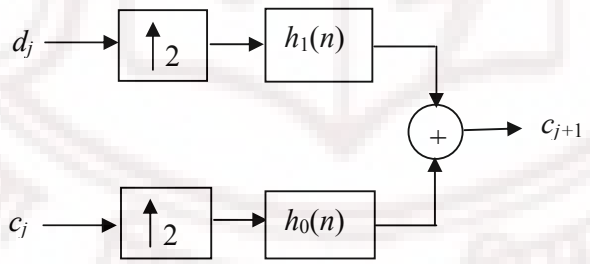

Figure 1. 10: One stage Two-Band Synthesis Bank

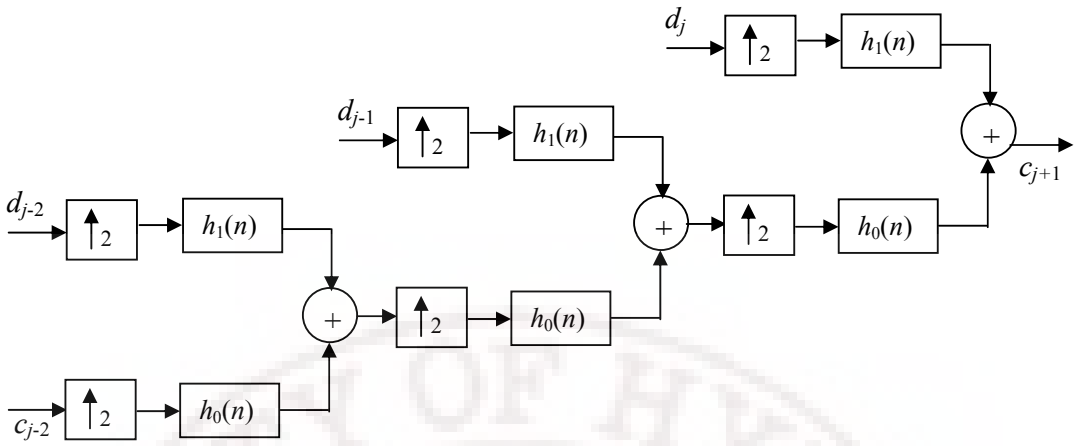

Figure 1. 11: Three stage Two-Band Synthesis Bank

1.12 Wavelet Families

There are number of standard basis functions which can be used as a mother wavelet functions in wavelet transforms. Figure (1.12) illustrates some of the commonly used wavelet functions. Haar wavelet is the one of the oldest and simplest wavelet.

Therefore, any discussion of wavelets starts with the Haar wavelet. Daubechies wavelets are the most popular wavelets. The Haar, Daubechies, Symlets and Coiflets are compactly supported orthogonal wavelets. The Meyer, Morlet and Mexican Hat wavelets are symmetric in shape.

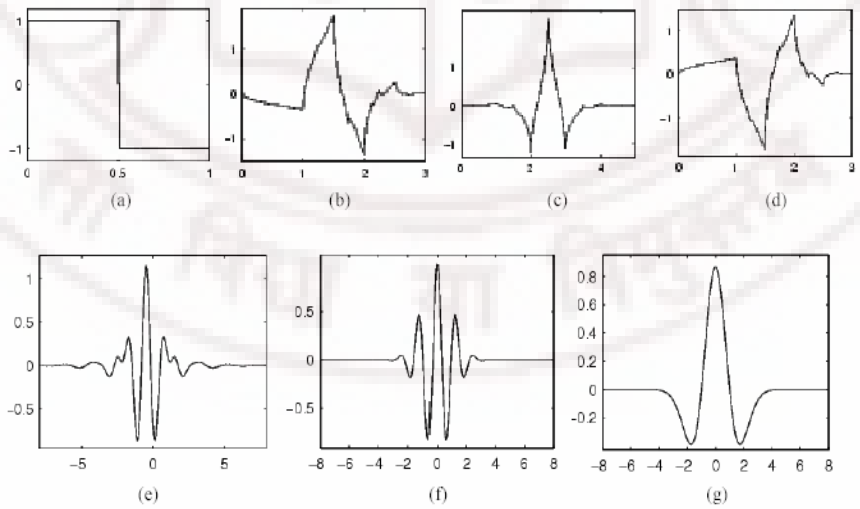

Figure 1. 12: Wavelet families (a) Haar (b) Daubechies4 (c) Coiflet1 (d) Symlet (e) Meyer (f) Morlet (g) Mexican Hat

1.13 Properties of MRA filters, scaling and wavelet functions

1. Orthogonality of Wavelets: The baby wavelets are orthogonal and have unit energy

$$\int_{-\infty}^{\infty} \psi_{j,k}(t)\,\psi_{m,n}(t)\,dt = \delta(j-m)\,\delta(k-n) \tag{1.48}$$

2. Orthogonality of scale: The translates $\varphi(t-k)$ $-\infty < k < \infty$ are orthogonal and have unit energy ($<\varphi(t), \varphi(t)>$)

$$\int_{-\infty}^{\infty} \varphi(t)\varphi(t-n) = \delta(n) \tag{1.49}$$

3. Completeness: The translates $\varphi(t-k)$ $-\infty < k < \infty$, span the same space as wavelets

$$\omega_{j,k}(t), \quad -\infty < j < 0 \quad \text{and} \quad -\infty < k < \infty \tag{1.50}$$

4. Double Shift Orthogonality of the Filters

$$\int_{-\infty}^{\infty} \varphi(t)\varphi(t-n)dt = \delta(n) = \sum_{k} h_0(k)h_0(k-2n) \tag{1.51}$$

$$\int_{-\infty}^{\infty} \omega(t)\omega(t-n)dt = \delta(n) = \sum_{k} h_1(k)h_1(k-2n) \tag{1.52}$$

$$\int_{-\infty}^{\infty} \varphi(t)\omega(t-n)dt = \delta(n) = \sum_{k} h_0(k)h_1(k-2n) \tag{1.53}$$

These equations (1.51-1.52) are called the double shift orthogonality relations of the filters. They lead to a number of other properties of the filters. They are

a) If we take n=0

$$\sum_{k} h_0(k)^2 = 1 \quad \text{and} \quad \sum_{k} h_1(k)^2 = 1 \tag{1.54}$$

b) If we integrate both sides of the equation we will get

$$\sum_{k} h_0(k) = \sqrt{2} \quad \text{and} \quad \sum_{k} h_1(k) = 0 \tag{1.55}$$

c) The even and odd terms of both filters are

$$\sum_{k} h_0(2k) = \sum_{k} h_0(2k+1) = \frac{1}{\sqrt{2}} \tag{1.56}$$

$$\sum_{k} h_1(2k) = -\sum_{k} h_1(2k+1) = \pm\frac{1}{\sqrt{2}} \tag{1.57}$$

5. Support of the scaling function: The support of a function $\varphi(t)$ is the range of t where the function is non zero. The recursion equation imposes a restriction on the support of the scaling function. If $N+1$ is the length of low pass filter $h_0(n)$, then the support of $\varphi(t)$ is the in the interval $0 \leq t \leq N$.

1.14 Applications of Wavelet Transforms

There is a wide range of application for wavelet transforms in different fields ranging from signal processing to biometrics, and the list is still growing.

One of the prominent applications is Data compression [Rao and Bopadikar, 1998]. Apart from its original intention of analyzing non-stationary signals; wavelets have been most successful in image processing and compression applications. Due to the compact support of the basis functions used in wavelet analysis, wavelets have good energy concentration properties. In DWT, the most prominent information in the signal appears in high amplitudes and the less prominent information appears in very low amplitudes. Data compression can be achieved by discarding these low amplitudes. The wavelet transforms enables high compression ratios with good quality of reconstruction. Recently, the wavelet transforms have been chosen for the JPEG 2000 compression standard [Marcellin et al., 2000 and Rabbani and Joshi, 2002].

Compression property has been further explored by Iain Jonstone and David Donoho [Jonstone and Donoho, 1995a] and they have devised the *wavelet shrinkage denoising (WSD)*. The idea behind WSD is based on recognizing the noise level, which will show itself at finer scales, and discarding the coefficient that fall below a certain threshold at these scales will remove the noise.

Wavelets also find applications in speech processing, which reduces transmission time in mobile applications. They are used in edge detection, feature extractions, speech recognition, echo cancellation, and others. They are promising for real time audio and video compression applications. Wavelets have numerous applications in digital communications, study of distant universes [Bijaoui et al., 1996], fractal analysis, turbulence analysis [Meyer, 1993] and financial analysis.

Wavelets have often been employed to analyze wind disturbances such as gravity waves [Shimomai et al., 1996] and to remove ground and intermittent clutters, such as due to airplane echoes, in the atmospheric radar data [Jordon et al., 1997, Boisse et al., 1999 and Lehmann & Teschke, 2001] using standard wavelets such as Daubechies 20.

Wavelets place important role in Biomedical Engineering owing to the nature of all biological signals being non-stationary. Further wavelets are useful the analysis of ECG (electro cardiogram) for diagnosing cardiovascular disorders and of electro encephalogram (EEG) for diagnosing neurophysiologic disorders, such as seizure detection, or analysis of evoked potentials for detection of Alzheimer's disease [Polikar et al., 1997]. Wavelets have also been used for the detection of micro calcifications in mammograms and processing of computer tomography [CT] and magnetic resonance image [MRI]. The popularity of wavelet transforms is growing because of its ability to reduce distortion in the reconstructed signal while retaining all the significant features present in the signal.

As mentioned above, though elegant and powerful wavelet based tools are being applied in number of areas, their application to radar signal processing has been rather limited. Considering the vastness of the area of radar signal processing it appears that wavelet base techniques haven't been applied to their full potential in this area. The main objective of the this work is to explore wavelet transform based signal processing to atmospheric radar i.e. MST radar with a view to extract Doppler spectra from the noisy data with improved signal to noise ratio to extend height coverage and improve the accuracy of the parameters extracted from the spectra.

Chapter 2

MST Radar Technique and Signal Processing

This chapter gives basic concepts of MST radar, signal and data processing as applied to the MST radars, which form the background to the subsequent chapters.

2.1 Introduction to Radar

The basic techniques for radar were used for the first time by Sir Edward Victor Appleton in his ionosphere research in the 1920s. The pulse radars are used to detect range and the radar scattering cross-section of a remotely located object (e.g. aircraft). When the detected target is in motion, the returned signal is Doppler shifted from the transmitted frequency and the measurement of the Doppler shift provides the line-of-sight velocity of the target. The radars having this capability are referred to as pulse Doppler radars. In addition to the above, if the location of the target is to be uniquely determined, it is necessary to know its angular position as well. The radars having this capability employ large antennas of either phased array or dish type to generate narrow beams for transmission and reception. There are several pulse radars that have been developed with varying degrees of complexity to meet the demands of application in various fields.

2.2 Atmospheric radars

Besides detection and characterization of hard targets e.g. aircraft, radar can be employed to probe the soft or distributed targets such as earth's atmosphere. A kind of radar whose target is earth's atmosphere is called as *atmospheric radar*. The turbulent fluctuations in the refractive index of the atmosphere serve as a target for these radars. This is the one of the features which makes the atmospheric radar unique and different from other kinds of radars. Atmospheric radars are used to measure temperature, pressure, humidity and wind velocities of atmosphere. The atmospheric radars of interest to the current study are known as clear air radars and they operate typically in the VHF (30–300

MHz) and UHF (300 MHz–3GHz) bands [Rotteger and Larsen, 1990]. Examples of atmospheric radars are ST (Stratosphere Troposphere), MST (Mesosphere Stratosphere Troposphere), Lidar and Meteor radar. Operational atmospheric radars have antennas with diameter of 10-300 m.

There is another class of radars known as weather radars which observes precipitation as its principal target and they operate in the SHF band (3-30 GHz) [Doviak and Zrnic, 1984 and Battan, 1973].

A major advance has been made in the radar probing of the atmosphere with the realization in early seventies. The pioneering work of Woodman and Guillen [1974], it is shown that it is possible to explore the entire Mesosphere-Stratosphere-Troposphere (MST) domain by means of a high power VHF backscatter operating ideally around 50 MHz. It led to the concept of MST radar and this class of radars has come to dominate the atmospheric radar scene over the past few decades.

2.3 Principles of MST Radar

MST Radar is used to investigate the motion of the middle atmosphere on all temporal and spatial scales and also to study the interactions among the three different regions of the atmosphere namely, *Mesosphere, Stratosphere, Troposphere*. It is high power phase coherent pulse Doppler radar operating typically around 50 MHz with an average power-aperture product exceeding about $5x10^7$ Wm^2. It receives echoes due to the scattering and reflection from variation in radio refractive index of neutral atmosphere which in turn depends on variability of humidity, temperature and electron density induced by turbulence in the lower and middle atmosphere. It provides estimates of atmospheric winds on a continuous basis at high temporal and spatial resolutions required to study of various dynamical processes of the atmosphere. MST radar uses the echoes obtained over the height range of 1-100 km to study winds, waves, turbulence and atmospheric stability.

2.4 Scattering mechanism of MST Radar and Radar equation

The scattering and reflection mechanism responsible for the MST radar signal return have been described in some detail by Balsley and Gage [1980] and Gage and Balsley [1980] among others. They are classified generally as (i) Turbulent scatter (ii) Fresnel (Partial) reflection/scatter and (iii) Thermal (incoherent or Thomson) scatter. The

first two mechanisms provide coherent scatter which results from macroscopic fluctuations in refractive index associated with clear air turbulence (CAT). The third arises from Thomson scatter by free electrons in the ionosphere and the signal return is characterized by the statistical fluctuations of electron density due to random thermal motions of electrons and ions [Evans, 1969]. While the turbulent scatter and the Fresnel reflection are the dominant mechanisms for the MST signal return, it has been shown that it is possible to map the mesospheric wind fields using the Thomson backscatter technique as well [Harper,1978]. The radio refractive index, n relevant to the MST radar return is expressed approximately as [Balsley and Gage, 1980]

$$\begin{aligned} n-1 &= 77.6\times10^{-6}\,\rho/T \quad \text{(Upper Troposphere and Strtosphere) Dry term} \\ &\quad + 3.73\times10^{-1}\,e/T^2 \quad \text{(Lower Troposphere) Wet Term} \\ &\quad - N_e/2N_c \quad \text{(Mesosphere) Electron Density} \end{aligned} \tag{2.1}$$

Where,

e = Partial pressure of water vapor (in Mb)

ρ =Atmospheric pressure (in Mb)

T =Absolute temperature (^0K)

N_e = Number density of electrons

N_c = Critical electron density corresponding to the operating radar frequency

The first two terms, in the above expression, represent the contributions due to the bound electrons of water vapor and dry air, while the third expresses the contribution due to the presence of free electrons. The refractive index fluctuations arising from the first two terms contribute to the radar returns from troposphere and stratosphere. The neutral turbulence induced electron density fluctuations represented by the third term become the major factor contributing to the radar return from the mesosphere. Figure (2.1) shows height profile of water-vapor, dry-air and free electron contributions to the radio refractive index n.

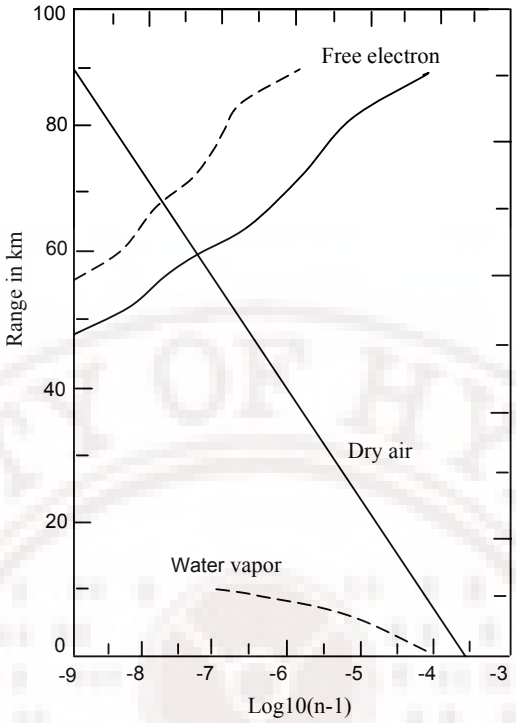

Figure 2. 1: Height profile of water-vapor, dry-air and free electron contributions to the radio refractive index n.

The main received echo power due to volume scatter is given by

$$P_r \alpha \frac{P_t A_e \eta \, r}{4 \pi R^2} \tag{2.2}$$

Where,

P_t = Transmitted power

A_e = Effective antenna area

R = Range resolution

R = Range of reflecting volume

η = Volume reflectivity coefficient

The value on η will depend on the mechanism of reflection which in turns is a function of the height.

2.5 MST radar Techniques

There are two main techniques.

1. Doppler Beam Swinging (DBS) technique
2. Spaced Antenna Drifts (SAD) technique

2.5.1 Doppler Beam swinging technique: This technique uses a narrow beam in at least three directions and measures the Doppler shift of echoes from irregularities. A beam in the Zenith direction and at least two more means in scattered off- Zenith in two perpendicular directions are used to measure the radial velocity in each beam direction. The vertical and horizontal components of the wind vector are estimated from the resultant radar returns. Figure (2.2) Shows beam configuration in wind profiling.

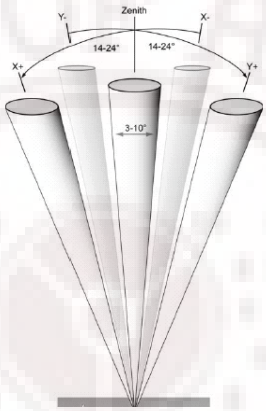

Figure 2. 2: Beam Configuration in wind profiling [Jain and Narayana Rao, 1995]. [Typical beam configuration in wind profiling consists of three beams: one vertical and two tilted 15^0 from the Zenith (to the East and North, for example). Under some circumstances, two additional beams are needed (such as South and West)]

2.5.2 Spaced Antenna Drifts (SAD) technique: This method uses three or more spaced antennas and the received signals are cross correlated to determine the offset of cross- correlation functions, yielding the horizontal velocity components.

Figure (2.3) shows the functional block diagram of India MST radar system. The main subsystems are

- Antenna and feed network
- Transmitter
- Receiver
- Data acquisition & signal processing
- System controller & Timing signal generator
- Computer system

2.6 MST Radar System Design Using Doppler Beam Swinging Technique

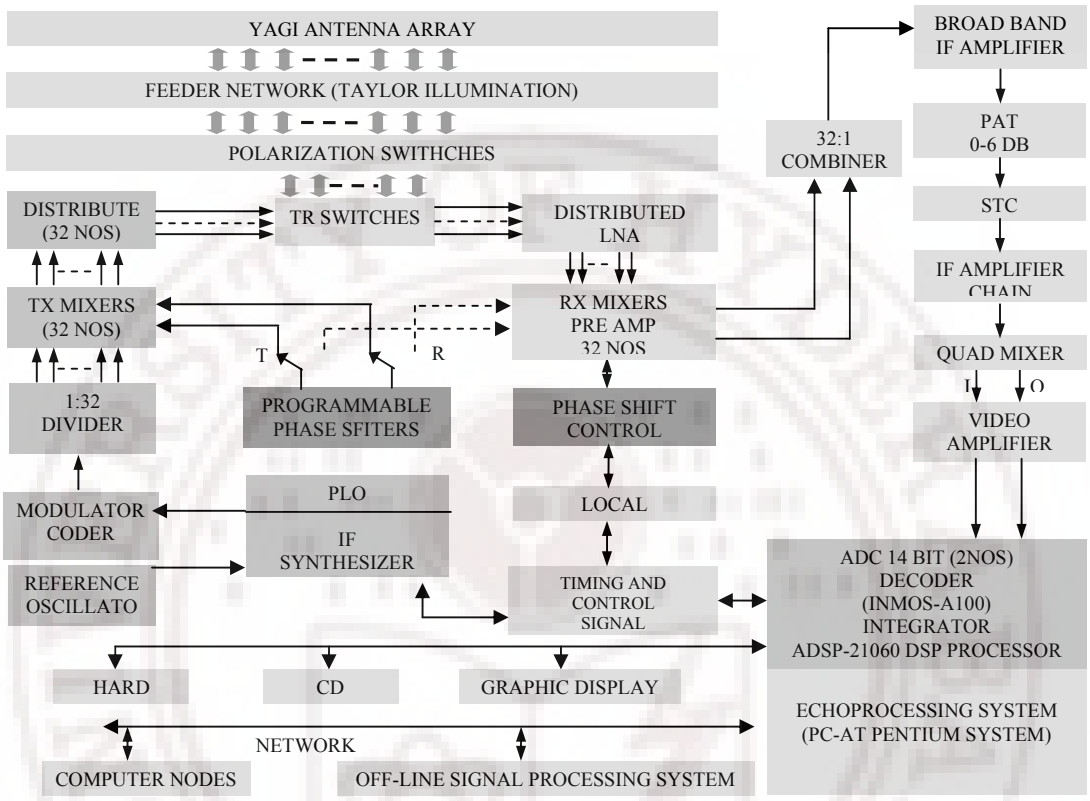

Figure 2. 3: A functional block diagram of the Indian MST

2.6.1 Antenna Array and Feeding System: To achieve the required power aperture product a large antenna is required. This is realized by a phased antenna. The beam steering is achieved through electronic control of phases at the feed points. The required side lobe levels are realized by using different illumination functions like Taylor illumination function etc. The elements of the phased array may consist of dipoles or yagis. This selection of the elements depends upon gain and bandwidth. The intermittent spacing among the elements is selected such that no grating lobes occur. The feeder network consists of high power low loss cables, duplexers, polarization switches, directional couplers etc. The tapering of the antenna illumination is achieved by using directional couplers.

Indian MST radar uses a phased array of crossed 3 elements, yagis arranged in a 32 x 32 matrix (1024 elements). A modified Taylor distribution is used as illumination

function. This is achieved by a complex feeder network consisting of power dividers and directional couplers and a set of 32 transmitters and receivers with different power levels.

The radar beam in principle can, be positioned at any angle, but it is currently programmed to sequence automatically any combination of seven angles: Zenith in X and Y polarizations, $\pm 20^0$ off-Zeniths in magnetic East west and North South, and 14.8^0 due North to look transverse to the Earth's magnetic field. The phase angles for transmit and receive beams for the seven beam positions are stored in four EPROMs, each serving 8 transmit and receive channels. A local processor (8085 A), located in each of the four transmitter huts, adds the phases read from the EPROM to the calibration phases and provides the control signals to 8-phase shifters.

2.6.2 Transmitter System: Since MST radar needs coherence between transmit and receive systems, MOPA (Master Oscillator Power Amplifier) type transmitter is used. The large peak power (2.5 MW) is achieved using appropriate power amplifiers. The large power is distributed among the various elements of antenna as per the illumination function. The transmitter is capable of operating from 1 μsec to 32 μ *sec* and with the pulse compression using complementary codes.

2.6.2.1 Waveform selection: The system sensitivity and high resolution depend upon the average power of transmitter and the pulse width. A large pulse width is necessary to increase average power to maximize the signal to noise ratio (SNR). But to observe some of the atmospheric phenomena typical resolution of the order of 150 m corresponding to a pulse width of 1 μs is required. This lower pulse width will not cause problem for troposphere measurements, because there will be a strong signal from those low altitudes. However, for mesospheric studies the lower pulse width will cause very weak return signals and useful data can be obtained only when strong turbulence exists, so a pulse width as high as 32 μs will be needed for probing the Mesosphere. While a maximum duty cycle and a high average power are preferred, a large pulse width reduces height resolution. Pulse compression techniques are often used to achieve a good height resolution, with large pulse widths. MST radar provides for a choice of transmitted waveforms depending upon the experiment planned.

2.6.2.2 Pulse compression Techniques: A good height resolution at the maximum average power can be achieved by using pulse compression techniques. *Phased coded*

pulse compression method is popular in MST radar. In this technique a long duration pulse of width "T" is divided into "N" sub-pulses of width '*t*'. The phase of each sub-pulse alters between 0 and 180 deg. And a Barker codes and complementary codes are extensively used in atmospheric radars. For MST radar applications complementary codes offer optimum side lobe suppression of range side lobes.

2.6.3 Receiver: Receiver is a conventional super heterodyne system employing highly stable local oscillator derived from the same reference as master oscillator feeding the transmitter to ensure phase coherency for extraction of Doppler information. The radar echo is fed to a receiver through a TR (Trans Receive) - switch which protects the receiver from damage caused by the high power transmitter during the transmission. The received RF signal, being a replica of the transmitted signal, is pre-amplified by a radio frequency (RF) amplifier. The RF signal is mixed with a coherent local (LO) signal, and is down converted to an intermediate frequency (IF) signal.

After maximizing a peak signal to noise power ratio in the IF amplifier, the IF signal is detected by a quadrature detector which produces a time series of sine and cosine components of the received signal. The detected signal is finally converted to a digital signal by an analog-to-digital converter (ADC), and then transmitted to a digital signal processing system. Normally the receivers have provision for selective range gating for height regions of interest.

2.6.4 Data Acquisition and Signal Processing: The purpose of Radar signal processing is to extract desired information from radar data. The accuracy of the data available from radar is limited by thermal noise introduced by the radar receiver echoes from targets of no interest (known as clutter), and externally generated interference. As a result radar signal processing is also used to enhance signals and to suppress clutter and externally generated signals. Especially in the case of MST radar, though the technique is same as in the case of radars used to detect hard targets, the extraction of signal requires great care. In normal radar the target will be hard target having better reflection coefficient. In the case atmospheric radar the target is soft target and it is buried 40 to 50 dB below the back ground noise/clutter and sophisticated signal processing technique is required to extract the signal. Figure (2.4) shows the basic processing steps involved in the extraction and estimation of atmospheric parameters.

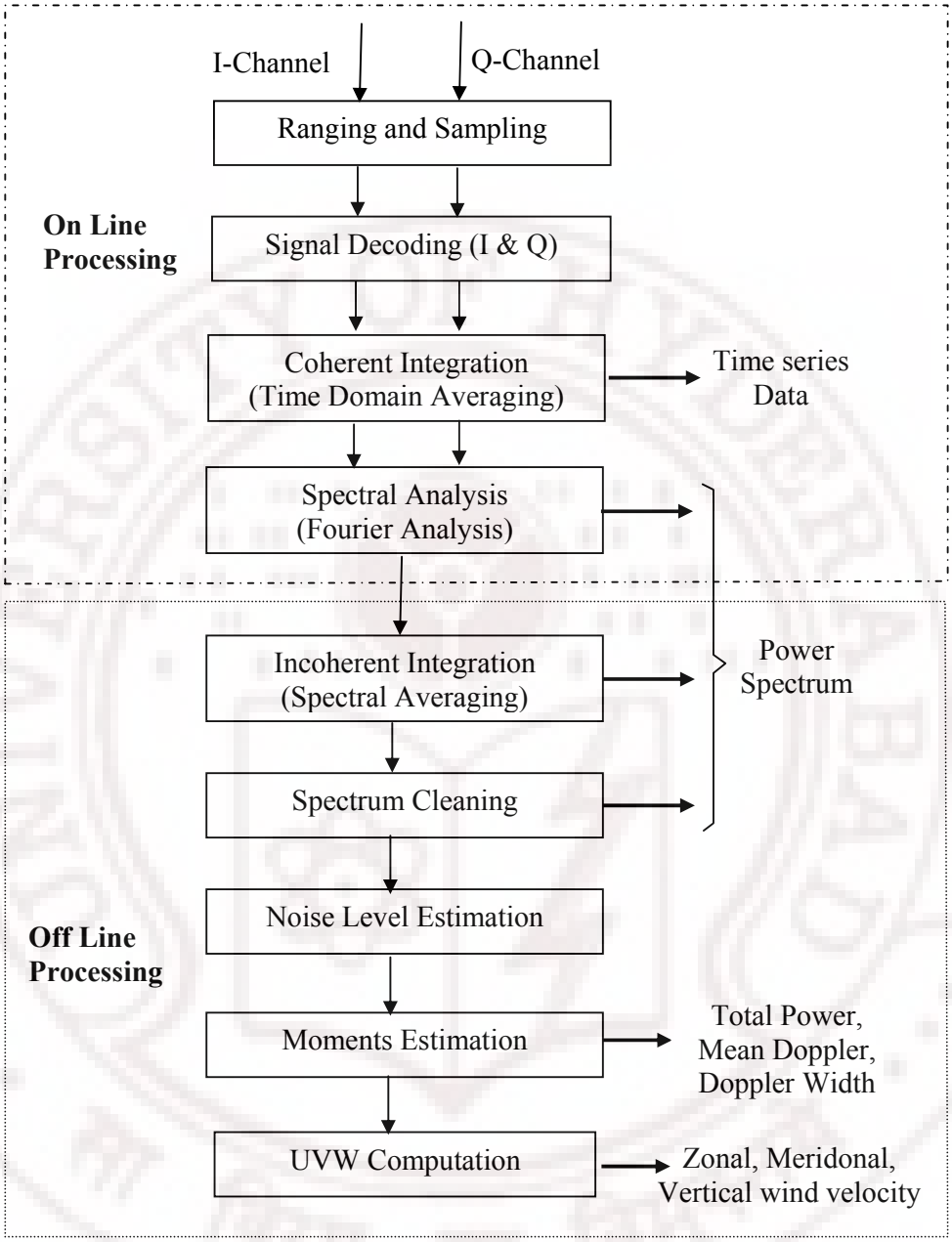

Figure 2. 4: Flow diagram of a typical digital signal processing scheme for MST radar

2.6.4.1 Ranging: The sampled digital signals are arranged as a function of trip-around time from transmission and reception, which is generally called ranging.

For monostatic pulse radar, the distance R, or range, to the scatterer from the radar is

$$R = ct_R / 2 \tag{2.3}$$

Where, t_R is a time interval between the pulse transmission and detection, and c is the speed of light (3×10^8 m/s). The denominator 2 appears in (2.3), because t_R corresponding to a round trip time of propagation for the distance R.

Figure (2.5) schematically shows a time-height chart between the range and the time interval from transmission to reception of a radar echo. An interval of successive pulse transmissions t_{IPP} is called an inter-pulse-period (IPP), and a corresponding frequency is called a pulse-repetition-frequency (PRF). Normally MST radars are operated with uniform IPP, which is, for an example, set equal to 1 *m sec* in Fig (2.5).

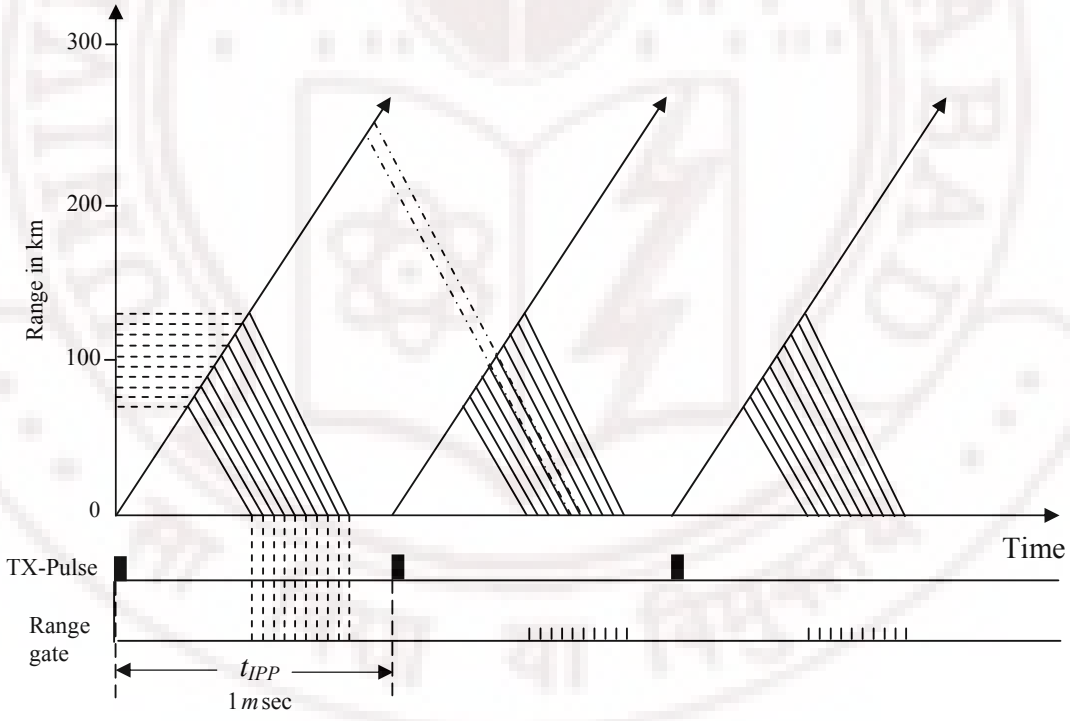

Figure 2. 5: A time height chart for MST radar observations when t_{IPP} is 1 *msec*. Thick and thin solid lines corresponding to propagation of transmitted and scattered radio wave respectively. The received signal is sampled for 10 times with equally spaced range gates as indicated by a dash line. A dot line shows a second -around echo due to ionospheric scattering.

IPP should be long enough so that after a pulse is transmitted by radar, before the transmission of the next pulse, the radar receives echoes from all the ranges. Therefore the IPP is determined by the longest range at which targets are expected. If the IPP is too short, echo signals from some targets might arrive after the transmission of the next pulse as indicated by a dot-dash line in Fig (2.5). This ambiguity in the ranging is called a range aliasing. The signals that arrive after the transmission of the next pulse are generally called second-time-around (or multiple-time-around) echoes. The range $ct_{IPP}/2$ is also called the maximum unambiguous range, beyond which targets appear as second-time-around echoes.

2.6.4.2 Decoding: The received signal may include phase modulation due to a pulse compression technique, which has to be decoded after digitization. The decoding of the signal is essential to get back the original signal from its coded nature. This is nothing but a correlation operation on received signal with its original coded waveform used for transmitting the signal. This essentially would not result in any process gain.

2.6.4.3 Coherent integration: The detected quadrature signals are coherently integrated for many pulse returns which lead to an improvement in the SNR. When M returns in time domain are averaged, SNR is enhanced by a factor of M [John, 2002]. The coherent integration is made possible because of the over sampling of the Doppler signal resulting from the high PRF relative to the Doppler frequency. Since the integration is a linear operation it can also be performed before any decoding is carried out of the phase-coded pulse returns [Woodman et al., 1980].

2.6.4.4 Spectral Analysis: The decoded signal for any range gate represented by the complex time series Z_k (range index is suppressed) is subjected to Discrete Fourier Transform (DFT) to obtain the frequency spectrum of the signal. The coefficients of the n^{th} harmonic component A_n (n = 0 to K-1) is given by

$$A_n = (1/K)\sum_{k=0}^{K-1} Z_k W^{kn} = (1/K)\left[\sum_{k=0}^{K-1} X_k W^{kn} + j\sum_{k=0}^{K-1} Y_k W^{kn}\right] = a_n + jb_n \qquad (2.4)$$

Where, $$W = \exp\left[-j2\pi T_i / T_s\right] = \exp(-j2\pi / K) \qquad (2.5)$$

The DFT computation is carried out usually by means of a Fast Fourier Transform (FFT) algorithm for the significant computational advantage that it offers [Brigham, 1988]. From the DFT coefficients, the power spectrum can be estimated as:

$$P_n = (1/K)(A_n A_n^*) = (1/K)(a_n^2 + b_n^2) \tag{2.6}$$

2.6.4.5 Incoherent integration: The power spectrum computed by above Eq. (2.6) is usually quite noisy and several estimates of it need to be averaged to reduce the noise and thereby improve the signal detectability. This process is known as Incoherent integration. When *M* spectra are averaged, the standard deviation of the noise spectral density is reduced and the detectability is enhanced by a factor of √M [John, 2002].

2.6.4.6 Spectrum cleaning: This step is optional in signal processing. Due to various reasons the radar echoes may get corrupted by ground clutter, system bias, interference, image formation etc. The data is to be cleaned (Clutter/DC, spikes/glitches removal) from these problems before going for analysis.

2.6.4.7 Noise level estimation: The observed Doppler spectra are invariably contaminated by noise. It is obviously practical importance to know the spectral power density below which the spectrum is dominated by the noise rather than by the signal received from the atmosphere target. We shall refer to this spectral power density as the noise threshold. Before calculating the moments the noise platform must be removed from the spectra as far as possible. Since the noise level is not expected to vary considerably within an experimental period, it is sufficient to take measurements once in a while.

There are many methods adopted to find out the noise level estimation basically all methods are statistical approximation to the near values. The method implemented here is based on the variance decided by a threshold criterion. The noise level threshold shall be estimated to the maximum level L, such that the set of spectral points below the level S, nearly satisfies the criterion,

$$\frac{\text{variance(S)}}{\text{mean(S)}} \le 1 \quad \textit{over number of spectra averaged} \tag{2.7}$$

2.6.4.8 Moments estimation: The extraction of lower order spectral moments (zeroth, first and second order moments) is the key task of signal processing for finding out the

various atmospheric and turbulence parameters in the region of radar sounding. The computation of moments will be accurate if the spectrum is free from noise, clutter and other interferences.

The low order spectral moments are computed from the averaged power spectrum which provides the total signal power P_r, the mean Doppler frequency $\overline{f_D}$ and the spectral width f_W^2. The moments are expressed as [Woodman, 1985],

$$P_r = m_0 = \int P(f)df \tag{2.8}$$

$$\overline{f_D} = m_1 = (1/m_0)\int fP(f)df \tag{2.9}$$

$$f_W^2 = m_2 = (1/m_0)\int \left(f - \overline{f_D}\right)^2 P(f)df \tag{2.10}$$

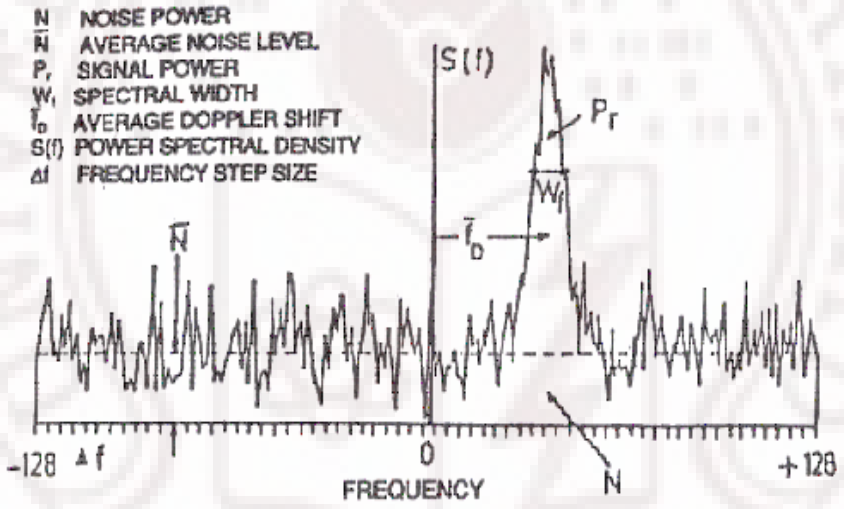

Figure 2. 6: Typical power spectrum showing measurement parameters [Jain and Narayana Rao, 1995].

Figure (2.6) shows typical power spectrum showing measurement parameters. In practice, the moments are estimated by numerical integration using the discrete power spectrum P_n of finite extent given by Eq. (2.6). In case the spectrum is Gaussian, which seems to be the case mostly [Anandan et al., 2005] the three moments convey all the information that one can obtain from the spectrum. They are the measure of three important physical properties of the medium: turbulence intensity, mean radial velocity and velocity dispersion.

2.6.4.9 UVW computation:

Calculation of radial velocities: For representing the observation results in physical parameters, the Doppler frequency and range bin have to be expressed in terms of corresponding radial velocity and vertical height.

$$\text{Velocity} \quad V = \frac{c * f_D}{2 * f_C} \quad or \quad \frac{f_D * \lambda}{2} \; m/\sec \tag{2.11}$$

$$\text{Height} \quad \mathrm{H} = \frac{\mathrm{c} * t_R * \cos\theta}{2} \tag{2.12}$$

Where, c = Velocity of light

f_D = Doppler frequency

f_C = Carrier frequency

λ = Carrier wavelength

θ = Beam tilt angle

t_R = Range time delay

Computation of wind velocity vectors: After computing the radial velocity in for different beam positions, the absolute velocity (UVW) can be calculated. To compute UVW, at least three non-planar beam radial velocities are required (East, North and Zenith or West, South and Zenith).

Line of sight component of the wind vector $V\,(V_x, V_y, V_Z)$ is

$$V_d = V \cdot \mathrm{i} = V_X \cos\theta_X + V_Y \cos\theta_Y + V_Z \cos\theta_Z \tag{2.13}$$

Where, **i** is the unit vector along the radar beam and θ_X, θ_Y, and θ_Z are the angles that the radar beam makes with the X, Y and Z axes, respectively. If V_d is measured at three radar beam positions which do not constitute a plane, the velocity vector can be determined from

$$\begin{bmatrix} V_X \\ V_Y \\ V_Z \end{bmatrix} = \begin{bmatrix} \cos\theta_{X1} & \cos\theta_{Y1} & \cos\theta_{Z1} \\ \cos\theta_{X2} & \cos\theta_{Y2} & \cos\theta_{Z2} \\ \cos\theta_{X3} & \cos\theta_{Y3} & \cos\theta_{Z3} \end{bmatrix}^{-1} \begin{bmatrix} V_{d1} \\ V_{d2} \\ V_{d3} \end{bmatrix} \tag{2.14}$$

On solving this Eq. (2.14) we can derive V_x, V_y and Vz, which are corresponding to U (Zonal), V (Meridonal) and W (Vertical) components of velocity. When observations are

made at more than three beam positions, the velocity V can be determined in a least squares manner by minimizing the residual [Sato, 1989].

2.7 Typical Indian MST Radar experimental Doppler profiles

Figure (2.7) shows a typical power spectra in five beam directions (East, West, Zenith, North and South), which are obtained using Indian MST radar system using 16 μs coded pulses with a 1 μs baud, providing height resolution of 150 m. The signal can be seen up to about 12 km on oblique beams, and beyond Tropopause level on the Zenith beam (although not continuous in the range) with four incoherent integrations. The vertical component of the wind velocity is quite small compared to horizontal components. It can be observed that the Doppler traces for oblique beams of East and West as well as North and South would be almost mirror images.

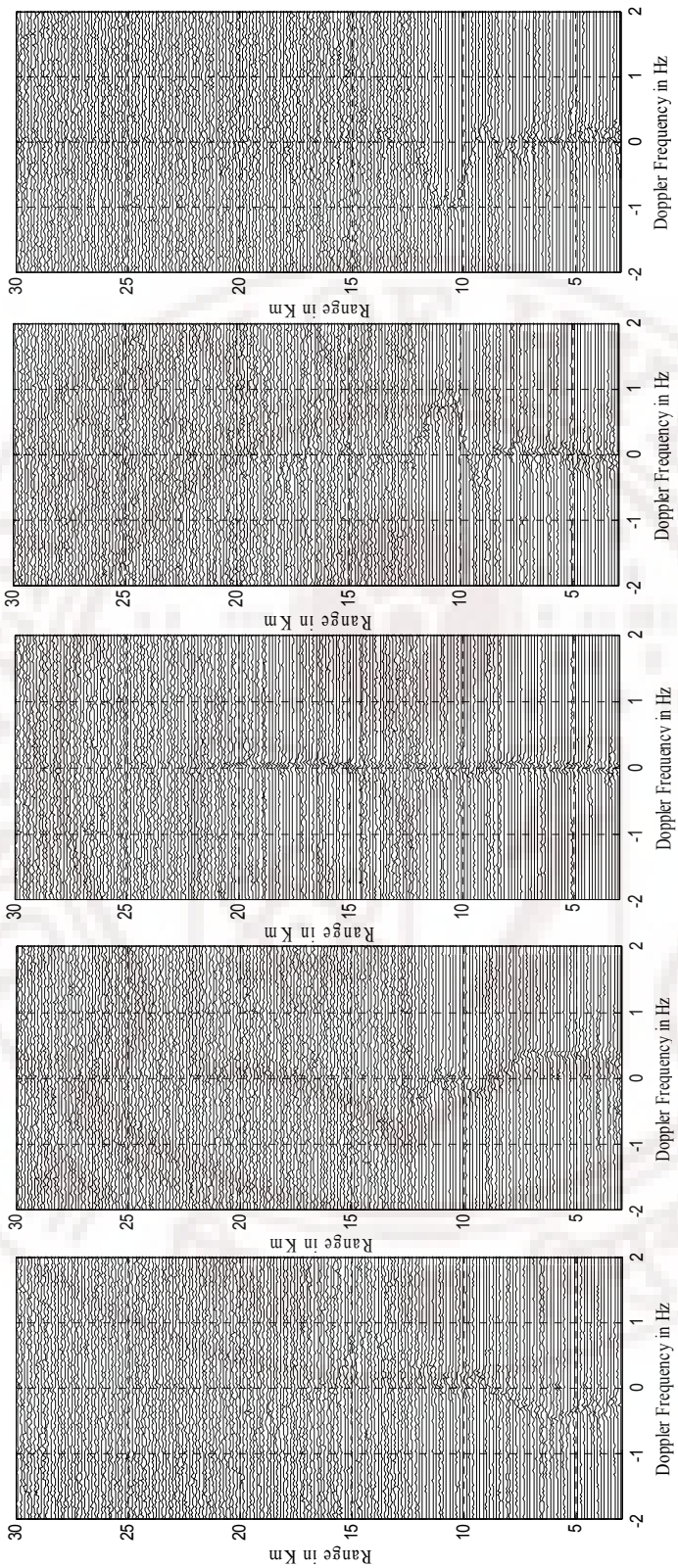

Figure 2.7: A Doppler spectra taken on a typical five beam scan in ST mode operation on December 14, 2004 at 14:35:57 IST. The panels from left to right correspond to East and 10^0 West 10^0, Zenith, North 10^0 and South 10^0 beams. The radar parameters are pulse width, 16 µsec; t_{IPP}, 1 *msec*; number of range bins, 250; coherent integrations, 64; FFT points, 512; FFT points, 512; and incoherent integrations, 1

2.8 Indian MST radar system specifications

System:

Location	:	Gadanki (11.5^0N, 79.2^0E)
Operating frequency	:	53 MHz
Peak Power Aperture Product	:	3 x 10^{10} Wm2
Height range	:	5-100 Km
Range Resolution	:	150 m - 4.8 km
Angle	:	3^0 (beam width)
Waveform	:	Selectable pulse width & PRF's (Including pulse compression)
Signal processing	:	Real time Digital (FFT based)

Subsystems

Antenna	:	Phased array with 1024 (32 X 32) crossed Yagi elements (36 dB nominal)
Beam width	:	3^0
Beam position	:	Zenith, $\pm 20^0$ % off-Zenith in EW & NS directions
Side lobe	:	-20 dB
Size	:	130 m x 130 m
Transmitter	:	Coherent: modulator with variable pulse width & PRF
Peak power	:	2.5 MW
Duty ratio	:	2.5%
Pulse width	:	selectable 1-32 μs
Receiver	:	2 channel I & Q coherent
Overall gain	:	110 dB
Dynamic range	:	70 dB
Data acquisition & signal processing	:	Real time computer controlled
No. of range gates	:	Up to 256-512 (Design goal)
Velocity resolution	:	0.1 m/sec
No. of coherent integrations	:	1-512
Max. No. of FFT points	:	64-2048
Data type	:	Raw data/Spectral Data

2.9 SNR issues and present detection possibilities

In general MST radar signal is a weak signal as they are generated due to the weak scattering at refractive index variations in the atmosphere. And as the range increases SNR (ratio of signal power to the noise power) decreases. It is estimated that the signal strength drops typically by about 2 dB per kilometer [Anandan et al., 2005] and the signal is buried in noise beyond the above range (when the SNR is below -10dB).

Hence the range up to which discernable clear-air Doppler echo signal can be observed in MST radar data is limited to 12-14 km, when only standard signal averaging and filtering techniques are used [Anandan et al., 2005] despite considerable improvements in radar design and transmitted power. Different averaging techniques were employed [Fischler & Boltes, 1981, May & Strauch, 1989 and Wilfong et al., 1993] to extract signals to improve SNR and statistical averaging techniques were used to eliminate contamination from ground clutter and fliers [Merritt, 1995].

In conventional MST radar signal processing, signal is processed by tracing the prominent spectral peak with highest amplitude in each range bin. This technique may be satisfactory for processing lower altitude ranges where SNR is quite high. But at higher altitudes where SNR is low, the algorithm may pickup false spectral peaks. In addition, the presence of electromagnetic interference or outliers, the reliable detection of the signal is still difficult. An adaptive tracking signal processing algorithm is developed to tackle these problems with better performance.

2.9.1 Adaptive tracking signal processing: Here, in each range bin, Doppler echo is identified based on information provided by previous range bins. Different adaptive techniques [Anandan et al., 2005, Clothiaux et al., 1994, Goodrich et al., 2002] and Morse et al., 2002] were used to trace the signals to higher range (up to 16-22 km). Similarly higher order spectral estimation technique was used to account for non-Gaussian nature of the Doppler echoes [Anandan et al., 2001]. All these methods have yielded reliable detection of the Doppler echoes to a maximum range of about 22 km under favorable conditions.

2.10 Aim of this thesis

The main goal of this thesis is to show the denoising algorithms based on Discrete Wavelet Transform that can be applied successfully to MST radar signals to improve the SNR of Doppler spectra with a view to increase the height coverage and improve the accuracy of the parameters extracted from the spectra.

Chapter 3

Wavelet Designing and Denoising

As described in the Chapter 1 the wavelet transformation will provide compact representation of the signal under suitable conditions. That means most of the energy of the signal gets concentrated into few wavelet coefficients resulting in a sparse representation of the signal. Of course the representation is sparse only if the functional form of the signal is such that few basis functions are sufficient to synthesize the signal. In the extreme case where the signal has exactly the same functional form as the basis function one coefficient (at appropriate scale and shift) is sufficient to represent the signal (similar to sinusoidal signals having delta representation in the frequency domain). This feature of wavelet decomposition can be used to separate useful signal from the noise and selectively remove the noise.

The key for the effectiveness of wavelet decomposition based denoising, therefore, is in the ability to find a wavelet basis function that has a functional form close to that of the signal of interest. Most of this cases one of the known wavelets is selected for this purpose. In the case of atmospheric radars, standard wavelet such as Daubechies was used to analyze wind disturbances such as gravity waves [Shimomai et al., 1996, Jordon et al., 1997 and Boisse et al., 1999] and to remove ground and intermittent clutters, such as due to airplane echoes in the atmospheric data [Lehmann V and Teschke, 2001] uses Daubechies 2 wavelet. However it is possible to improve the effectiveness of the denoising process if a better wavelet is designed. Therefore a wavelet suitable for clear-air echo signals of the MST radar is designed in this work. This chapter presents the details of the wavelet designing methodologies and denoising Techniques. First part of this chapter deals with criteria for selection of wavelet for an application, design aspects and reviews of existing wavelet designing methods, where as second part introduces the denoising technique based on wavelet thresholding. It also provides details about standard threshold selection rules such as Adaptive, Universal, Heuristic and Minimax threshold selection rules and different thresholding methods (hard and soft).

3.1 Motivation for Designing Wavelet

One of the advantages of the wavelet transform is the basis function is not completely fixed as in the case of other transforms such as Fourier and Laplace Transform. Thus the form of the basis function can be chosen, of course while satisfying the requirements of a basis function of wavelet, in such a fashion that it resembles the functional form of the signal of interest. Then it provides a sparse representation of the signal, wherein the entire energy in the signal is within few wavelet coefficients, providing good signal to noise separation.

The application of wavelet analysis in radar systems has become an active research area. In [Elsehely and Sobhy, 1999] Wavelet analysis is used to detect radar pulse edges. Wavelet denoising technique was previously used in electromagnetic waves radar [Ehara et al., 1994 and Elsehely and Sobhy, 2000]. The noise is removed by thresholding the wavelet transform coefficients of the received RF radar pulses. In the wideband radars, delay and scale variation have been computed by wavelet transforms [Peng et al., 1996], [Jiang and Zhang, 2001] and in the ad-hoc detection of radar targets, wavelet based denoising has been employed [Liu et al., 2001, Guohuo and Siliang, 2003 and Saidi, 2003]. This technique was also used for Wind Profiler signal processing for removing ground and intermittent clutters (due to air-plane echoes) [Lehmann and Teschke, 2001] using standard wavelet Daubechies 2.

In the previous work standard wavelets (Daubechies) were used. These wavelets may not adequate; however it is possible to improve previous work results if a better wavelet is designed. Therefore instead of using standard wavelets, wavelet suitable for MST radar clear-air echo is proposed to design. Therefore the first phase of the work reported in this thesis pertains to design a basis function suitable for the MST radar clear-air echo. It can be envisaged to extend this work further to separate clear air echoes from those of precipitation, in which case the wavelets presently being used may not be adequate.

3.2 Wavelet design aspects

There are few important aspects of wavelets to take into account (in decreasing order of importance) while designing wavelet:

1. Perfect reconstruction
2. Compact support

3. Vanishing moments in the wavelets,
4. Smoothness of the wavelets.
5. Symmetry/Regularity

1. Perfect reconstruction: When doing a transform in order to get better representation of a signal, it should be ensured that the signal can be reconstructed with minimal artifacts from its original representation. Otherwise the representation may be completely or partly meaningless. If the filters (low pass and high pass) used for wavelet analysis are not ideal, then perfect reconstruction can't be achieved. Although it is not possible to realize ideal filters, one should design filters close to ideal filters to achieve perfect reconstruction

2. Compact support: A function is said to be compact support if it is zero outside the compact set i.e. $\psi(x) = 0$ if $|x| > M$ for some M. This property is useful because it limits the range of integration. Most compactly supported wavelets are designed to have a rapid fall-off, so Examples: Daubechies, Symlets, Coiflets, etc. Compact support allows

a. Reduced computation complexity
b. Better time resolution, but
c. Poorer frequency resolution

3. Vanishing moments: Vanishing moments are important because if we use a wavelet with enough number of vanishing moments to analyze a polynomial then all detail coefficients will be zero hence will exhibit excellent compression ratios [Burrus et al., 1998 and Daubechies, 1992].

If we expand the wavelet transform equation (Eq.1.4) into the Taylor series at $t = 0$ until order n (let $b = 0$ for simplicity)

$$W_x(a,0) = \frac{1}{\sqrt{a}}\left[\sum_{P=0}^{n} f^{P}(0)\int \frac{t^{p}}{p!}\psi\left(\frac{t}{a}\right)dt + O(n+1)\right] \tag{3.1}$$

Here f^p stands for the p^{th} derivative of f and $O(n+1)$ means the rest of the expansion. Now the moments of wavelet is defined as

$$m_p = \int t^p \psi(t)dt \tag{3.2}$$

Then Eq. (3.1) can be rewritten as

$$W_x(a,0) = \frac{1}{\sqrt{a}}\left[f(0)m_0 s + \frac{f^1(0)}{1!} m_1 s^2 + \frac{f^2(0)}{2!} m_2 s^3 + \ldots + \frac{f^n(0)}{n!} m_n s^{n+1} + O(s^{n+2}) \right] \quad (3.3)$$

From the admissibility condition we already have that the zeroth moment $m_0 = 0$, so that the first term in the right-hand side of Eq. (3.3) is zero. If we now manage to make the other moments up to m_n zero as well, then the wavelet transform coefficients $W_x(a, b)$ will decay as fast as s^{n+2} for a smooth signal $f(t)$. But most practical signals do not look anything like polynomials but any function can be written as a polynomial when expanded into its Taylor series. This is what makes wavelets so successful in compression. The moments do not have to be exactly zero; a small value is often good enough. In fact, the number of vanishing moments required depends heavily on the application.

4. Smoothness/Regularity: Regularity/smoothness is roughly the number of times a function can be differentiated at any given point. Regularity is closely related to the number of vanishing moments. The more is the number of vanishing moments, the smoother is the wavelet. This is important because it provides

- Numerical stability
- Better reconstruction properties
- Necessary for certain applications, such as solution of differential Equations

5. Symmetry: Symmetric or anti-symmetric wavelets give rise to linear phase filters. Orthogonal wavelets with compact support cannot be symmetric. Linear phase FIR filters can be constructed from biorthogonal wavelets. Most orthogonal wavelets also satisfy biorthogonality. However, such wavelets do NOT satisfy symmetry requirements, e.g., Daubechies wavelets

3.3 Relation between MRA filter coefficients

The DWT is usually implemented as an iterated digital filter bank tree, so the design of a wavelet transform amounts to the design of a filter bank. And in the case of orthogonal wavelet systems, knowledge of scaling filter is sufficient for design of the analysis and synthesis filters [Strang and Nguyen, 1996]. By restricting to the orthogonal

case, we need the only scaling filter coefficients to implement DWT. For a given even size FIR analysis scaling filter $h_{0A}(k)$, we have

$$\left.\begin{aligned} h_{1A}(k) &= (-1)^k h_{0A}(N-k-1) \\ h_{0S}(k) &= h_{0A}(N-1-k) \\ h_{1S}(k) &= h_{1A}(N-1-k) \end{aligned}\right\} \tag{3.4}$$

Where, $h_{1A}(k)$ is analysis wavelet filter, $h_{0s}(k)$, is synthesis scaling filter and $h_{01}(k)$, is synthesis wavelet filter.

3.4 Wavelet design methods

In recent years, several authors have developed systematic and efficient design algorithms for signal adapted filter banks. Daubechies classic technique [Daubechies, 1988] for finding orthogonal wavelet bases with compact support is often used as the default in many wavelet applications. However, the wavelets produced are independent of the signal being analyzed. Tewfik, Sinha, and Jorgenson [1992] have developed a technique for finding the optimal wavelet basis for representing a specified signal within a finite number of scales. Gopinath, Odegard, and Burrus [1994] extended the results of Tewfik et al., by assuming band limited signals and finding the optimal m-band wavelet basis for representing a desired signal.

The wavelet design techniques developed by Mallat and Zheng [1993] and Chen and Donoho [1994], build non orthonormal wavelet bases from a library of existing wavelets in such a way that some error cost function is minimized. These techniques are constrained by the library of functions used and do not satisfy the need for optimal correlation in both scale and translation. Sweldens [1996] developed the lifting scheme for constructing biorthogonal wavelets. Aldroubi and Unser [1993] match a wavelet basis to a desired signal by either projecting the desired signal onto an existing wavelet basis. Few of the design methods are briefly described below.

3.4.1 Wavelet design by using Gröbner bases: [Jerome and Selesnick, 2004]: This method is used to construct wavelet filters for which the usual spectral factorization approach (used for example to construct the well known Daubechies filters) is not applicable to many of the other wavelet design problems where additional constraints are

imposed. Here design equations can be written as a multivariate polynomial system of equation. These equations were solved by using Gröbner bases.

3.4.2 Lifting based Wavelet Design: [Sweldens, 1996] The Lifting scheme is a new method for constructing biorthogonal wavelets. The main difference with conventional constructions is that is doesn't rely on the Fourier transform. This way the lifting can be used to construct second generation wavelets, wavelets which are not necessarily translates and dilates of one function.

The basic idea behind the lifting scheme is very simple. It starts with a trivial wavelet, the "Lazy wavelet"; a function which essentially doesn't do a thing, but which has the formal properties of a wavelet. The lifting scheme then gradually builds a new wavelet, with improved properties, by adding in new basis functions. This is the inspiration behind the name "lifting scheme".

Lifting scheme has following advantages:

- It allows a faster implementation of a wavelet transform
- The lifting scheme allows a fully in place calculation of the wavelet transforms i.e. no auxiliary memory is needed and the original can be used replaced with its wavelet transform.

3.4.3 Signal adaptive wavelets based on genetic algorithms: Soon-Huat [2002] proposed a method based on genetic algorithm for constructing signal adapted wavelets for the ammunition Doppler radar system. In order to implement genetic algorithm for the construction of the wavelets, the filter coefficients must be represented in some form such as trigonometric form. There are two methods for encoding the wavelet filter coefficients for the representation of the wavelet filter are given below:

- **Direct method:** The coefficients of a $2n$-tap orthogonal filter with one vanishing moment satisfy n+2 non-linear simultaneous equations as follow [Daubechies, 1988]

Equations for normalization: $$\sum_{i=0}^{2n-1} h(i) = \sqrt{2} \tag{3.5}$$

n -equations for Orthogonality: $$\sum_{i=0}^{2n-1} h(i)h(i-2k) = \delta(k) \tag{3.6}$$

Equation for zero at π in the frequency response:

$$\sum_{i=0}^{2n-1}(-1)^i h(i+1) = 0 \tag{3.7}$$

There are *n*-2 free coefficients for optimization. The problem with this method is due to non-linear nature of the simultaneous equations. It can't be guaranteed that the filter coefficients satisfy the simultaneous equations exactly. As a consequence, this may affect the properties like Orthogonality and Frequency response of the derived wavelet.

- **Trigonometry Method:** The filter coefficients satisfying equations (3.5) to (3.7) can be represented in terms of trigonometric functions Sine and Cosine. For any set of parametric angles ($\alpha_1, \alpha_2, \ldots. \alpha_k$), if sum of all the parametric angles is π/4, then the expansion/decomposed terms of cosine function Cos($\alpha_1+\alpha_2+\ldots+\alpha_k$) form the even filter coefficients ($h_0, h_2, h_4, \ldots.$,) and sine function Sin($\alpha_1+\alpha_2+\ldots+\alpha_k$) form the odd filter coefficients ($h_1, h_3, h_5, \ldots.$,) [Soon-Huat, 2002].

The advantage of using the trigonometry method to encode the wavelet filter coefficients are the dimension of the search space is reduced from 2*n* to ln(*n*)/ln(2) , thus alleviating the complexity of the optimization problem.

The search space of the parametric angles is large but finite. The genetic algorithm is used by Soon-Huat to construct the signal adapted best basis algorithm by minimizing the best basis entropy of the wavelet packet basis transform (WPBBT).

3.5 Denoising by wavelet thresholding

The problem of estimating a signal that is corrupted by additive noise has been of interest to many researchers. The problem is to recover the original signal from the noisy data. We want the recovered signal to be as close as possible to the original signal, retaining most of its important properties (e.g. smoothness). Traditional denoising schemes are based on linear methods, where the most common choice is the Wiener filtering [Proakis and Manolakis, 1996]. Recently, nonlinear method, denoising based on wavelets have become increasingly popular, due to its simplicity. One of the first reports about this approach was by Weaver et al. [1991]. A systematic theory was developed mainly by Donoho and Johnstone [1994a and 1995b]. They have shown that wavelet thresholding has near-optimal properties in the minimax sense, and guarantees better rate of convergence of noise, despite its simplicity.

Wavelet denoising attempts to remove the noise present in the signal while preserving signal characteristics, regardless of its frequency content. The general wavelet denoising procedure involves three steps:

1. Linear forward wavelet transform [Wavelet decomposition] to the noisy signal to produce noisy wavelet coefficients to the level which we can properly distinguish the signal occurrence.
2. Nonlinear thresholding by selecting appropriate threshold limit and threshold method to best remove the noises.
3. Linear inverse wavelets transform [Wavelet reconstruction] of the thresholded wavelet coefficients to obtain a denoised signal.

Figure (3.1) shows the steps involved in wavelet based denoising.

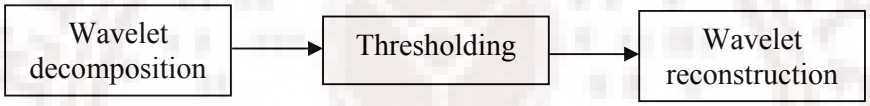

Figure 3. 1: Block diagram of Wavelet based Denoising

Forward and inverse wavelet transforms are linear operations but thresholding is non linear operation, where all the coefficients below a threshold value are set to zero as described below.

Let assume that the observed data contains the true signal $S(t)$ with additive noise $N(t)$ as functions in time t to be sampled. That is

$$X(t) = S(t) + N(t) \tag{3.8}$$

Let $w(\cdot)$ and $w^{-1}(\cdot)$ denote the forward and inverse wavelet transform operators. Let $D(\cdot, T)$ denote the denoising operator with soft/hard threshold (*vide infra*) T. We intend to wavelet denoise $X(t)$ in order to recover $\hat{S}(t)$ as an estimate of $S(t)$. Then the above mentioned three steps can be formally written as

$$\left.\begin{aligned} Y &= W(X) \\ Z &= D(Y,T) \\ \hat{S} &= W^{-1}(Z) \end{aligned}\right] \tag{3.9}$$

These three equations summarize the wavelet denoising procedure. Of course, this summary of principles does not reveal the details involving implementation of the operators W or D, or selection of the threshold T.

Wavelet denoising is quite different from smoothing; smoothing only removes the high frequencies and retains the lower ones. Whereas denoising attempts to remove whatever noise is present and retain whatever signal is present regardless of the spectral content of the noisy signal. For example, to denoise music corrupted by noise, the high frequencies of the music should not be eliminated. Instead, both the treble and the bass should be preserved. This example of denoising music offers an important application of wavelet based denoising for further investigation.

3.6 Thresholding

In general the idea of thresholding is to set all the coefficients that are below a certain threshold to zero since they are considered to contain only noise. Figure (3.2) illustrates the thresholding procedure of signal coefficients. The horizontal solid line indicates threshold level. After thresholding all the coefficients below the threshold value are removed while coefficients which fall above the threshold level are allowed.

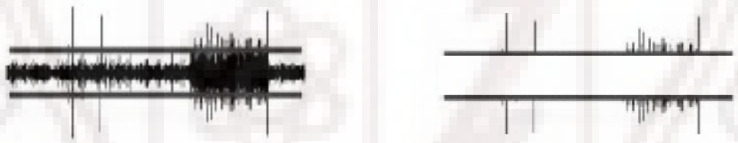

Figure 3. 2: Thresholding of coefficients (a) Before thresholding (b) After thresholding (Solid horizontal line is threshold level)

The signal $S(t)$ can be represented via a few wavelet coefficients, while the noise has wideband characteristics and spreads out on all coefficients. For example this holds true if $S(t)$ is a low pass signal, while $N(t)$ is white noise, this is the case in most of the practical signals. The thresholding procedure is then sets the small wavelet coefficients representing $N(t)$ to zero, while the large coefficients due to S(t) be slightly affected. Thus, provided the threshold T is chosen appropriately, the signal $\hat{S}(t)$ reconstructed from the manipulated wavelet coefficients will contain much less noise that S(t) does.

Figure (3.3) illustrates simple wavelet based denoising example. The original signal, top panel is before corrupting with noise where as second panel is same signal but

corrupted with random noise. Then this noisy signal is wavelet transformed using standard Symlet 8 wavelet, thresholded at level 3 using soft heuristic thresholding method (explained in following section) and inverse-transformed. The result is cleaned-up signal that still resembles the original signal. The resultant signal i.e. denoised signal is shown at the bottom panel.

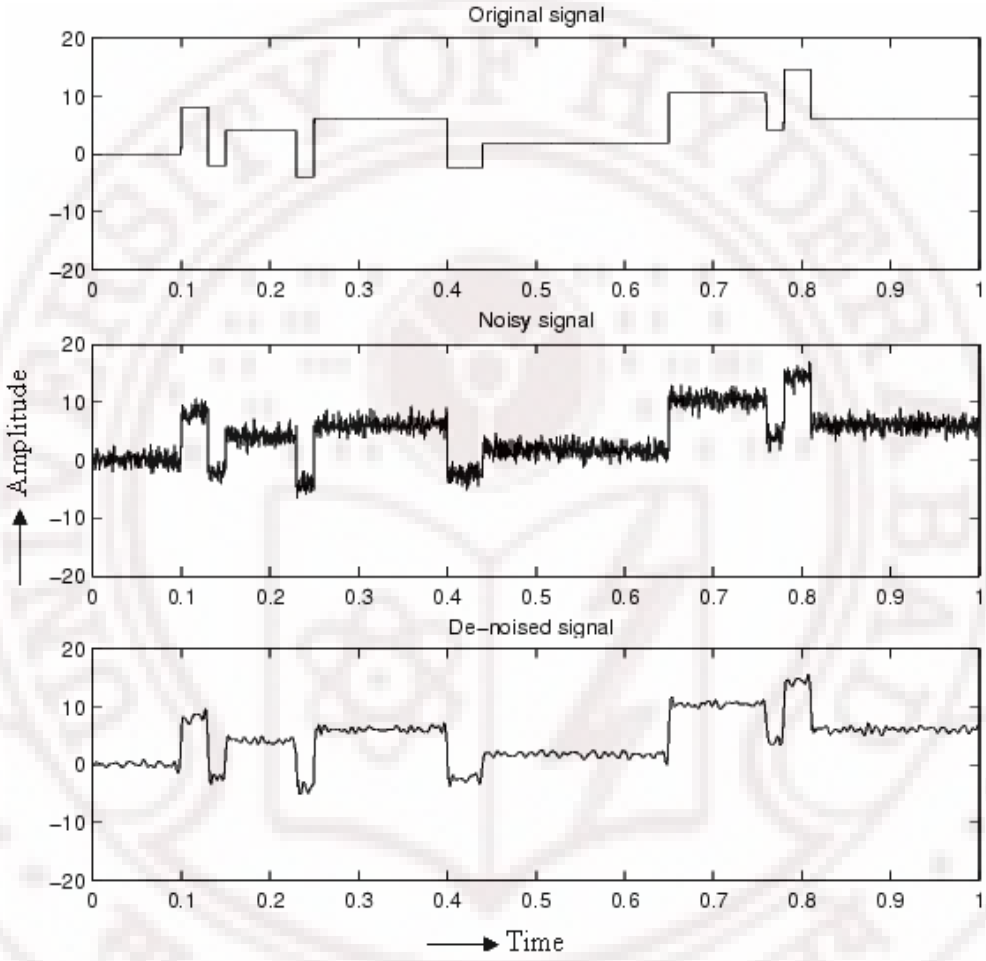

Figure 3. 3: Example of wavelet denoising [Matlab V7.0, 2006]

The efficacy of the wavelet denoising depends heavily on the choice of a thresholding parameter. In practice the problem is to choose this threshold value because the amount of noise is usually not known a priori. If threshold value is too small, the noise will not be efficiently removed. If it is too large, the signal will be distorted. However researchers have developed various techniques for choosing denoising parameters so far. There is no best universal threshold determination technique.

3.7 Threshold selection Rules

The selection of the threshold value T plays an important role in, the de-noising process. Different methods for estimating the threshold value (based on the noise variance) have been developed by Donoho and Johnstone [1994b, 1998 and Donoho, 1995a].

According to the noise model, there are four threshold selection rules [Dai-fei et al., 2000] that are as follows:

1. Threshold selection rule based on Stein's Unbiased Estimate of Risk (or Rigrsure threshold method) [Donoho, 1994b]**:** Donoho and Johnstone [2005] introduced a level dependent threshold selection scheme (unlike Universal threshold where a single threshold value is used for all levels, for each level j of the wavelet decomposition a threshold T_j will be computed and applied to the wavelet coefficients W_j at that level) based on Stein's unbiased estimate of risk (SURE) Hence this method is also called as an adaptive thresholding method.

For computing threshold value T at scale j, the squared coefficient is first computed.

$$A_k = (W_{j,k})^2 \tag{3.10}$$

Where $W_{j,k}$ is the element of the j^{th} scale coefficients in W, and sorted in ascending order. Then the cumulative total of the A_k is computed by

$$B_k = \sum_{i=1}^{k} A_i \tag{3.11}$$

Further, a vector C with the same size of the coefficient number of the scale j, n_j, is designed by

$$C_k = A_k - k \tag{3.12}$$

Thus, the first element is n_j-1 and the last element is 0. A risk value for every coefficient, R_k is then computed by

$$R_k = \frac{(n-1) + B_k + A_k C_k}{n_j} \tag{3.13}$$

The coefficient that has minimum R_k is selected as the threshold value for that scale j.

$$T = \min(\mathrm{R_k}) \tag{3.14}$$

It should be noted that the absolute value of the coefficient is used for computing threshold value.

2. Fixed or Universal or Sqtwolog form threshold selection rule: [Donoho, 1995a]**:** This rule uses a fixed threshold yielding good performance. The threshold value is proportional to *log*(*length*(*x*)). This type of threshold is defined by

$$T = \sqrt{2 \log (n)} \tag{3.15}$$

Where n is sample size. The Universal threshold is the default method and yields the largest threshold. As a result this method results in a relatively high degree of smoothness.

3. Mixed or Heursure threshold selection rule: Mixed rule is a mixture of the two previous rules. First calculate the variables A and B as in Eq. (3.16), then find which larger, then fixed form threshold is as Eq. (3.15) is used when A is less than B, else threshold selection rule based on stein's unbiased estimate of risk is adopted. A and B are defined by [Dai-fei et al., 2000]

$$\left.\begin{aligned} A &= \frac{\left(\sum_{i=1}^{n} |x_i|^2 - n\right)}{n} \\ B &= \sqrt{\frac{1}{n} \left(\frac{\log(n)}{\log(2)}\right)^3} \end{aligned}\right\} \tag{3.16}$$

4. Minimax-performance threshold selection rule: [Donoho and Johnstone, 1998]: This selection of threshold is based on the minimax principle and soft shrinkage. Here the goal is to find a good estimate $W(j,k)$ of the original signal $w(j,k)$. The predictive performance of $w(j,k)$ is measured by the risk (called the mean square error) defined by

$$MSE = \frac{1}{n} E \left\| W\text{-}w \right\|^2 \tag{3.17}$$

Where n is sample size and E is the expectation over the observed noisy signal S. Hence it has a good predictive performance. Here a fixed threshold is selected to obtain the minimum of maximum mean square error that is obtained over the worst function in a given set when compared against an ideal procedure. The threshold value is typically

smaller than the universal threshold and thus results in less smoothing. The algorithm of the threshold selection is

$$Thr = 0.3936 + 0.1829 * \frac{\log(n)}{\log(2)} \quad (3.18)$$

It can be noticed that threshold computed by Fixed and Minimax threshold value depends only on sample size (n) but not on signals where as Stein's selection rule threshold value depends both on n and signal.

3.8 Hard and Soft thresholding

There are different ways to apply the thresholds to the wavelet coefficients. The most common methods are *hard thresholding* ("keep or kill") and *soft thresholding* ("shrink or kill"). In both cases, the coefficients that are below a certain threshold are set to zero. In hard thresholding coefficients above threshold values are left unchanged where as in soft thresholding the magnitudes of the coefficients above threshold are reduced by an amount equal to the value of the threshold, which corresponds to the following equations.

Hard thresholding
$$x_H = \begin{cases} 0, & if \ |x| \le T \\ x, & if \ |x| > T \end{cases} \quad (3.19)$$

Soft thresholding
$$x_S = \begin{cases} 0, & if \ |x| \le T \\ \mathrm{sgn}(x)(|x| - t), & if \ |x| > T \end{cases} \quad (3.20)$$

Where, T is the threshold value.

Figure (3.4) shows an example of linear signal thresholding, here threshold value T is considered as 2.6. After the hard thresholding, signal is completely suppressed below 2.6 and left unchanged after 2.6 as shown in Fig (3.4b). Similarly soft thresholding suppressed the signal below 2.6 but shrank the signal towards zero above 2.6 as in Fig (3.4c).

Hard thresholding is creating discontinuities at $x = \pm T$. Soft thresholding avoids those discontinuities by shrinking the coefficients, but it can produce high attenuation of the signal, especially when the threshold values are big. For all these reasons, the suitability of one or the other method depends on each particular application.

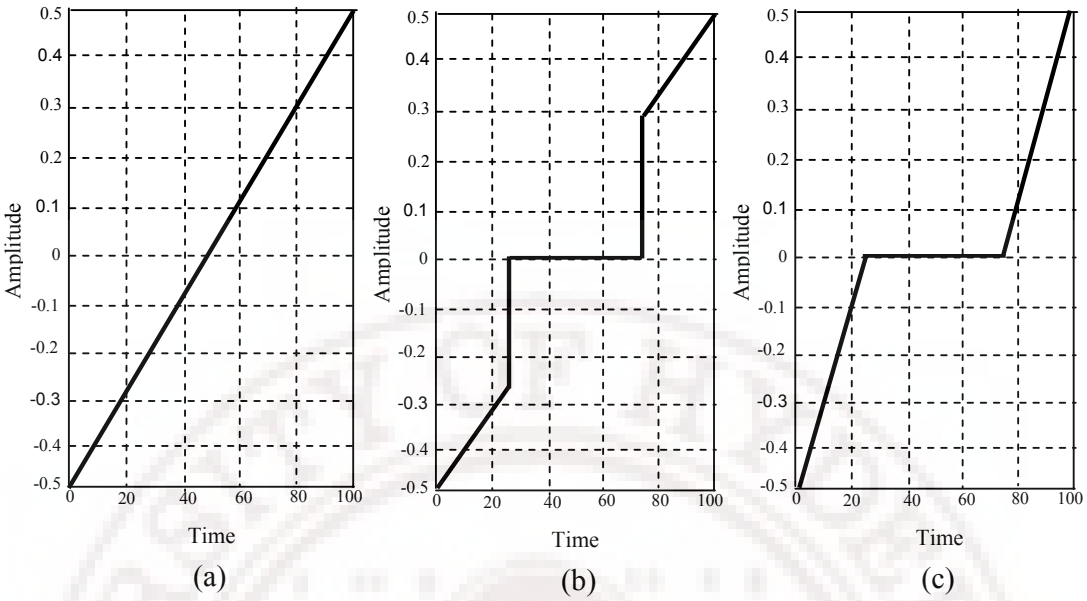

Figure 3. 4: An example of linear signal (a) Before thresholding (b) thresholded using hard-thresholding, and (c) thresholded using soft-thresholding

Chapter 4

Design of Wavelet for MST Radar clear air echo

As mentioned earlier, a wavelet suitable for the clear-air echoes of MST radar is designed in this work. Details of this design methodology and the wavelet thus obtained and its properties are described in this chapter. The MRA filter coefficients computed for this wavelet are also presented in this chapter. The wavelet designed in this work is compared with standard wavelets in its efficacy in providing sparse representation of clear air echoes. This methodology is on the same lines of one which is developed by Soon-Huat [2002] described in the Chapter 3, but instead of Genetic algorithm, Levenberg-Marquardt's algorithm is used as an optimization technique.

4.1 Selection of mother wavelet to MST radar data

As the MST radar clear-air Doppler echo is of have predominantly Gaussian distribution in off-vertical direction [Anandan et al., 2005], it can be assumed that the wavelet basis function is a shifted Gaussian in frequency domain, which can be written as

$$X(f) = \frac{1}{\sqrt{2\pi}\sigma} \exp\left(\frac{(f - f_0)^2}{2\sigma^2}\right) \tag{4.1}$$

Then chosen mother wavelet in time domain is given by the following equation.

$$x(t) = \phi(t) = \exp\left(-2\pi^2\sigma^2 t^2\right)\exp\left(j\omega_0 t\right) \tag{4.2}$$

For typical values of σ = 0.12 and f_o =0.4 Hz (which are typical values of line width and Doppler shifts of MST radar clear-air echoes) shape of chosen mother wavelet centered on 3.5 sec is shown in Fig (4.1). The corresponding frequency domain spectrum is shown in Fig (4.2).

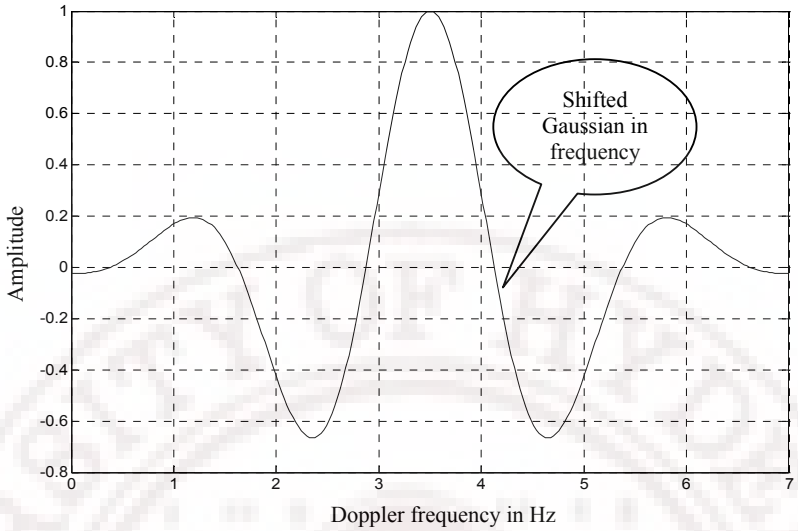

Figure 4. 1: Proposed wavelet basis suitable to MST Radar clear air echo in time domain.

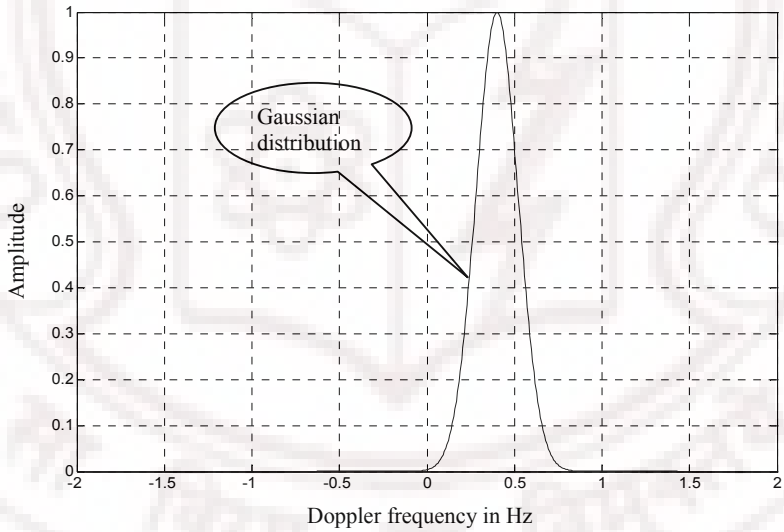

Figure 4. 2: The frequency domain representation of the proposed mother wavelet.

4.2 Computing MRA filter coefficients

A wavelet function should exhibit normalization, orthogonally properties and it should have one zero at π in the frequency response. It should be ensured that the chosen wavelet basic function and the corresponding MRA filter coefficients satisfy these properties. Then according to Soon-Huat the corresponding MRA filter coefficients can be calculated by representing the scaling filter coefficients in terms of trigonometric functions of Sine and Cosine represented by parametric angles, such that the above conditions are satisfied. As explained in following result section it was found that eight filter coefficients can represent chosen mother wavelet.

Using trigonometric encoding method [Soon and Huat, 2002] an 8-tap filter is represented by 3 parametric angles *a*, *b*, and *c* where

$$c = \frac{\pi}{4} - a - b \tag{4.3}$$

The coefficients of 8-tap low pass filter are described in terms of the above angles, by the following equations (Soon and Huat, 2002)

$$\left.\begin{aligned}
h(0) &= \cos(a) * \cos(b) * \cos(c) \\
h(1) &= \sin(a) * \cos(b) * \cos(c) \\
h(2) &= -\cos(a) * \sin(b) * \sin(c) \\
h(3) &= -\sin(a) * \sin(b) * \sin(c) \\
h(4) &= -\sin(a) * \sin(b) * \cos(c) \\
h(5) &= \cos(a) * \sin(b) * \cos(c) \\
h(6) &= -\sin(a) * \cos(b) * \sin(c) \\
h(7) &= \cos(a) * \cos(b) * \sin(c)
\end{aligned}\right\} \tag{4.4}$$

The parameters *a, b* and *c* can be obtained by solving the recursive relation between scaling function and low pass filter/scaling filter coefficients discussed in Chapter 1, Eq.(1.25) repeated below

.

$$\phi(t) = \sqrt{2}\sum_{n=0}^{N} h(n)\phi(2t-n) \tag{4.5}$$

Substituting 8-tap filter coefficients Eq. (4.4) in recursion relation Eq. (4.5), and replacing c with Eq. (4.3) we get

$$\phi(t) = \sqrt{2}\begin{pmatrix} \left(\cos(a)*\cos(b)*\cos(\pi/4 - a - b)\right)\phi(2t) \\ +\left(\sin(a)*\cos(b)*\cos(\pi/4 - a - b)\right)\phi(2t-1) \\ +\left(-\cos(a)*\sin(b)*\sin(\pi/4 - a - b)\right)\phi(2t-2) \\ +\left(-\sin(a)*\sin(b)*\sin(\pi/4 - a - b)\right)\phi(2t-3) \\ +\left(-\sin(a)*\sin(b)*\cos(\pi/4 - a - b)\right)\phi(2t-4) \\ +\left(\cos(a)*\sin(b)*\cos(\pi/4 - a - b)\right)\phi(2t-5) \\ +\left(-\sin(a)*\cos(b)*\sin(\pi/4 - a - b)\right)\phi(2t-6) \\ +\left(\cos(a)*\cos(b)*\sin(\pi/4 - a - b)\right)\phi(2t-7) \end{pmatrix} \tag{4.6}$$

Levenberg-Marquardt's (LM) algorithm, details of which are given in following section, finds the values of these parameters by optimizing (minimizing) mean square error between wavelet computed by recursion equation Eq. (4.6) and mother wavelet (Eq. (4.2)). LM optimizing algorithm needs some guess values as initial values to these parameters, then this algorithm tries to optimize mean square error of optimizing function Eq. (4.6) with respect to mother wavelet i.e. Eq. (4.2) by adjusting parameter values iteratively. This procedure is terminated when the mean square error satisfies minimum value in two successive iteration steps.

As described in Chapter 3, for the relations between low pass and high pass filter coefficients and synthesis and analysis filter coefficients for an orthogonal wavelet are given as

$$\left.\begin{aligned} h_{1A}(k) &= (-1)^k h_{0A}(N-k-1) \\ h_{0S}(k) &= h_{0A}(N-1-k) \\ h_{1S}(k) &= h_{1A}(N-1-k) \end{aligned}\right\} \tag{4.7}$$

Where, $h_{0A}(k)$ and $h_{1A}(k)$ are analysis scaling/low pass filter and wavelet/high pass filter coefficients respectively, where as $h_{0S}(k)$ and $h_{1S}(k)$ are synthesis scaling/low pass filter and wavelet/high pass filter coefficients respectively.

Therefore, as orthogonality condition is imposed while encoding filter coefficients, Eq. (4.7) can be used to calculate remaining MRA filter coefficients from analysis scaling filter coefficients.

4.3 Levenberg-Marquardt's (LM) algorithm

The LM algorithm is an iterative technique that locates a local minimum of a multivariate function that is expressed as the sum of squares of several non-linear, real-valued functions. It became a standard technique for nonlinear least-squares problems, widely adopted in various disciplines for dealing with data-fitting applications. LM can be thought of as a combination of steepest descent and the Gauss-Newton method. When the current solution is far from a local minimum, the algorithm behaves like a steepest descent method: slow, but guaranteed to converge. When the current solution is close to local minimum, it becomes Gauss-Newton method and exhibits fast convergence. Detailed analysis of LM algorithm is available in [Madsen et al., 2004, Nocedal and Wright, 1999 and Kelley, 1999]. A complete LM algorithm is shown in pseudo code below [Manolis, 2005]

Input: A vector function $f: R^m \rightarrow R^n$ with $n \geq m$,
A measurement vector $x \in R^n$ and initial parameters
Estimate $P_0 \in R^m$
Output: A vector $P^+ \in R^m$ minimizing $|| x-f(P) ||^2$.
Algorithm:
$k: = 0$; $v := 2$; $P := P_0$
$A: = J^T J$; $\epsilon_p: = x - f(P)$; $g := J^T \epsilon_p$;
Stop: = ($||g||_\infty \leq \varepsilon_1$); $\mu := T * \max_{i=1,\ldots,m}(A_{ii})$;
While (notstop) and ($k<k_{max}$)
    $k: = k+1$;
    Repeat
        Solve $(A+\mu I)\, \delta P = g$;
    If ($||\delta_P|| \leq ||P||$)
        Stop: =true;
    Else
        $P_{new}: = P + \delta_P$;
        $\rho : = (||\epsilon_p||^2 - || x-f(P_{new}) ||^2) / (\delta^T{}_P(\mu\delta_P+g))$;
    If $\rho>0$
        $P=P_{new}$;
        $A: = J^T J$; $\epsilon_p: = x-f(P)$; $g := J^T \epsilon_p$;
        Stop: = ($||g||_\infty \leq \varepsilon_1$);
        $\mu: = \mu * \max (1/3, 1-(2\rho-1)^3)$; $v: = 2 * v$;

```
        Else
            μ: = μ* v; v: = 2* v;
        End if
        End if
    Until (ρ>0) or (stop)
End while
P+=P;
```

Figure 4. 3: LM Algorithm

In above algorithm vectors and arrays appear in bold face and ^{T} is used to denote transposition. Also, $\|.\|$ and $\|.\|_{\infty}$ respectively denote the 2 and infinite norms. Let f be an assumed functional relation which maps a *parametric vector* $P \in R^m$ to an estimated *measurement vector* $\hat{X} = f(P)$, $\hat{X} \in R^m$. An initial parametric estimate P_0 and a measured vector X are provided and it is desired to find the best vector P^+ that best satisfies the functional relation f locally, i.e. minimizes the squared distance $\epsilon^T \epsilon$ with $\epsilon = X - \hat{X}$ for all P. The LM algorithm terminates when at least one of the following conditions met [Manolis, 2005]:

- The gradient's magnitude drops below a threshold ϵ_1
- The relative change in the magnitude of δ_P drops below a threshold ϵ_2
- A maximum number of iterations k_{max} is reached

4.4 Results

LM algorithm optimizes the measurement vector by adjusting the optimizing parameters. In this work recursion equation Eq. (4.5) is considered as a measurement vector ($\hat{X}$ in standard LM algorithm) because this equation can be represented in terms of parameter vector Eq. (4.6) and it is equivalent of mother wavelet Eq. (4.2), so it can be compared with mother wavelet for optimization. Appendix A shows Matlab code used in this work for LM algorithm and necessary functions for it. The main program ***waveletfitfn2para.m*** takes X and Y data (X vector in standard LM algorithm), input parameter vector (P_0 in standard LM algorithm) with some initial guess values and it calls the ***lmfit.m*** program which is the actual optimizing program. It can allow maximum of three functions for optimization. In this work Y data is the amplitude of mother wavelet with respect to time X data and two functions, real and imaginary parts of recursion relation (RecWaveletreal.m and ImagWaveletimag.m) are used as optimizing functions.

These two functions are represented in terms of parameter vector (or angles). The LM algorithm computes real and imaginary parts of a wavelet using recursion relation for initial guess values of given parameter vector, and then calculates mean square error between this wavelet and mother wavelet (X and Y data) i.e. $X - \hat{X}$ in standard LM algorithm. If this mean square error doesn't satisfy minimum allowed value i.e. 0.0001, it adjusts parameter vector (*a, b, c,...*) and this process is continued. LM algorithm terminates when the mean square error satisfies minimum value in two successive iteration steps. In this work various filters, 4- tap filter with 2 parameter vector, 8-tap with 3 parameter vector, 16- tap filter with 4 parameter vector and 32- tap filter with 5 parameter vector and with different sets of initial values were studied. The filter type and initial guess parameter vector, which result desired frequency response of the filter coefficients derived using these values is selected as a best filter type and initial guess parameter vector. After extensive study it was found that 8-tap filter represented with 3 parameter vector Eq. (4.4) and initial guessed parameter vector P = [π/4, π /4], corresponding parameter vector values (*a*=1.0404, and *b*=1.6215) resulted as desired frequency response as shown is Fig (4.4).

Substituting *a* and *b* in equation (4.3), we get third parameter *c*=-1.8766. Then scaling filter coefficients $h_{0A}(k)$ are computed with these parametric angles using Eq. (4.4) and remaining MRA filter coefficients were computed from Eq. (4.6). Table (4.1) shows MRA filter coefficients of a chosen wavelet to MST radar clear air echo. It can be noticed that the sum of low pass coefficients is √2 and high pass coefficients is zero as required by Eq. (1.55).

Table 4. 1: MRA filter coefficients of the designed wavelet

Analysis Filters		Synthesis Filters	
Low-pass filter Coefficients $h_{0A}(k)$	High-pass filter coefficients $h_{1A}(k)$	Low-pass filter coefficients $h_{0S}(k)$	High-pass filter coefficients $h_{1S}(k)$
0.0077	-0.0245	0.0245	0.0077
0.0132	-0.0417	-0.0417	-0.0132
0.4818	0.1521	-0.1521	0.4818
0.8216	0.2593	0.2593	-0.8216
0.2593	-0.8216	0.8216	0.2593
-0.1521	0.4818	0.4818	0.1521
-0.0417	-0.0132	0.0132	-0.0417
0.0245	0.0077	0.0077	-0.0245

4.5 Frequency response of MRA filter coefficients

One immediate factor to be examined is whether the filters corresponding to the designed wavelet posses the right frequency response. The frequency response of computed MRA filter coefficients derived for the designed wavelet as explained above is shown in Fig (4.4). Here solid line indicates low pass filter where as dot dash line indicates high pass filter. The frequency response of a standard wavelet (Daubechies wavelet db10) is shown in Fig. (4.5). As can be seen from these plots the frequency response of these filter coefficients were found to be as desired i.e. say, compares with that of db10 quite well, though the roll off of the designed wavelets are not as steep as in the case of db10. However this comparatively extended roll of the designed wavelets did not pose any difficulty in the envisaged application, *viz.,* the denoising of the MSR radar signals. In any case, it should be possible to make the cutoff much sharper by increasing the length of the filter coefficients, which is not attempted in this work.

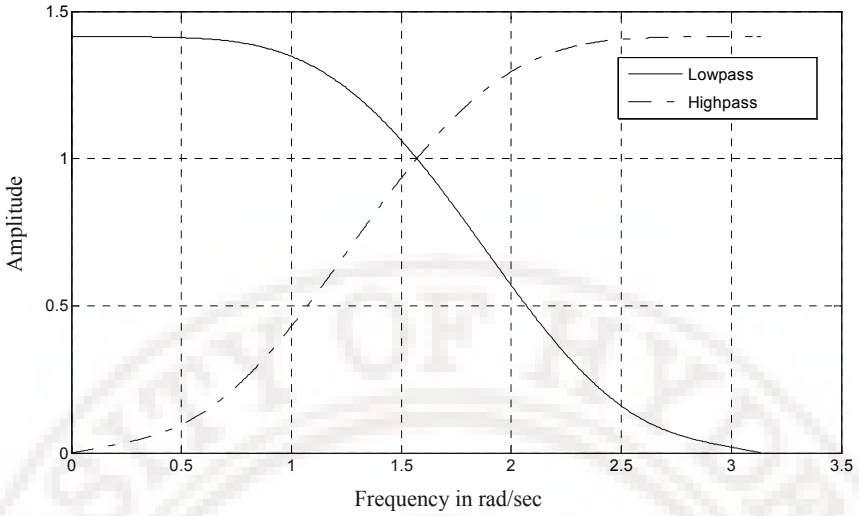

Figure 4. 4: Frequency response of a designed wavelet

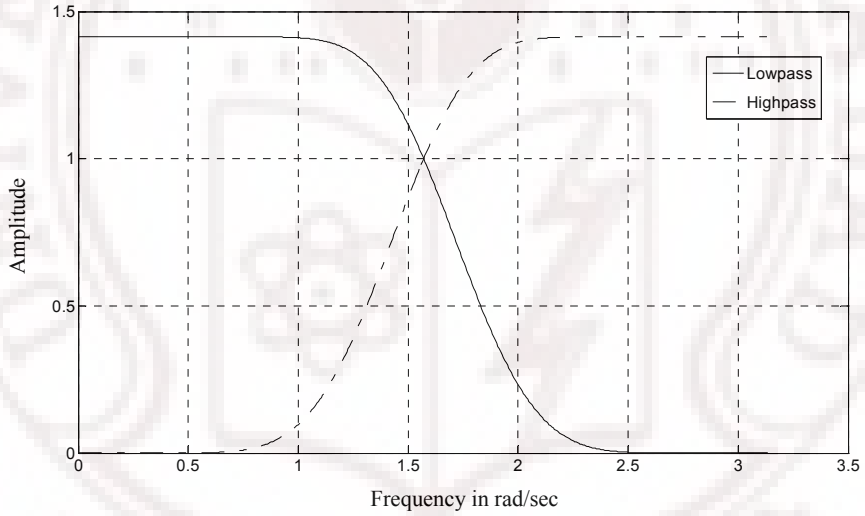

Figure 4. 5: Frequency response of a standard Daubechies db10 wavelet

4.6 Reconstruction with MRA filters coefficients

The next check on the designed wavelet is to verify its ability to decompose and reconstruct MST radar signal perfectly with minimal artifacts. This is verified in the following way. First MST radar signal is decomposed using newly designed wavelet and then reconstructed back by performing inverse wavelet transform using same wavelet. Fig (4.6) illustrates the perfect reconstruction of designed wavelet. The signal in Fig (4.6a) is

the experimental MST radar signal before applying wavelet analysis; where as signals in figures (4.6b and 4.6c) are after wavelet analysis (wavelet decomposition and reconstruction) using designed wavelet and standard wavelet Daubechies db10 respectively. It can be observed that the signal is reconstructed without any observable artifacts similar to standard wavelet.

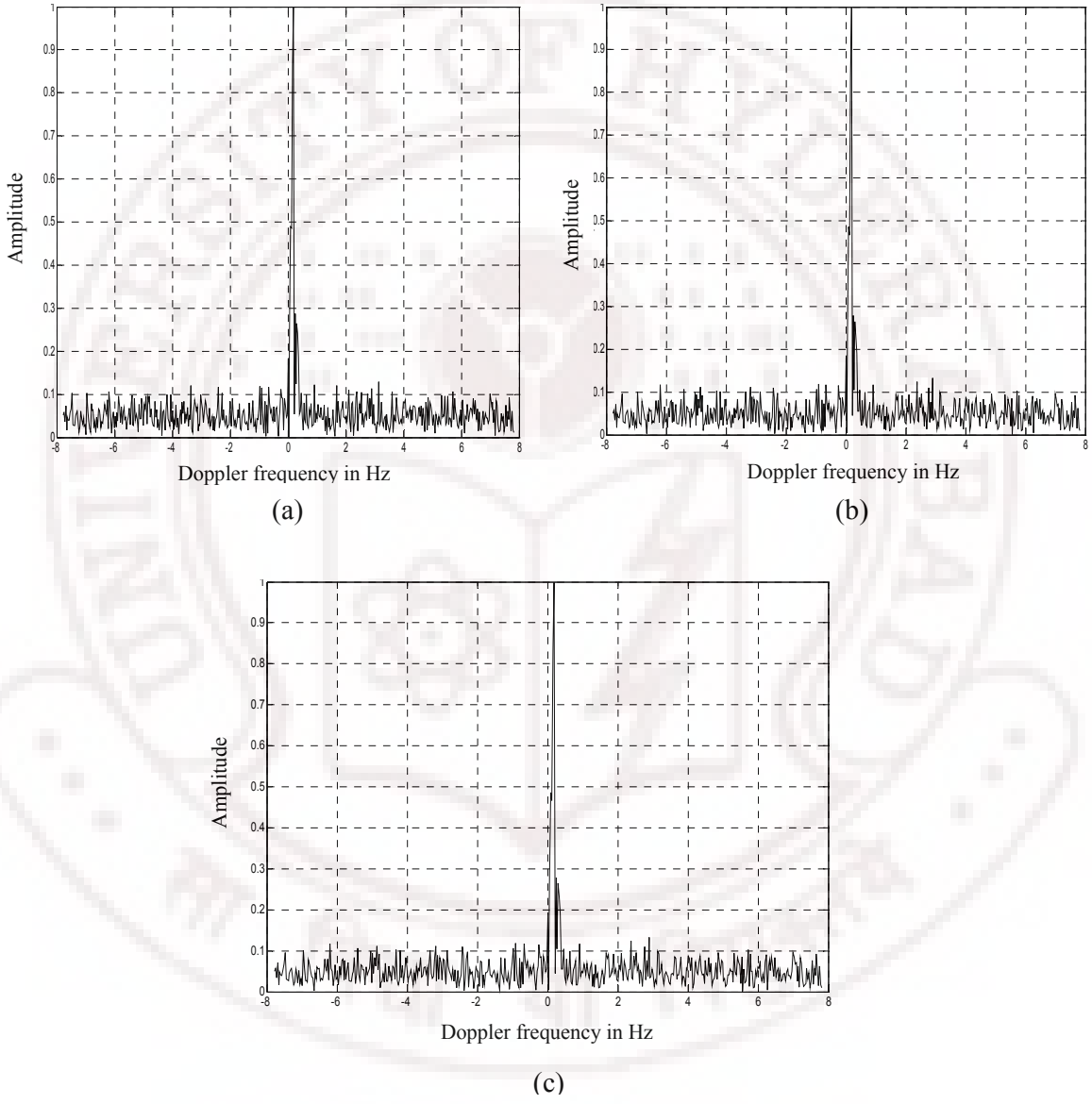

Figure 4. 6: Experimental MST radar data (a) Original data (before wavelet analysis) (b) and (c) After wavelet decomposition and reconstruction using newly designed wavelet and standard Daubechies db10 wavelet respectively.

4.7 Conclusions

The wavelet suitable for MST radar clear-air Doppler echo is designed. The corresponding MRA filter coefficients were computed. The frequency response of computed filter coefficients satisfies the desired frequency response as in the case of standard Daubechies wavelet (db10).

Chapter 5

Wavelet Denoising Techniques on MST radar Data

The aim of the work reported in this thesis is to develop wavelet based denoising technique for MST radar data. It was proposed to achieve this by first designing a wavelet suitable for clear-air echoes and then optimizing the denoising technique to suite MST radar data. While the details of the wavelet design for MST radar data is presented in the Chapter 4, the optimization of denoising technique is presented in this chapter. This optimization involves determining adequate levels of wavelet decomposition following by determining the best suited threshold levels for each of these sub-bands. Since it is expected that the noise levels essentially remain the same for all ranges except at very low ranges where ground clutter is expected to result in additional noise [Anandan et al., 2005]. A set of threshold levels should be adequate to denoise all the data collected during a given experimental conditions.

This optimization process was performed utilizing the experimental data. Both moderately strong signals as well as noisy signals were used in each of the above two cases.

5.1 Number of decomposition levels for MST radar data

In principle a given data can be decomposed in any number of levels using wavelet transform, the theoretical limit arising from the number of data points present in the data (as the data are decimated by a factor 2 after every decomposition). At every level, the filtering and sub sampling will result in half the number of samples (and hence half the time resolution) and half the frequency band spanned (and hence doubles the frequency resolution). The optimal decomposition levels suitable for MST radar data was determined by trial and error method. The data were decomposed to different decomposition levels (2, 3, 4, 5 and 6) using designed wavelet. In each case both approximation and detailed coefficients were denoised with suitable threshold values computed as described in the next section. The thresholded signals were reconstructing

back (by performing inverse wavelet transform) and signal to noise ration was computed. The MST radar signal collected at height 7.5 km, 20^0 off-Zenith North directions is shown in Fig (5.1). It is a strong signal and we can identify Doppler echo position on this signal. It can be observed that Doppler echo is at 0.18 Hz. The maximum frequency of this signal is 7.8 Hz and the computed SNR value is 0.87 dB

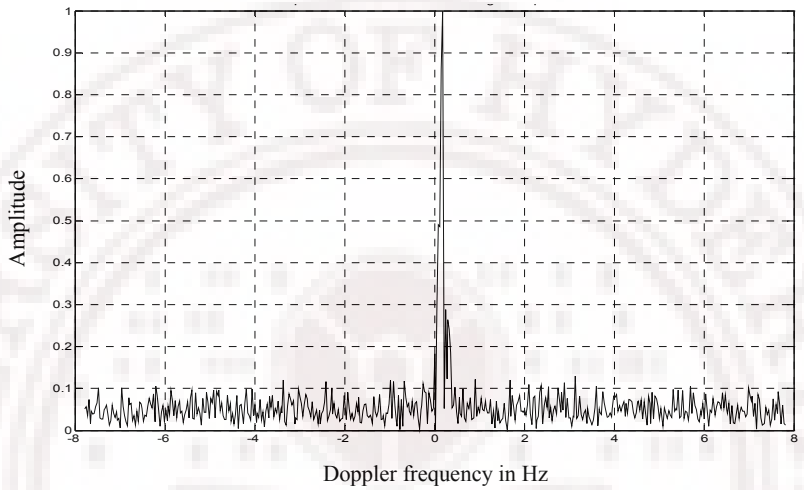

Figure 5.1: Experimental MST radar echo

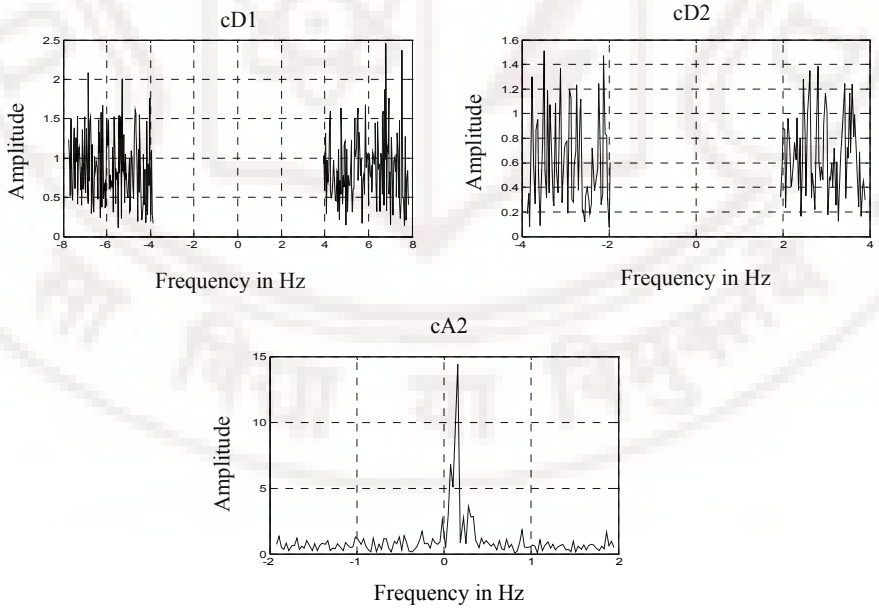

Figure 5.2a: Two level wavelet decomposition sub-bands (cD1, cD2 and cA2)

Figure (5.2a) shows the result of wavelet decomposed into two levels, with the resulting bands (approximation cA2, detailed cD1 and cD2). Approximation coefficients cA2 span the frequencies 0-1.95 Hz where as detailed coefficients cD2 and cD1 span the frequencies 1.95-3.9 Hz and 3.9-7.8 Hz and respectively. Since Doppler echo of original signal is at 0.18 Hz, Doppler echo should appear in cA2 band. Then these coefficients were thresholded with best threshold values (0.09 for all the coefficients) and used to reconstruct back the original MST radar signal. The original signal properties are retained in the reconstructed signal as show in Fig (5.2b) and some of the noise is removed. However noise present around the lower frequencies was not removed properly. The SNR value of this denoised signal is 2.83 dB which is little more than three fold increase compared to the original signal.

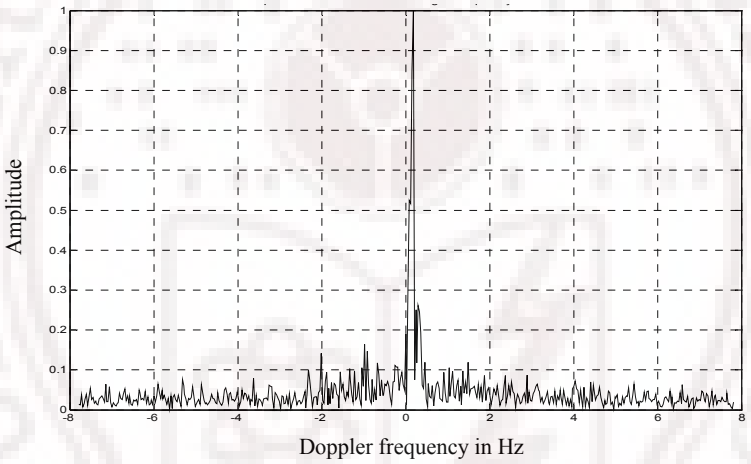

Figure 5.2b: Experimental MST radar signal denoised with 2-level wavelet analysis

Further decomposition divides the approximation band to two bands and hence noise spread over to these bands i.e. some of the noise is separated from the signal. Therefore a three level decomposition divides approximation band to two bands approximation cA3 and detail cD3 as shown in Fig (5.3a). Figure (5.3a) shows decomposition bands before thresholding. These bands are thresholded using same threshold values as in case one. Here also original signal properties are retained in the reconstruction as shown is Fig (5.3b). The SNR value of denoised signal in this case is 3.71 dB. Comparing figures (5.2b and 5.3b); it can be observed that noise present in lower frequencies is removed further with three level decomposition improving SNR to 3.71 dB.

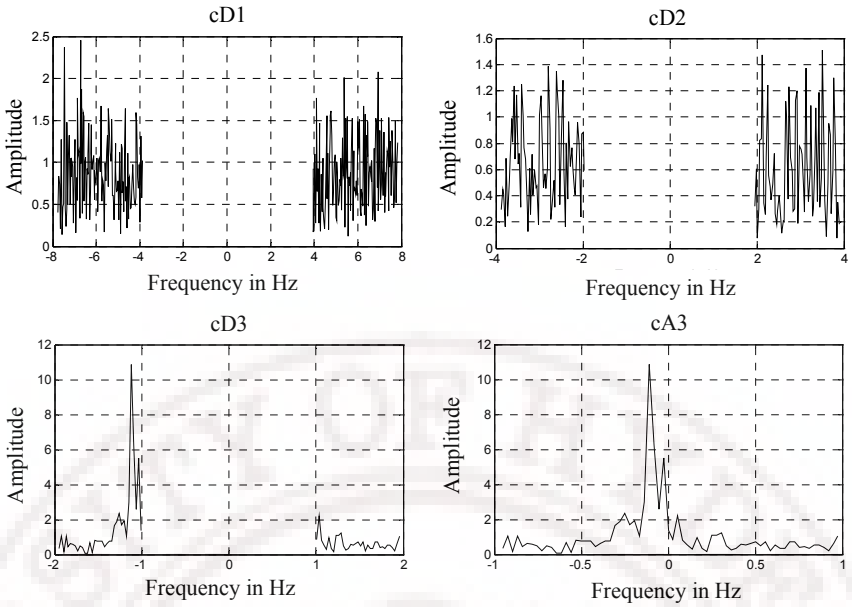

Figure 5.3a: Three level wavelet decomposition sub-bands (cD1, cD2, cD3 and cA3) spectra before thresholding

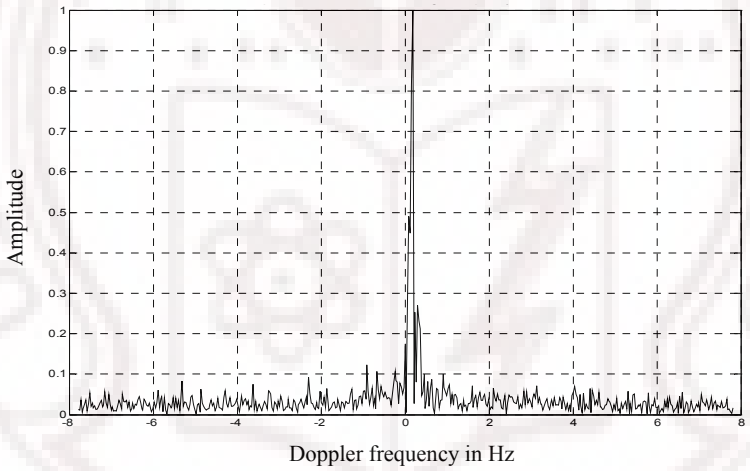

Figure 5.3b: Experimental MST radar signal denoised with 3-level wavelet analysis

This procedure is repeated with four level and five level decompositions. These results are shown in figures (5.4 and 5.5) and SNR values are summarized in Table 1. It can be observed that 3-level decomposition gives 0.9 dB more improvement in SNR than 2-level decomposition and no considerable improvement from 4-level decomposition onwards. However computational time and resources increase. Hence it can be concluded as 3-level decomposition is adequate for this data. So 3-level decomposition will be used for Indian MST signal in all wavelet analysis in following sections.

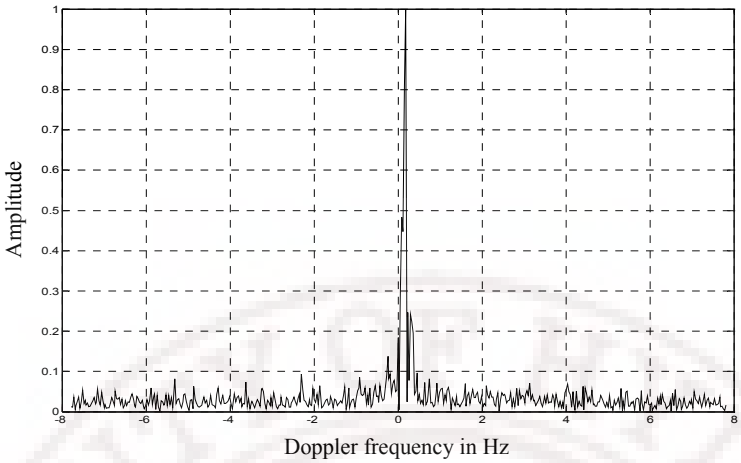

Figure 5.4: Experimental MST radar signal denoised with 5-level wavelet analysis

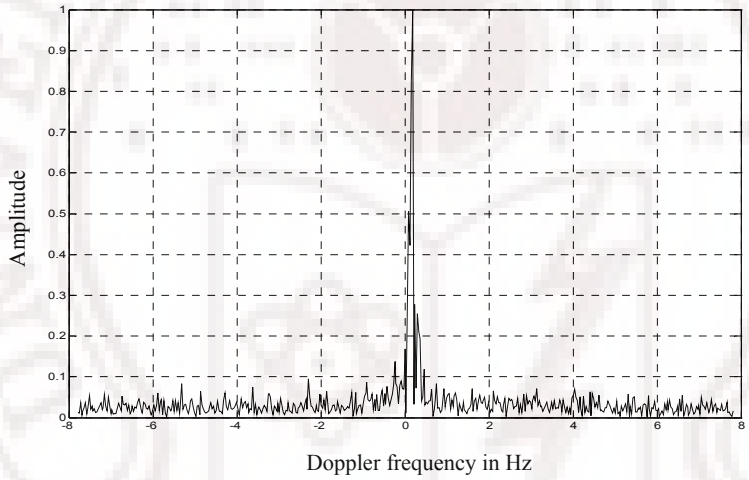

Figure 5.5: Experimental MST radar signal denoised with 5-level wavelet analysis

Table 5.1: SNR values of MST radar signal with different decomposition levels

Decomposition level	Before denoising SNR value in dB	After denoising SNR value in dB
Two	0.87	2.8262
Three	0.87	3.7144
Four	0.87	3.9665
Five	0.87	4.0261
Six	0.87	4.0392

5.2 Computation of suitable threshold values to MST radar data.

As mentioned earlier, it is important to choose the right levels for the thresholds in different sub-bands to be able to perform effective denoising which removes most of the noise while leaving the signal unaltered. There are different standard threshold selection techniques (as discussed in Chapter 3); such as Adaptive threshold, Universal threshold, a Heuristic threshold and Minimax (minimum of maximum) threshold selection method were considered on reasonably strong and weak echoes. The aim is to find a set of threshold values those suite the MST radar data at all levels.

Table 5.2 summarizes threshold values of MST radar Doppler echo at 7.5 km height computed from standard threshold methods. Universal, Heuristic and Minimax threshold methods result relatively larger threshold values and sometimes suppress the weaker signals as well. After extensive study, it is found that an Adaptive threshold selection technique provides suitable threshold values for MST radar data since it provides smaller threshold values compared to other threshold techniques and hence weaker signals will suppress. The threshold values found using an Adaptive method are slightly adjusted manually in order to have single set of thresholds for all the ranges for both simulated and experimental data.

Table 5.2: Threshold values of MST radar Doppler echo computed from standard threshold selection techniques

Band	Rigrsure		Heursure		Sqtwolog		Minimaxi	
	Designed wavelet	db10 wavelet	Designed wavelet	db10 wavelet	Designed wavelet	db10 wavelet	Designed wavelet	db10 wavelet
cD1	0.13	0.16	3.33	3.34	3.33	3.34	0.93	0.93
cD2	0.14	0.16	3.13	3.15	3.13	3.15	1.68	1.71
cD3	0.11	0.10	2.91	2.96	2.91	2.96	1.51	1.55
cA3	0.47	0.47	2.91	2.96	2.91	2.96	1.51	1.55

After extensive study it is found that threshold value 0.09 to all four bands (cD1, cD2, cD3 and cA3) is best threshold set to both stronger and weaker signals and similarly analysis is done by using standard Daubechies db10 wavelet and found that threshold set i.e. 0.085 to all bands is best threshold set. Table 5.3 summarizes threshold values to MST radar data using both designed and db10 wavelet.

Table 5.3: Best threshold values to MST radar data

Band	For Designed wavelet	For standard Daubechies db10 wavelet
cD1	0.09	0.085
cD2	0.09	0.085
cD3	0.09	0.085
cA3	0.09	0.085

These values of the thresholds seem to be good for all the collected data during a given period with out changing the operating conditions of the facility. Further, these values may have to be adjusted only slightly even if the operating conditions of the MST are retuned resulting in slightly different noise levels etc. Therefore these threshold levels seem to be characteristic to a given MST radar facility.

5.3 Thresholding method to MST radar data

As explained in Chapter 3 there are two thresholding methods, *viz.,* soft and hard thresholding. It is verified which of these techniques suite MST radar signals at three different altitudes (7.5 km, 16.35 Km, 20.85 Km). Towards this signals at these altitudes were denoised using both hard and soft thresholding methods. The SNR values thus computed are given in Table 5.4. It can be seen that the soft thresholding results in better SNR values, compared to hard thresholding in the case of strong signals whereas hard thresholding is better in the case of weak signals. The signals at lower altitudes can be even tracked without denoising techniques and our main concern is about weak signals at higher altitudes. Hence hard thresholding is most suitable thresholding technique for MST radar data.

Table 5.4: SNR values using both hard and soft thresholding

Range	SNR in dB		
	Before Denoising	Soft thresholding	Hard thresholding
7.5 Km	0.87	6.05	3.71
16.35 Km	-17.54	-13.7	-12.12
20.85 Km	-19.46	-16.18	-15.82

5.4 Denoising Simulated MST radar data

The optimized denoising methods for MST radar data as described the above, were first tested using the simulated data, as the details of the signal are known in simulated data.

The simulated data that has characteristics similar to MST radar data were generated as following. The Doppler echo in these simulated spectra was chosen to have Gaussian distribution in frequency domain with width typical of observed Doppler echoes, with a chosen shift and unit peak value for the lowest range bin. Random Gaussian noise was added to this spectrum to obtain a noisy signal by using random number generator. Then the data for higher range bins were generated by reducing the Doppler echo strength by 2 dB per every kilometer [Anandan et al., 2005] keeping the noise power constant as expected in the case of a realistic MST radar data. Thus simulated MST radar profiles covering the same range as that experimentally recorded was generated. While the position of the Doppler echo in the experimentally collected data are not known, the same are known in the simulated data, making it possible to verify the ability of the denoising techniques developed in this work in detecting correct variation of the Doppler echo signals at high altitudes. Different variations of the Doppler echo positions in the simulated profiles were considered to cover all possible experimental conditions.

Similar to experimental data, suitable threshold values are computed for this simulated data using designed wavelet and standard Daubechies db10 wavelet. Table 5.5 summarizes best threshold values to simulated data.

Table 5.5: Best threshold values to simulated data

Band	For Designed wavelet	For standard Daubechies db10 wavelet
cD1	0.13	0.13
cD2	0.11	0.11
cD3	0.14	0.07
cA3	0.11	0.09

5.5 Results

The ability of the wavelet based denoising techniques, with the denoising conditions determined above (decomposition levels, threshold levels and denoising

method (strong/weak)) was verified by considering strong and weak signals. First simulated data were considered followed by experimental data. Figures (5.6 and 5.7) show the results of this denoising method on stronger (7.5 km) and weaker (12.15 km) simulated Doppler echoes respectively and Table 5.6 summarizes the SNR values of these echoes before and after denoising. The results of denoising using the standard Daubechies wavelet db10 are also shown for comparison.

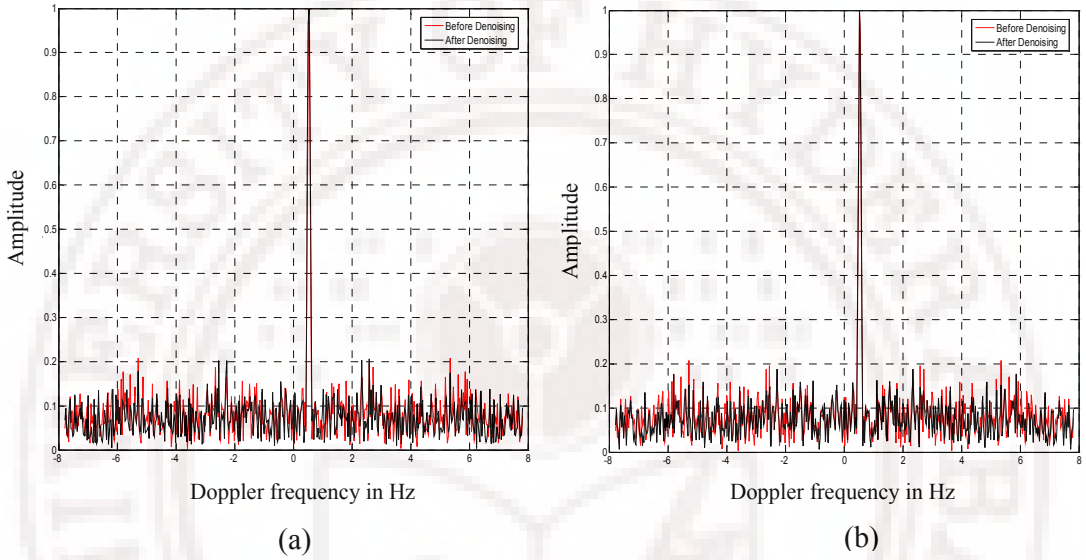

Figure 5.6: Relatively stronger simulated Doppler echo observed at lower ranges, original signal in red color and denoised signal (black color) (a) using designed wavelet (b) standard Daubechies db10 wavelet.

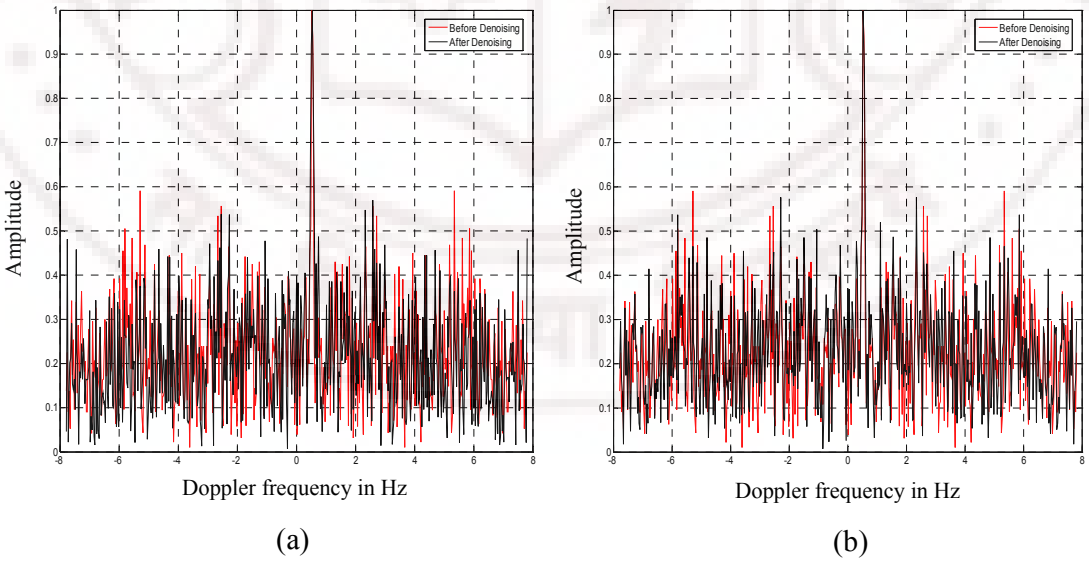

Figure 5.7: Relatively weaker simulated Doppler echo observed at higher ranges, original signal in red color and denoised signal (black color) (a) using designed wavelet (b) standard Daubechies db10 wavelet.

Table 5.6: SNR values of simulated stronger and weaker Doppler echoes

signal	SNR values in dB		
	Before denoising	After denoising	
		Designed wavelet	Standard Daubechies db10 wavelet
Strong signal at 7.5 Km	-0.32	1.24	0.48
Weak signal at 12.15 Km	-9.41	-8.25	-8.78

As can be seen the SNR of the both the signals improve substantially after denoising using both designed wavelet and standard wavelet db10, but the wavelet designed in this work performing better than the standard wavelet. The ability of this denoising method in tracking the signals to much higher altitudes (compared to original profiles) and improvement in accuracy of estimated parameters is also demonstrated in following chapters. An Adaptive Tracking of Doppler echo algorithm discussed in next chapter along with wavelet based denoising technique identifies the Doppler echoes correctly to much higher ranges compared to before denoising and designed wavelet performs better than standard wavelet db10. The wavelet analysis not only improves the range over which the Doppler echoes are reliably detected; it also improves the accuracy of the parameters derived (first three moments and SNR) from such data after denoising using both designed wavelet and db10.

Then the efficacy of this wavelet denoising technique is applied on experimental MST radar Doppler echoes. Figures (5.8 and 5.9) show the results of this denoising method on stronger (7.5 km) and weaker (12.15 km) signals of experimental MST radar Doppler echoes respectively. Table 5.7 summarizes the SNR values of these echoes before and after denoising using designed wavelet and standard Daubechies wavelet db10.

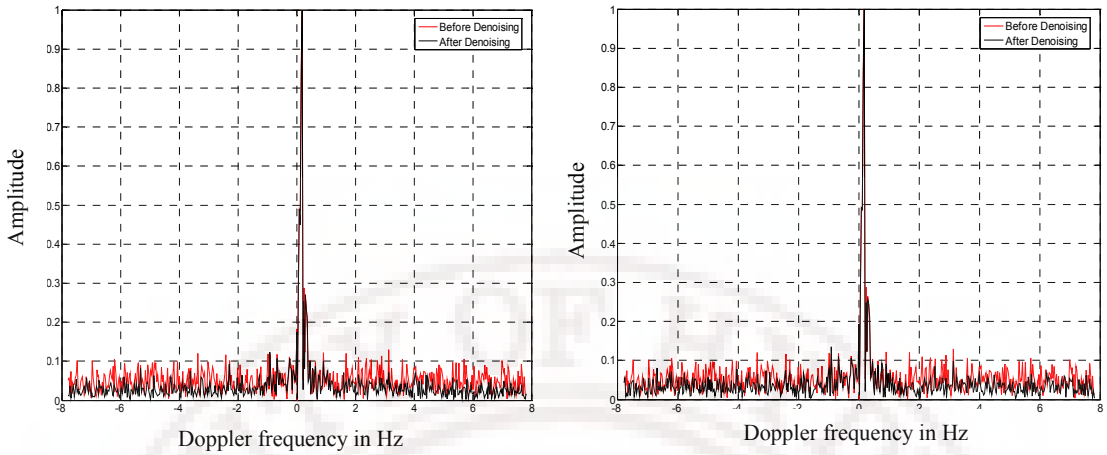

Figure 5.8: Relatively stronger experimental MST radar Doppler echo observed at lower ranges, original signal in red color and denoised signal (black color) (a) using designed wavelet (b) standard Daubechies db10 wavelet.

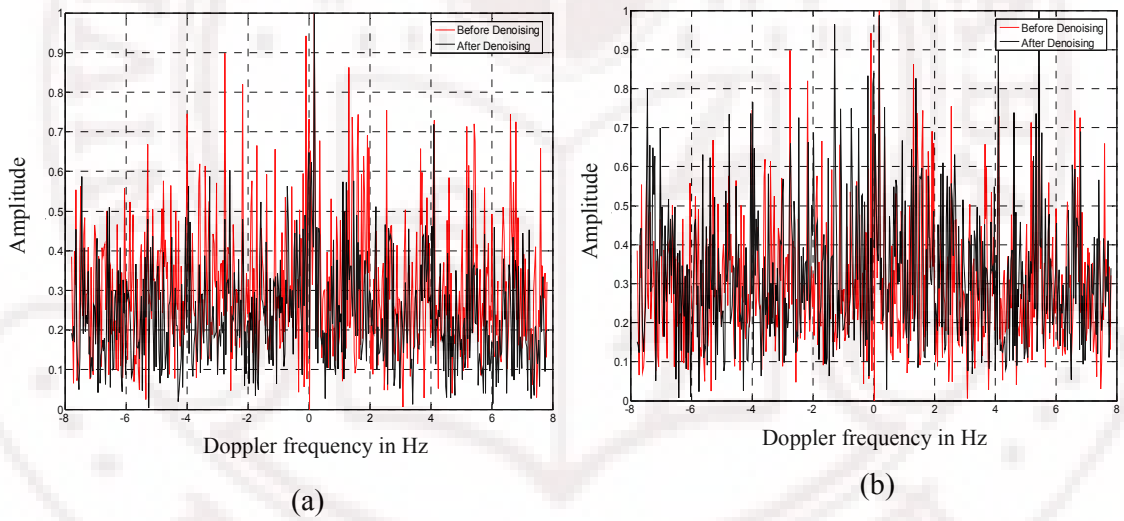

Figure 5.9: Relatively weaker experimental MST radar Doppler echo observed at higher ranges, original signal in red color and denoised signal (black color) (a) using designed wavelet (b) standard Daubechies db10 wavelet.

Table 5.7: SNR values of MST radar stronger and weaker Doppler echoes

signal	SNR values in dB		
	Before denoising	After denoising	
		Designed wavelet	Standard Daubechies db10 wavelet
Strong signal at 7.5 Km	0.87	3.71	3.21
Weak signal at 12.15 Km	-15.08	-12.33	-14.57

The results again show that the SNR of both the Doppler echoes improve substantially after denoising using both designed wavelet and standard db10 wavelet, but the designed wavelet performing better than the db10 wavelet, particularly in the case of weaker signals. Further, this denoising method in tracking the signals to much higher altitudes is also demonstrated on experimental MST radar profiles in Chapter 8. An Adaptive Tracking Method along with wavelet based denoising technique results that the detected echoes show mirror symmetry between North and South (East and West) beams to much higher ranges when they are denoised using both designed wavelet and db10 wavelet and designed wavelet performs better compared to db10 wavelet. It is again observed that the accuracy of the derived parameters improve due to this analysis even in ranges where other methods can also detect the Doppler echo.

Chapter 6

Adaptive tracking of Doppler Echoes

6.1 Introduction

Wind profile from MST radar data is computed by processing the Doppler profile obtained from the spectral data in at least three non-coplanar beam positions. The primary MST radar data consists of amplitude spectra spanning the desired Doppler frequency window for each range bin in the range window. This spectrum has to be processed for each range bin to get the total wind profile in the height region.

The method adopted for identifying the signal and computing the three low-order spectral moments is central to the problem of extracting information from the Doppler spectrum of the MST radar signal. The conventional method of analyzing the MST radar spectral data is done by tracking the prominent spectral peak with highest amplitude in each range bin and computing first three spectral moments and signal to noise ratio. This simple method is satisfactory for processing lower altitude ranges where the SNR is quite high. But at higher altitudes where SNR is low, this method may pick false spectral peaks. In edition, the presence of any electromagnetic interference or outliers make the reliable detection of the signal is still difficult.

6.2 Existing algorithms to improve Doppler peak detection

A median estimator or consensuses average method was suggested [Fischler and Boltes, 1981, May and Strauch, 1989 and Wilfong et al., 1993] to be used instead of a simple averaging of the spectra before computing the spectral moments to improve the performance of the Doppler peak detection algorithm. The main motivation for the consensus algorithm was to extend the reliable averages to low SNR signals. These methods eliminate contamination (echoes from flying objects such as aircraft, birds etc) in the average by editing the data before averaging. The problem with both the median and consensus methods, however, is that they depend upon the number of data points to

be good (noise free), which is around one third of the total samples in consensus algorithm, in order to give a reliable estimate. Merritt [1995] developed a more effective method that makes use of the signal statistics to selectively average the data and that is not restricted by the desired good data points. Approaches to filtering the time series data prior to spectral processing and modifications to the spectral processing were considered by May and Strauch [1998] and Jordan and Lataitis [1997] to address clutter issues. All of these statistical averaging techniques and filtering techniques are intended mainly to deal with spectral data contaminated with signals from non-atmospheric sources such as ground clutter, aircraft, birds, insects, etc.

For identifying signals from regions of low SNR, which would improve the reliability and height coverage of Doppler profiles, some kind of an adaptive method needs to be used. An adaptive method based on constructing chains of profiles by maximizing an energy function and using a neural network approach for detecting the most likely profile has been developed by Clothiaux et al. [1994]. The performance of the method has been successfully demonstrated with 404 MHz wind profiler spectral data taken in low-altitude mode that showed extensive periods when either the SNR was poor or the atmospheric signal power was significantly less than that of the ground clutter. A wind confidence algorithm [National center for Atmospheric Research (NCAR) Improved Moments algorithm (NIMA)] and an automatic moments estimation technique [NCAR Wind and Confidence Algorithm (NWCA)] were developed and implemented for wind profilers [Morse et al., 2002 and Goodrich et al., 2002]. The NIMA method implements combinational mathematical analysis, fuzzy logic synthesis, and global image processing algorithms. Anandan et al. [2001] developed another method of adaptive data processing that has been found to perform consistently well under a wide range of SNR conditions of atmospheric signals that are free from interference and ground clutter. The method is based on tracking the signal in the range-Doppler spectral frame making use of certain criteria for adaptively setting the parameters of the SNR threshold, Doppler velocity window and wind shear threshold. All these methods have yielded reliable detection of the Doppler echoes to a maximum range of about 22 km under favorable conditions.

6.3 Simplified Adaptive Tracking Method

An Adaptive Tracking Method (ATM) is developed in this work on the same lines of one which is developed by Anandan et al. [2001] with some simplifications to be used on the profiles which are processed by the wavelet based denoising technique described in the earlier chapters. This method works around parameters that get updated constantly so as to optimize the tracking performance. The parameters used for adaptive signal tracking in a range Doppler frame are the Doppler velocity window (DVW), wind shear and signal to noise ration (SNR). In the case of SNR, a threshold value is specified that applies for the entire range-Doppler frame. In the SNR computation, the noise power is computed over the full bandwidth of the amplitude spectrum. The SNR threshold is chosen to be 15dB (after several trails) above the mean noise level estimated for the highest range bin in noise region.

The tracking is initiated by the first range-bin whose highest peak was selected as Doppler echo as in almost all cases the SNR is invariably quite high (SNR of 7 dB or more) and the Doppler echo is quite prominent and easily detectable in several lower altitude bins.

From the second range bin onwards, the Doppler peak in a range bin (say i^{th} bin) is chosen in the following way. First a Doppler window is fixed based on the position of the detected Doppler echo of the previous (i-1) bin. Doppler velocity window limits are set at $\pm 10\%$ of the coherent integration filter band width on either side of the mean Doppler velocity associated with the previous bin since the signal is not to expect to change by more than 10% of the coherent filter bandwidth from one range bin to the next. The five most prominent spectral peaks are selected as candidate signals within the specified DVW. For example Fig (6.1) shows the spectral peaks in descending order of power level in a range bin. Peaks S_1, S_2, S_3, S_4 and S_5 represents selected prominent peaks in descending order of power level. For the selected candidate peaks, the three lower order spectral moments and SNRs are computed following Woodman [1985]. Here SNR is calculated by considering the noise in the same bandwidth as that of the signal. Out of the five peaks with in the Doppler velocity window, starting from the peak having highest total power, the peak satisfying the SNR criterion (SNR_{th}) was chosen as the Doppler echo. If none of the peaks satisfy the SNR criterion, the strongest peak which falls within the permissible wind shear is chosen as Doppler echo. The wind shear threshold was selected based on earlier two range bins. The wind shear threshold for present bin (say i^{th}

bin) is set by adding the full width of the Doppler velocity peak in present bin to the difference in mean Doppler velocity between present bin (say i^{th} bin) and previous bin (i-1). The wind shear threshold set for present bin is used for next range bin to identify prominent peak.

If no Doppler echo was detected in a given range bin that bin is skipped and DVW and wind shear threshold for the next bin is computed from the earlier bins. This algorithm is shown in flow chart Fig (6.2). The procedure is repeated sequentially for all range bins, there by fixing a height-varying DVW and wind shear for the entire frame.

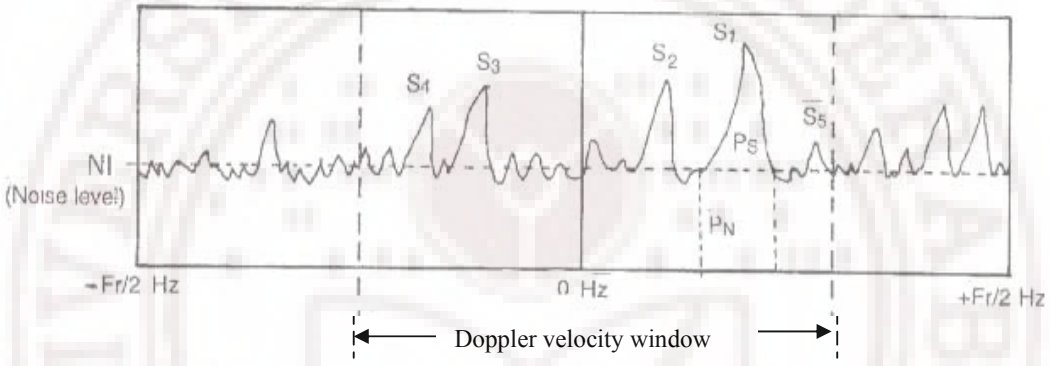

Figure 6.1: Amplitude spectrum in one range bin

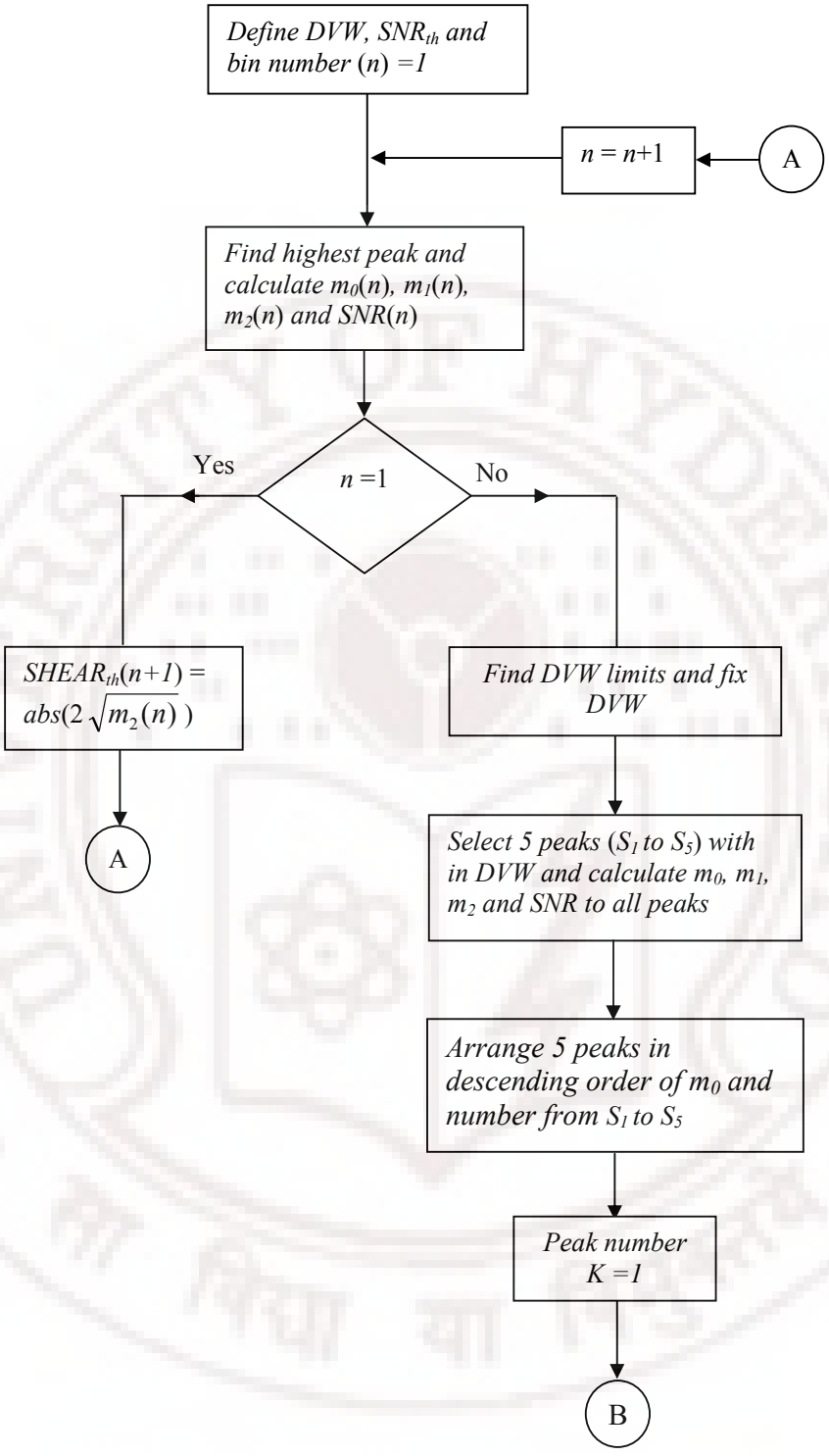
Define DVW, SNR_{th} and bin number (n) =1
$n = n+1$
A
Find highest peak and calculate $m_0(n)$, $m_1(n)$, $m_2(n)$ and $SNR(n)$
n =1
Yes
No
$SHEAR_{th}(n+1) = abs(2\sqrt{m_2(n)})$
A
Find DVW limits and fix DVW
Select 5 peaks (S_1 to S_5) with in DVW and calculate m_0, m_1, m_2 and SNR to all peaks
Arrange 5 peaks in descending order of m_0 and number from S_1 to S_5
Peak number K =1
B

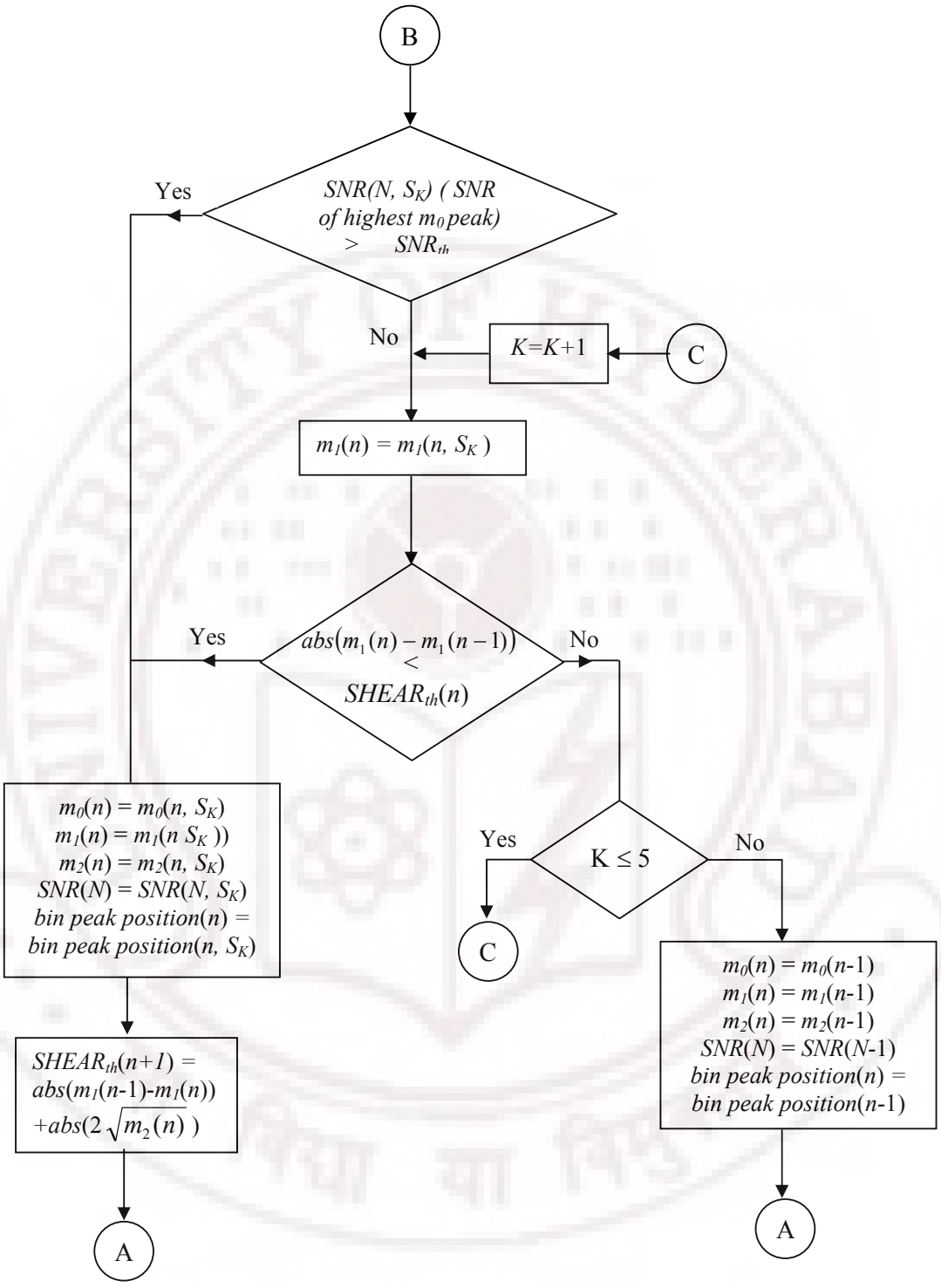

Figure 6.2: Adaptive Tracking Method

6.4 ATM on simulated signals

This algorithm is first applied on simulated signals (described in Chapter 5) before and after denoising to ascertain detectability of the correct Doppler echoes as echo position is known in that case. Figure (6.3) shows effect of Adaptive Tracking Method and denoising on simulated data.

Figure (6.3a) shows the simulated Doppler profile. Here signals were simulated up to range of 3-30 km (180 range bins with one bin for every 150m) as in the case of typical MST radar data. The Doppler shift was varied linearly from 0-2 Hz from lowest range bin to highest range bin as shown by the solid blue colored line in Fig (6.3b). The Doppler echoes were barely observable up to 15 km in this case. The Doppler echoes identified by above described ATM are marked with darker points in figures (6.3b and 6.3c). As can be seen from the Fig (6.3b), the ATM identifies the Doppler echoes correctly up to about 17 km before denoising. The selected peaks by ATM are deviating from the actual location of Doppler echoes from 17 km onwards and are completely off the target at higher ranges. Figure (6.3c) shows how the same ATM is able to pick the correct Doppler echoes after wavelet based denoising the data by using designed wavelet described in the Chapter 4. As can be seen from the Fig (6.3c) it is possible to track the signal up to 24 km after wavelet based denoising.

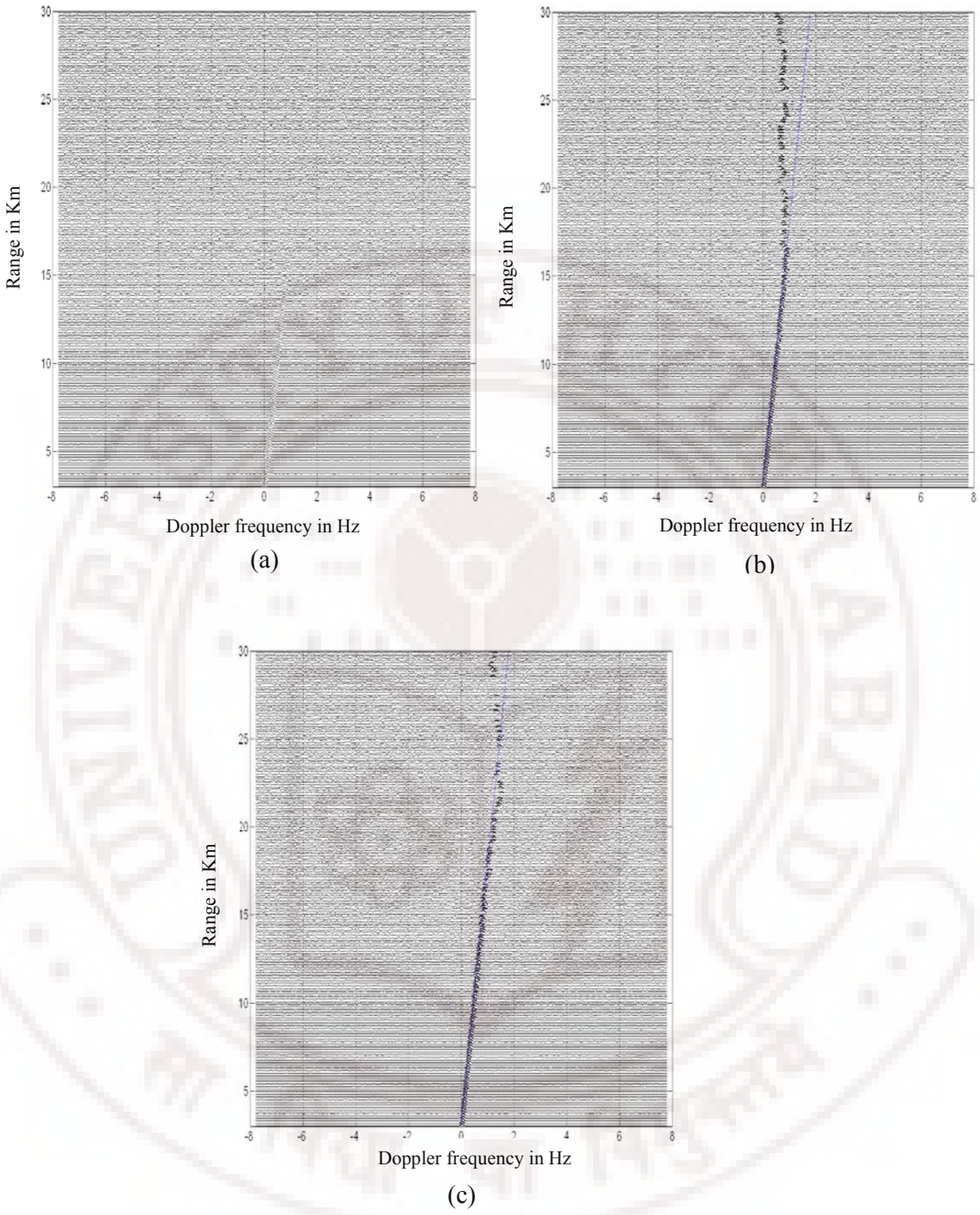

Figure 6.3: Simulated MST radar profiles (a) Raw data (b) with Adaptive tracking of the Doppler echo and (c) with denoising and Adaptive tracking of the Doppler echoes. Here blue solid line indicates the expected location of the Doppler echoes where as darker points indicate the peaks selected by the Adaptive Tracking Method.

Chapter 7

Simulation Data Analysis

The methods developed in previous chapters, for the wavelet denoising of the MST radar data are first tested using the simulated data as the details of the signal are known in simulated data. The generation of simulated data is explained in Chapter 5. This chapter presents results of the analysis of the simulated data using the methods developed in previous chapters. The results on the simulated data generated using different Doppler shift variations and different noise profiles are summarized and results are compared with the standard wavelet. The results on accuracy of estimated parameters from simulated data are also presented.

7.1 Denoising and adaptive techniques on simulated profiles

Different experimental situations were simulated by generating the profiles for different seed values of the noise generator and for different Doppler shift variations. To test the developed denoising algorithms and adaptive tracking of Doppler echoes, different simulated profiles with different Doppler echo variations were considered.

As we know in typical situations MST radar Doppler shift is less than 2 Hz. Hence in first case realistic MST radar data were simulated by varying Doppler shift linearly from 0 to 1.8 Hz from lowest range bin to highest range bin in steps of 0.01 Hz as shown by the blue colored line in the Fig (7) and range varying from 3-30 km (181 range bins with one bin for every 150 m). The peak value for the Doppler echo was chosen to be unit for the lowest range bin and the data for higher range bins were generated by reducing the Doppler echo strength by 2 dB per every kilometer [Anandan et al., 2005] keeping the noise power constant as expected in the case of a realistic MST radar data. The Doppler echoes are barely observable up to 15 km in raw data as shown in Fig (7.1a). The adaptive tracking of Doppler echoes of this raw data is shown in Fig (7.1b). As can be seen from the Fig (7.1b) the ATM identifies the Doppler echoes correctly up to about 16 km in the raw data. The selected peaks by ATM start deviating from the actual

location of Doppler echoes from 16 km and are completely off the target at higher ranges. Fig (7.1c) shows how the same ATM is able to pick the correct Doppler echoes after denoising the data using wavelet transform method with designed wavelet. As can be seen from Fig (7.1c) it is possible to track the signal up to 25 km, through with somewhat small scatter around 20km, whereas it is able to track up to 21 km only when standard db10 wavelet was used for denoising as shown in Fig (7.1d).

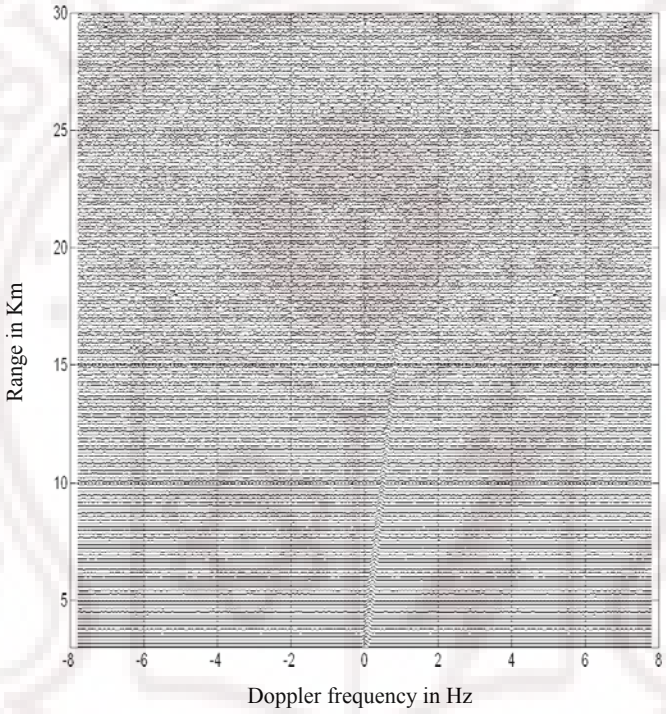

(7.1a)

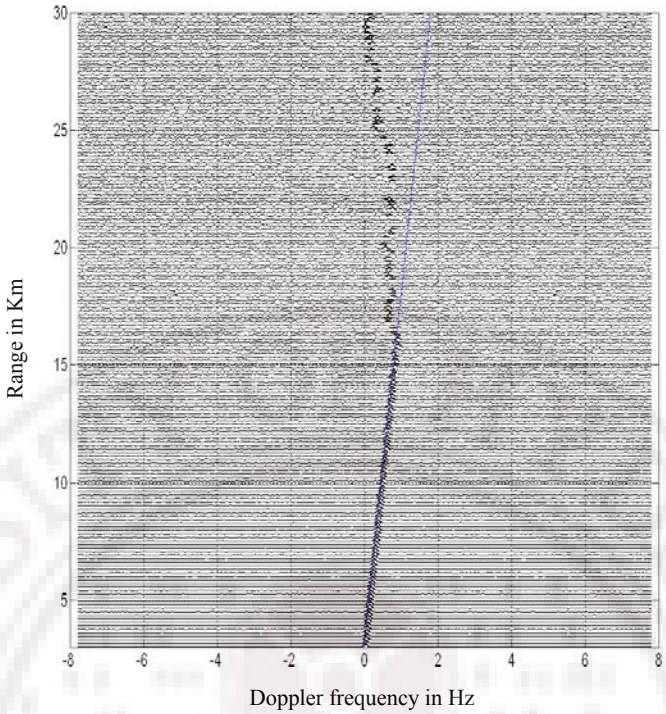
Range in Km
Doppler frequency in Hz

(7.1b)

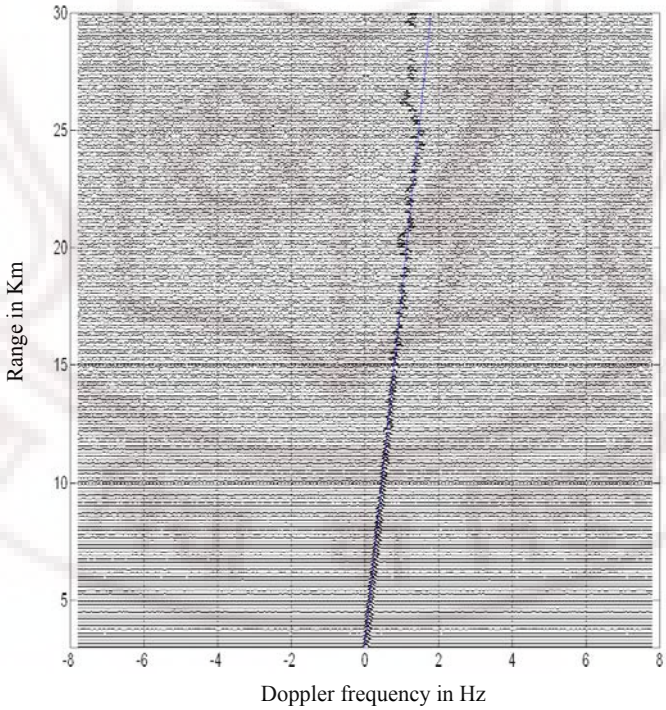
Range in Km
Doppler frequency in Hz

(7.1c)

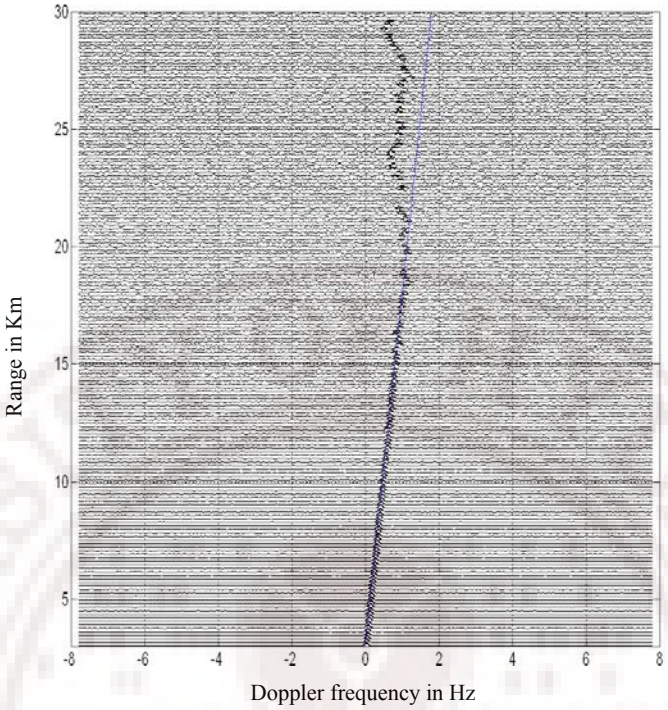

(7.1d)

Figure 7. 1: Simulated MST radar profiles with Doppler shift variation from 0-1.8 Hz (a) Raw data (b) with adaptive tracking of the Doppler echoes and (c) and (d) with denoising and adaptive tracking of the Doppler echoes using designed wavelet and standard Daubechies db10 wavelet. Blue colored line indicates the expected location of the Doppler echoes where as darker points indicate the peaks selected by the Adaptive Tracking Method.

Further, to check how well this technique tracks the Doppler echoes having larger Doppler shifts simulated profiles with Doppler shift variation from 1- 5.6 Hz as shown in Fig (7.2) were used. Here Doppler shift spans in detail coefficients sub-bands at decomposition level 1 and 2 (cD2 and cD3) where as previous profile Doppler shift spans in cA3 and cD3 sub-bands.

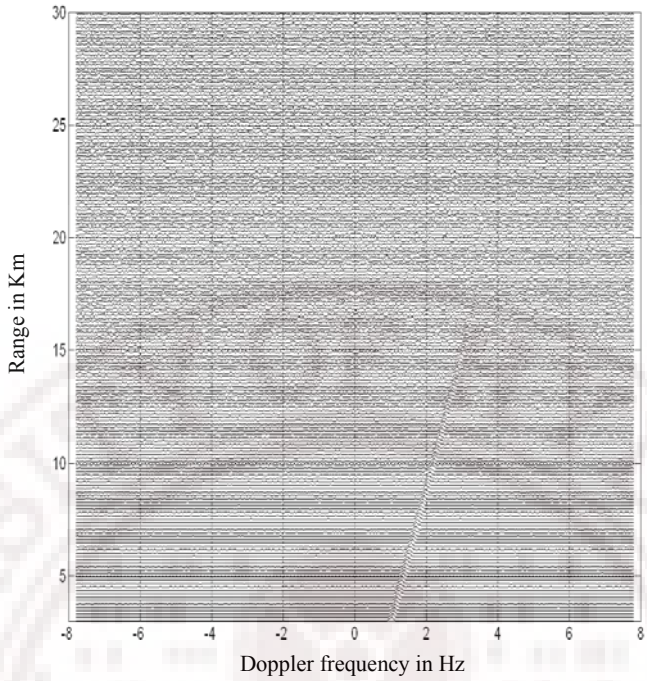
Range in Km
30
25
20
15
10
5
-8
-6
-4
-2
0
2
4
6
8
Doppler frequency in Hz

(7.2a)

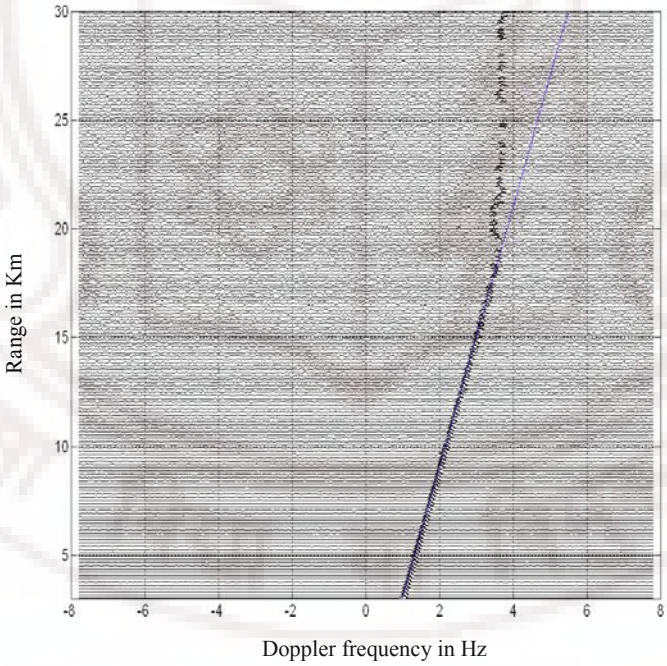
Range in Km
30
25
20
15
10
5
-8
-6
-4
-2
0
2
4
6
8
Doppler frequency in Hz

(7.2b)

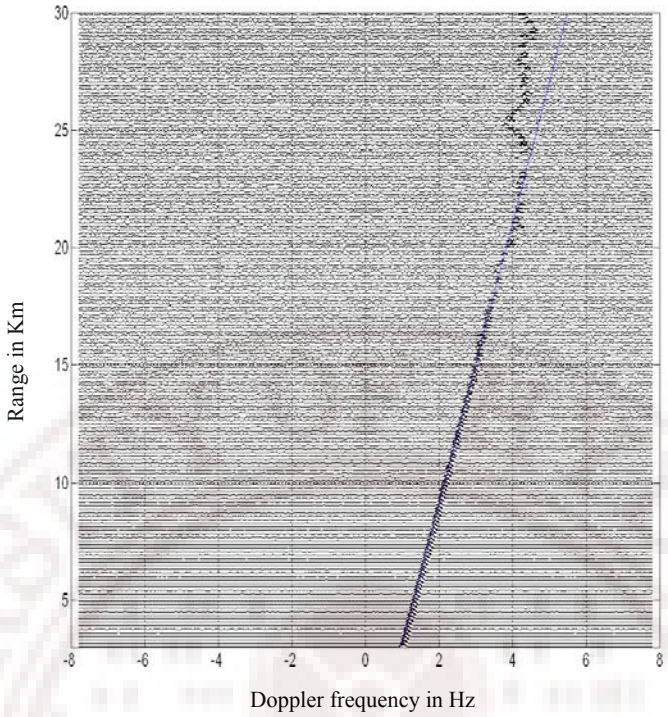

(7.2c)

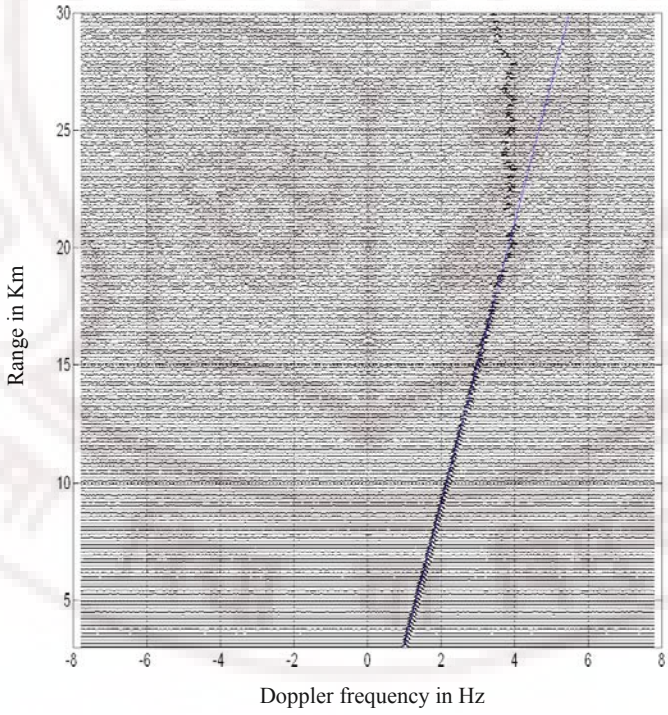

(7.2d)

Figure 7. 2: Simulated MST radar profiles with Doppler shift variation from 1-5.6 Hz (a) Raw data (b) with adaptive tracking of the Doppler echoes and (c) and (d) with denoising and adaptive tracking of the Doppler echoes using designed wavelet and standard Daubechies db10 wavelet. Blue colored line indicates the expected location of the Doppler echoes where as darker points indicate the peaks selected by the Adaptive Tracking Method.

The adaptive tracking of Doppler echoes of raw data is shown in Fig (7.2b). As can be seen from the Fig (7.2b) the ATM identifies the Doppler echoes correctly up to about 18 km in the raw data. Figures (7.2c and 7.2d) show how the same ATM is able to pick the correct Doppler echoes after denoising the data using designed wavelet and standard Daubechies wavelet respectively. As can be seen from Fig (7.2c) it is possible to track the signal up to 24 km using designed wavelet, whereas it is able to track up to 21 km only when standard db10 wavelet was used for denoising as shown in Fig. (7.2d).

7.2 Estimation of the accuracy of derived parameters

The method of denoising the MST radar data using wavelet analysis not only improves the range over which the Doppler echoes are reliably detected; it also improves the accuracy of the parameters derived from such data. This was demonstrated by considering several simulated profiles (about 10) corresponding to different seed values of the noise generator and same in all profiles Doppler shift (0-1.8 Hz). These sets have different noise values though echo positions and other related parameters remain the same. This situation is equivalent to several sets of experimental data collected in a short span under steady weather conditions. The Doppler echoes of all these profiles were identified by ATM. The first three moments corresponding to the Doppler spectra (m_0, m_1 and m_2), as described in Chapter 2, were computed for some chosen range gates. Then mean and standard deviations of these parameters over all the sets of data (about 10) were computed. Similar computations were performed after denoising these signals using the designed wavelet and standard db10 wavelet. And this process was repeated over all range bins of those ten sets of data. The Table 7.1 shows the results of these computations. The values in parenthesis are the standard deviations in the values of the parameters. As can be seen from the above table the SNR has considerably improved in all cases after denoising and designed wavelet gives better SNR values than standard wavelet db10. Further the standard deviations in parameters such as m_1 have considerably reduced even in lower altitudes where other methods can also detect the Doppler echo, increasing the accuracy of the measurements. The mean (standard deviation) value of m_2 computed over ten identical simulated profiles at an altitude 20.5 km before denoising was $2.25\text{x}10^{-3}$ ($9.9\text{x}10^{-4}$), where as after denoising using both designed wavelet and Daubechies wavelet it was $2.15\text{x } 0^{-3}$ ($9.9\text{x}10^{-4}$) and $2.15\text{x}10^{-3}$ ($9.9\text{x}10^{-4}$) respectively.

Mean and standard deviations of parameter m_0 are more or less same before and after denoising because in this work wavelet decomposition coefficients of MST radar data were thresholded using hard thresholding technique, which sets coefficients that are below a certain threshold to zero and coefficients above threshold values are left unchanged. Hence wavelet based denoising could not remove noise properly under this Doppler echo. From Eq. (2.8) m_0 is the area under Doppler echo, so there is no considerable improvement in mean and standard deviations of parameter m_0. Similar case in m_1 as it represents the width of the Doppler echo.

Table 7. 1: Mean and standard deviations of derived parameters computed over 10 sets of identical simulated profiles at different altitudes

Range in km	m_0 (x10^3)			m_1 *in Hz*			SNR in dB		
	Before Denoising	After Denoising (Designed Wavelet)	After Denoising (db10)	Before Denoising	After Denoising (Designed Wavelet)	After Denoising (db10)	Before Denoising	After Denoising (Designed Wavelet)	After Denoising (db10)
3.75	20.80 (0.58)	21.80 (0.59)	2.08 (0.58)	0.080 (0.0012)	0.080 (0.0010)	0.080 (0.0013)	6.88 (0.35)	8.75 (0.36)	7.50 (0.36)
4.65	13.67 (0.509)	13.80 (0.517)	1.365 (0.537)	0.139 (0.0014)	0.139 (0.0012)	0.140 (0.0014)	5.00 (0.18)	6.80 (0.21)	5.70 (0.23)
7.35	4.00 (0.308)	4.10 (0.306)	4.0 (0.274)	0.320 (0.0023)	0.320 (0.0022)	0.321 (0.0014)	-0.25 (0.09)	1.50 (0.11)	0.40 (0.104)
9.45	1.56 (0.144)	1.50 (0.143)	0.16 (0.142)	0.460 (0.0063)	0.459 (0.0060)	0.4613 (0.0057)	-4.40 (0.038)	-2.70 (0.04)	-3.75 (0.04)
13.2	0.35 (0.105)	0.30 (0.102)	0.03 (0.011)	0.712 (0.0135)	0.713 (0.0081)	0.7086 (0.0123)	-10.90 (0.025)	-9.80 (0.027)	-10.20 (0.03)
14.85	0.17 (0.057)	0.10 (0.047)	0.20 (0.061)	0.811 (0.0272)	0.817 (0.0266)	0.822 (0.0267)	-13.90 (0.015)	-13.95 (0.014)	-13.00 (0.015)
16.95	0.10 (0.041)	0.10 (0.037)	0.10 (0.047)	0.906 (0.1038)	0.923 (0.0580)	0.9519 (0.0617)	-16.25 (0.01)	-15.75 (0.01)	-16.85 (0.013)
18.9	0.07 (0.031)	0.20 (0.017)	0.10 (0.029)	0.924 (0.1640)	1.048 (0.0839)	1.0418 (0.1333)	-17.50 (0.007)	-17.00 (0.005)	-17.00 (0.007)
20.25	0.07 (0.017)	0.20 (0.021)	0.10 (0.017)	0.820 (0.2097)	1.134 (0.1177)	1.1015 (0.1202)	-17.80 (0.004)	-16.25 (0.005)	-17.70 (0.0048)
22.65	0.06 (0.018)	0.09 (0.022)	0.10 (0.018)	0.761 (0.2156)	1.293 (0.1355)	1.1417 (0.1550)	-18.20 (0.005)	-17.0 (0.0055)	-17.8 (0.0055)
24.15	0.05 (0.018)	0.07 (0.007)	0.04 (0.018)	0.712 (0.2394)	1.385 (0.1549)	1.1198 (0.1947)	-18.9 (0.0045)	-17.50 (0.002)	-18.20 (0.005)

Figure (7.3) shows mean and standard deviations of extracted parameters m_0, m_1 and SNR computed over ten identical sets as explained above. Here standard deviation is plotted around the mean value vertically. While the improvement in m_0 and SNR is nominal as shown in Figures (7.3a and 7.3c), the same in m_1 (Fig.7.3b) much more pronounced after denoising.

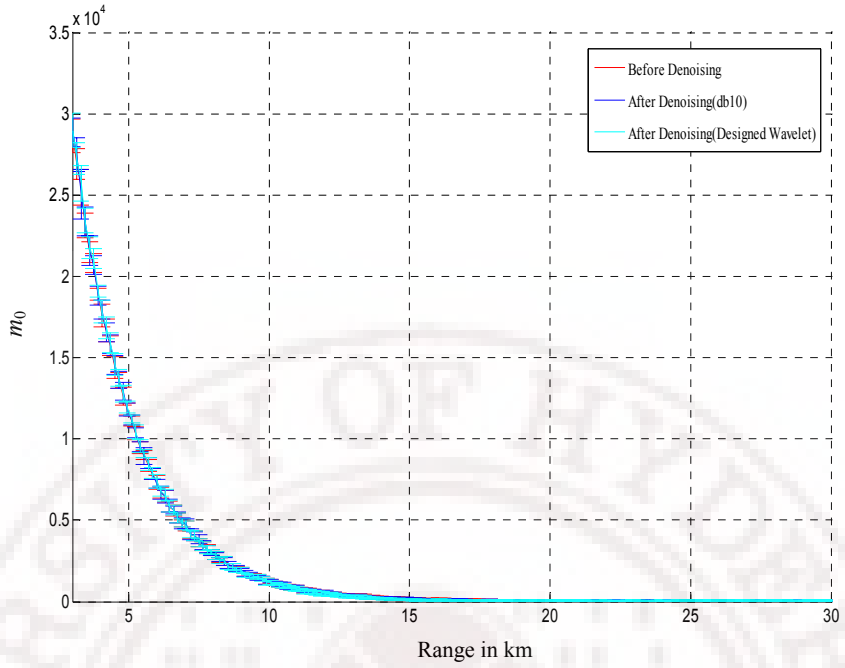
x 10^4
Before Denoising
After Denoising(db10)
After Denoising(Designed Wavelet)
m_0
Range in km

(7.3a)

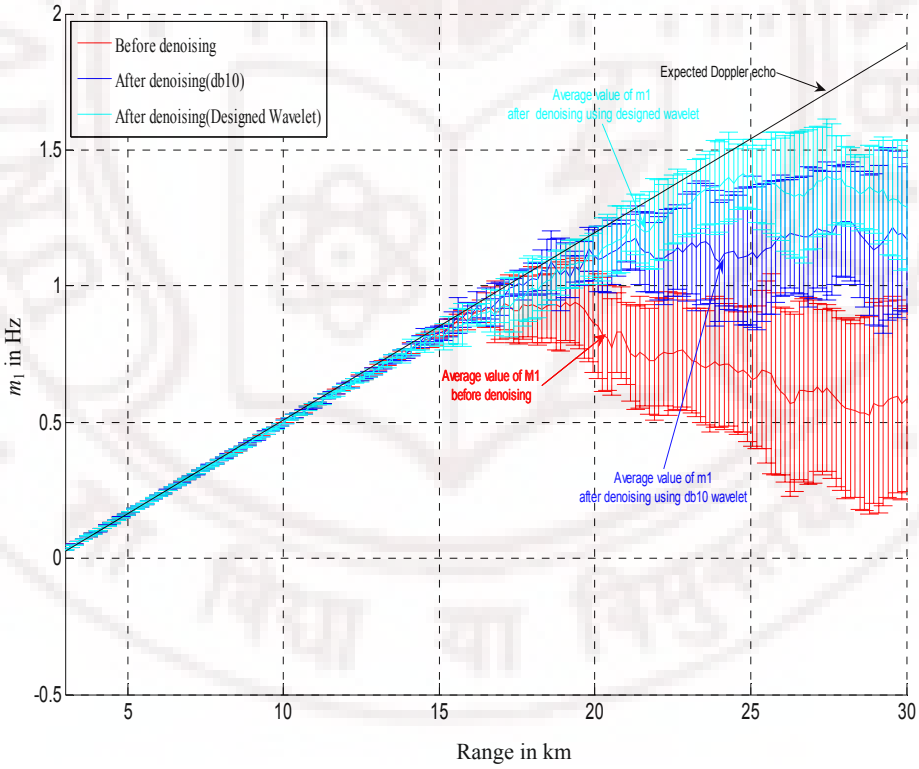
Before denoising
After denoising(db10)
After denoising(Designed Wavelet)
Expected Doppler echo
Average value of m1
after denoising using designed wavelet
Average value of M1
before denoising
Average value of m1
after denoising using db10 wavelet
m_1 in Hz
Range in km

(7.3b)

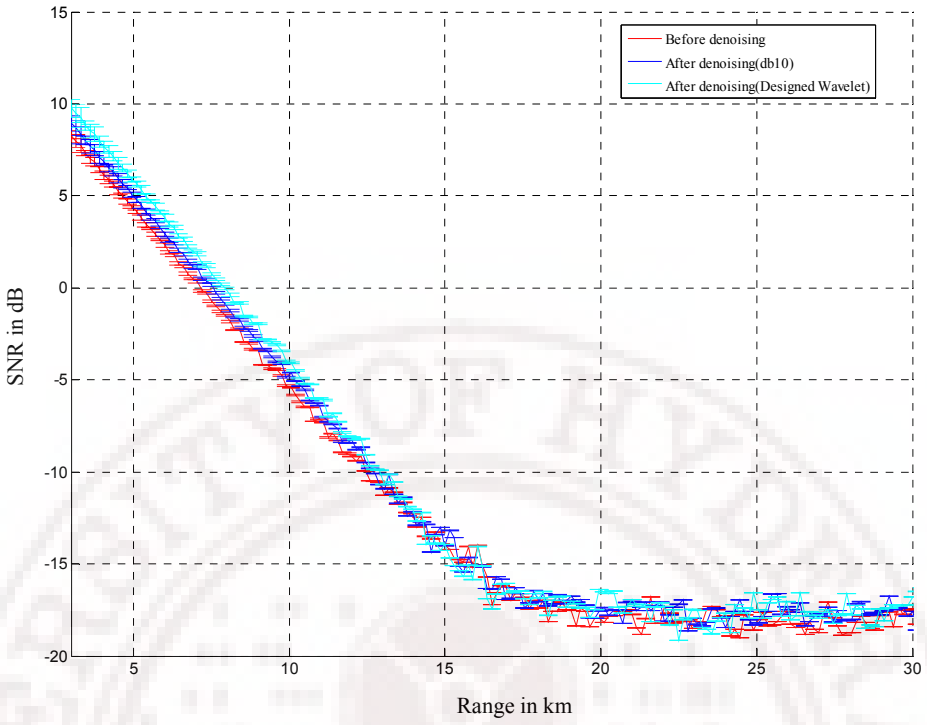

(7.3c)

Figure 7. 3: Mean and standard deviations computed over 10 sets of identical simulated profiles corresponding to different seed values of the noise generator (a) Zeroth moment m_0 (b) First moment m_1 and (c) *SNR*. Here length of error bar (vertical lines) indicates amount of deviation from average value.

Now we look at plot of standard deviation alone for m_1. The values of Standard deviations computed over ten simulated profiles (explained above) are shown in Fig (7.4). As seen the improvement in standard deviations after wavelet analysis is very small below 15 km, where as above 15 km this is a considerable improvement in standard deviation. And above 15 km designed wavelet gives better standard deviations than standard db10 wavelet.

`

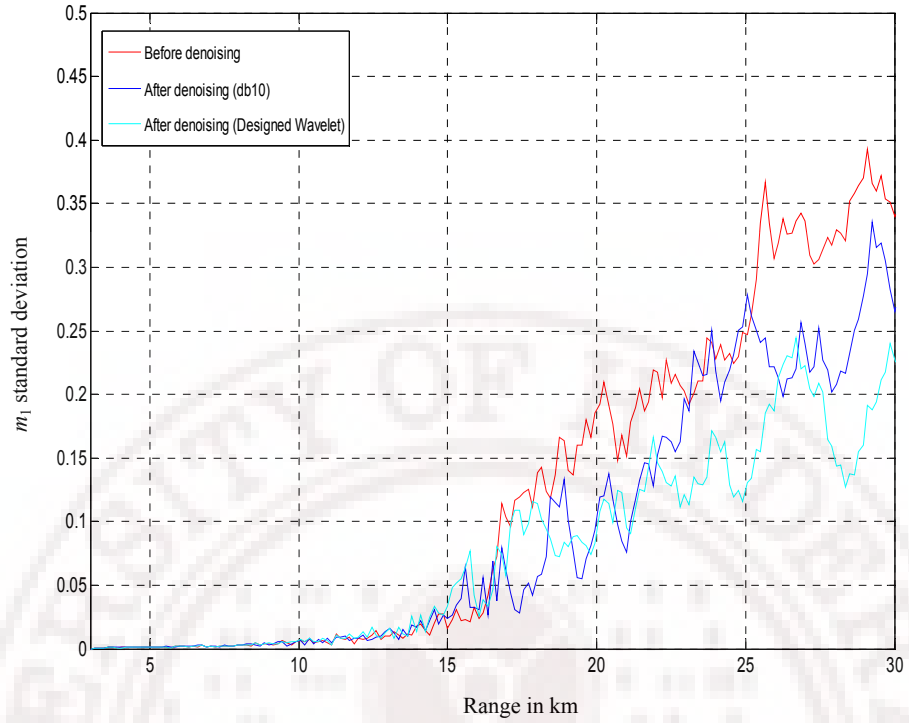

(7.4a)

Figure 7. 4: Standard deviations of First moment m1 computed over 10 sets of identical simulated profiles corresponding to different seed values of the noise generator

Figure (7.5) shows individual plots of mean values computed over ten identical simulated profiles. The mean values of m_0 and *SNR* before and after denoising are more or less same. The improvement in accuracy in measured parameters can be verified with mean values of m_1, where the expected value is known. As we know profiles considered in this demonstration are having same Doppler variations from lowest range bin to highest bin i.e. 0-1.8 Hz. Hence in idle case the mean Doppler shift value over ten profiles should be 0-1.8 Hz from lowest range bin to highest range bin. Figure (7.5b) shows mean values computed over ten simulated profiles for raw data, denoised profile using both designed wavelet and standard db10. Here black colored solid line indicates expected average mean value. The mean value computed over ten raw profiles is shown in red color; up to 15 km this mean values are same as expected mean value and after that completely off the expected value. The magenta colored solid signal shows the computed average mean value after wavelet based denoising the data by using designed wavelet. As can be seen from the Fig (7.5b) average value computed using designed wavelet is very

closer to the expected value up to 25 km, where as it is 20 km only when standard db10 wavelet is used for denoising which is indicated with blue colored signal in Fig (7.5b). Similarly, Fig (7.5c) shows that the SNR also improves due to the denoising using the wavelet designed in this work. As mentioned earlier mean values of m_0 were same before and after denoising as m_0 is the area under Doppler echo and wavelet analysis could not remove noise properly under Doppler echo.

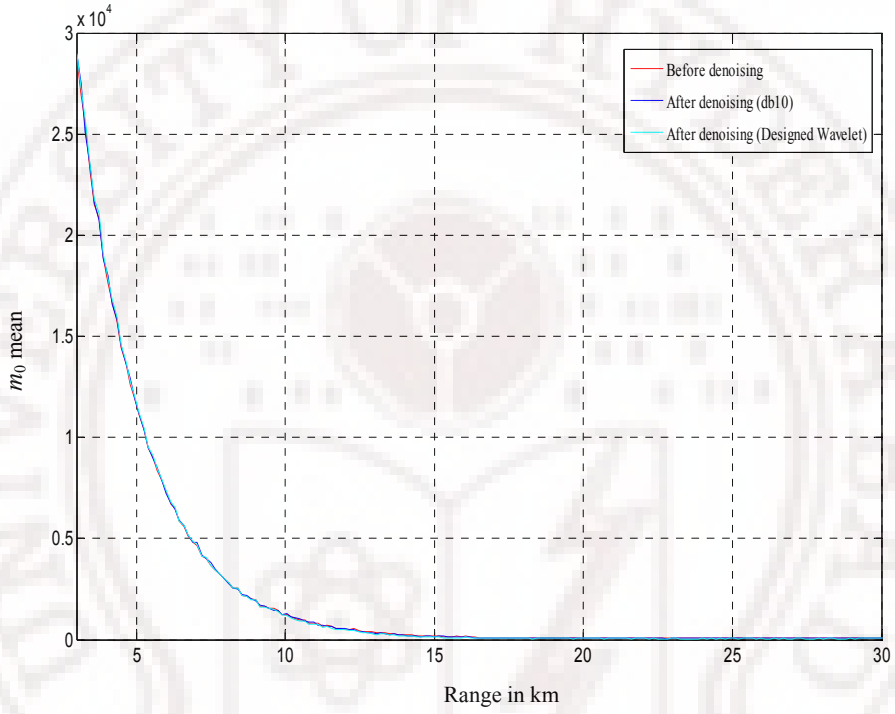

(7.5a)

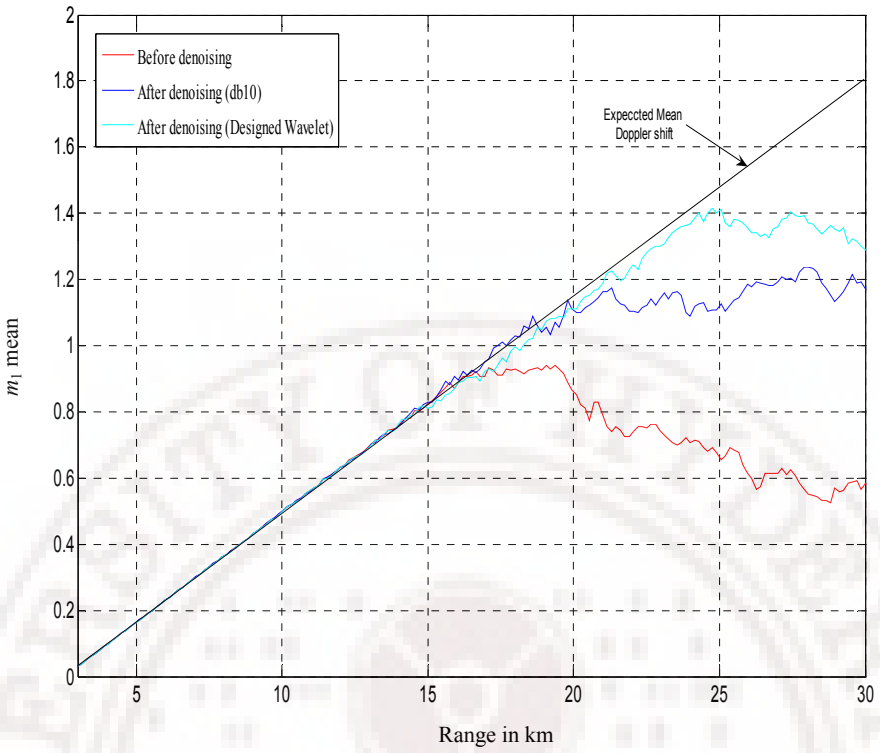

(7.5b)

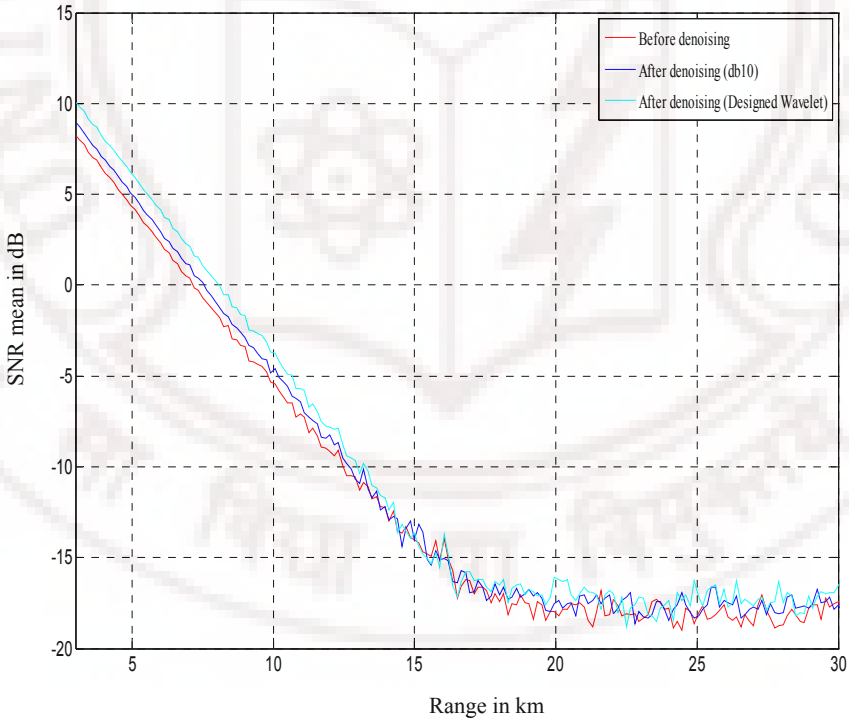

(7.5c)

Figure 7. 5: Mean values computed over 10 sets of identical simulated profiles corresponding to different seed values of the noise generator (a) Zeroth moment m_0 (b) First moment m_1 and (c) SNR

7.3 Conclusion

All these results show that the wavelet based denoising not only improves the range and also improves the accuracy in estimated physical parameters of such data. And this improvement is much more using designed wavelet compared to the Daubechies wavelet. When the data were denoised using the wavelet designed in this work and the Doppler echo was tracked using the Adaptive Tracking Method, the improvement in the range was typically about 60% higher compared to tracking the raw signal itself, where as standard wavelet and then the same adaptive tracking method was applied, the improvement in the range compared to raw signal was only about 30%. Further, SNR is improved considerably after denoising and designed wavelet provides improvement in accuracy of derived parameters and reduces standard deviations compared to Daubechies wavelet and raw data.

Chapter 8

Experimental Data Analysis

The wavelet denoising algorithms developed for the MST radar data were first tested using the simulated data, as the details of the signal are known in simulated data. These results are described in the Chapter 7. As shown in Chapter 7, wavelet denoising methodology improves the detectable range of the Doppler echoes. Subsequently the efficacy of this methodology in improving the detectability range of the Doppler echoes was tested using the experimental data. This chapter presents the results of analysis of the experimental data using wavelet denoising algorithms described in the earlier chapters. The results of the analysis on a large number of experimental data collected under different circumstances and the details of the improvement achieved both in the range of reliable detection of Doppler echoes as well as in the accuracies of the derived parameters are presented in detail.

8.1 MST Radar Range Improvement

The experimental data were collected using the MST radar facility at Gadanki, India (13.5^0N, 79^0E). The data from the all four directions East, West, North and South (making angle of 10° with the vertical beam) were collected. The data were denoised using newly designed wavelet described in the Chapter 4 and tracked using the Adaptive Tracking Method (ATM) developed in Chapter 5. The correctness of the detected Doppler echoes using developed algorithms can be ascertained by comparing the East and West (or North and South) beams, as the profiles of the Doppler echoes in these two directions should show mirror symmetry within the normal ranges.

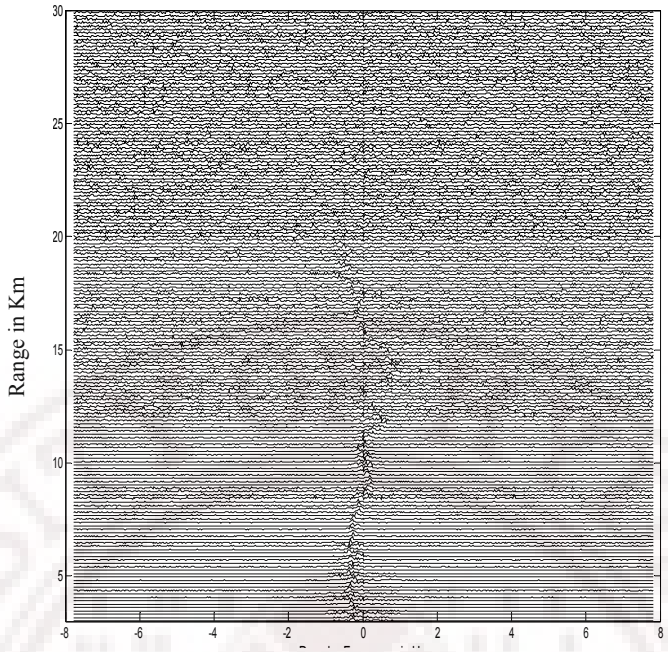

(8.1a)

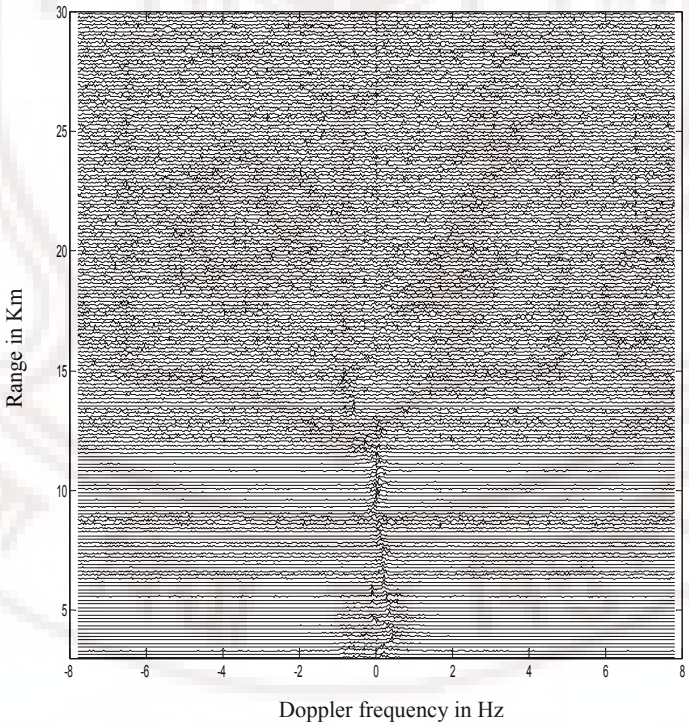

(8.1b)

Figure 8. 1: Experimental MST radar data (Raw dada) in (a) 10º East direction and (b) 10º West direction

Figures (8.1a and 8.1b) show profiles from 10^0 East and 10^0 West beam directions of the MST radar. As can be seen, in raw profiles with out adaptive tracking, the Doppler echoes are barely observable up to 10-12 km with expected mirror symmetry between the two beams.

Figure (8.2a) shows the position of Doppler echoes detected using the ATM, described in the Chapter 6 on this data. As can be seen the mirror symmetry exists only up to 13–14 km and presumably these are expected Doppler echoes. Beyond this the results of the East and West beams are not consistent and both appear on the same side of Doppler frequency = 0 axis indicating that the ATM method used here is unable to track the signal correctly above 14 km.

Figure (8.2b) shows the results of wavelet transform based denoising using designed wavelet in Chapter 4. After denoising the ATM is able to track the signal, with expected mirror symmetry between East and West beams, up to about 24 km. Further these results are compared with standard Daubechies wavelet. Figure (8.2c) shows the result of wavelet transform based denoising using Daubechies 10 wavelet. Here the ATM is able to track the signal up to 18 km satisfying mirror symmetry between East and West beams. These results show that the ATM is able to detect echoes more reliably when denoised using designed wavelet compared to Daubechies wavelet or raw data.

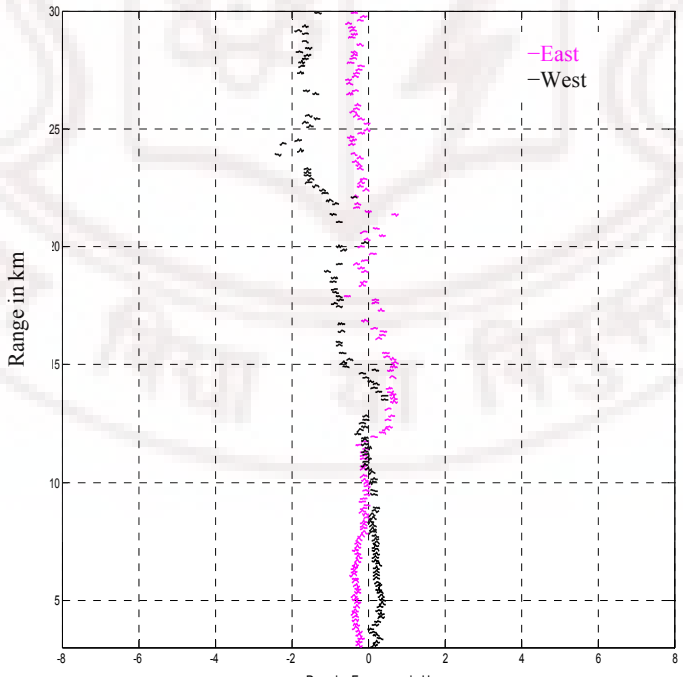

(8.2a)

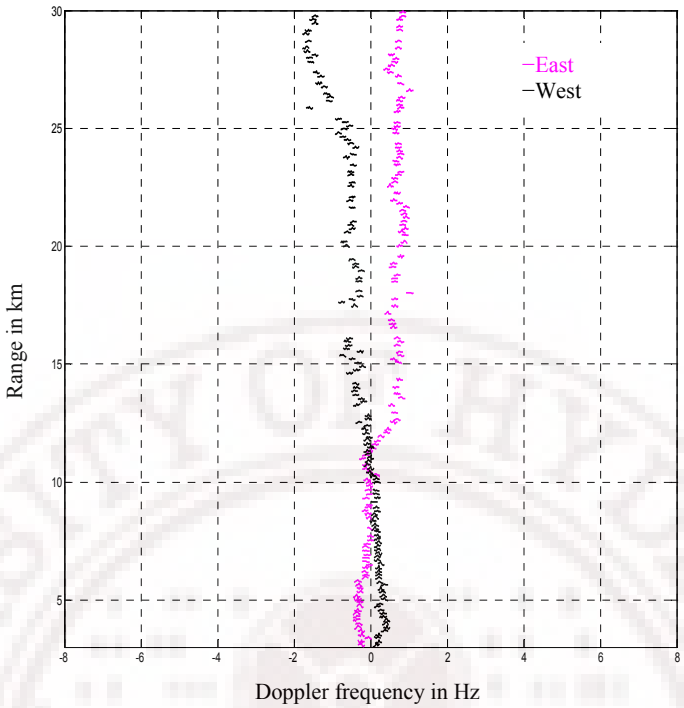

(8.2b)

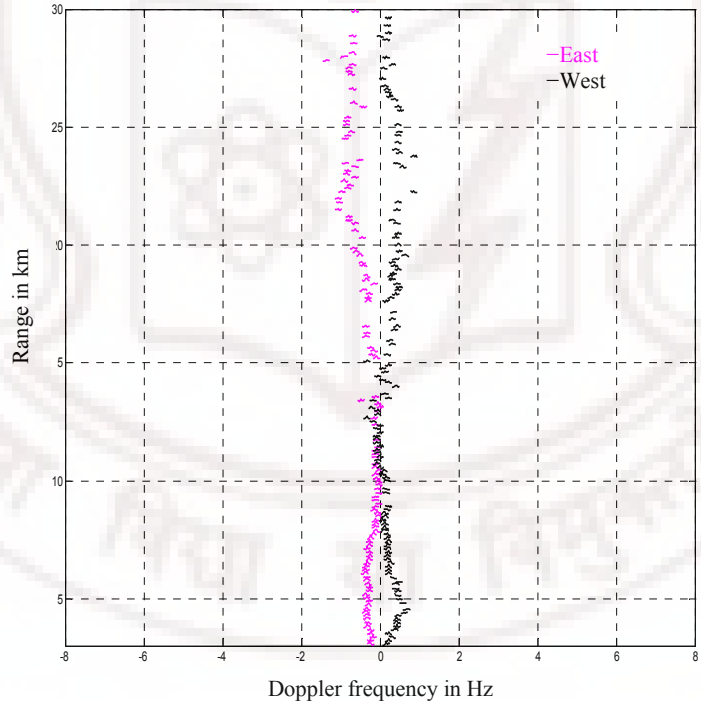

(8.2c)

Figure 8. 2: Experimental data Doppler echoes detected with ATM in 10° East and 10° West (Fig (8.1)) beam directions (a) Raw data (b) Denoised data using designed wavelet and (c) Denoised data using standard Daubechies db10 wavelet

8.2 Estimation of the accuracy of measured parameters from Experimental data

As is surmised in the Chapter 7 based on the simulated data, and as shown above in the case of experimental data, wavelet based denoising algorithm improves the range over which the Doppler echoes are reliably detected; besides, it also improves the accuracy of the parameters derived from such data. It is also verified on simulated data in Chapter 7. To examine to what extent the wavelet based denoising improves the accuracy of the measured parameters several sets of Indian MST radar Doppler profiles (over 10) in 10º East beam direction were collected in a very short span (about half an hour) under steady weather conditions. The assumption here is that wind parameters should not change with in this span of time and hence all sets of data should provide similar wind parameter values. An Adaptive Tracking Method developed in Chapter 6 was used to identify the Doppler echoes of all these profiles. The first three moments corresponding to the Doppler spectra (m_0, m_1 and m_2) were computed for some chosen range bins. Then mean and standard deviations of these parameters over all the sets of data (over 10) were computed. Similar computations were performed after denoising these signals using the designed wavelet. This procedure was repeated with standard wavelet db10 for denoising. Further, this process was repeated over all range bins of those ten sets of data. The Table 8.1 shows the results of these computations for some chosen range bins. The values above parenthesis are mean values and values in parenthesis are the standard deviations in the values of the estimated parameters. As can be seen from the Table 8.1, the SNR has considerably improved in all cases after denoising and designed wavelet gives better SNR values than standard wavelet db10. Further the standard deviations in derived parameters such as m_1 has considerably reduced even in lower altitudes where other methods can also detect the Doppler echo showing that the denoising using the designed wavelet increases the accuracy of the measurements even when the Doppler echoes are otherwise detectable. However, as it was seen in simulated data analysis in Chapter 7 there is no considerable improvement in parameters m_0 and m_2 standard deviations as these parameters are corresponds to area and width of the Doppler echo and wavelet denoising couldn't remove noise properly under the Doppler echo. . The mean (standard deviation) value of m_2 at an altitude 14.85 km computed over ten experimental raw profiles as explained above is 2.45×10^{-2} (1.04×10^{-2}). When the same data were denoised using

designed wavelet this was $1.6\text{x}10^{-3}$ ($0.569.9\text{x}10^{-4}$) and $2.05\text{x}10^{-3}$ ($0.52\text{x}10^{-4}$) for Daubechies wavelet.

Table 8. 1: Mean and standard deviations of derived parameters computed over 10 sets of Experimental profiles in 10^0 East beam direction at different altitudes.

Range in km	m_0 (x 10^3)			m_1 in Hz			SNR in dB		
	Before Denoising	After Denoising (Designed Wavelet)	After Denoising (db10)	Before Denoising	After Denoising (Designed Wavelet)	After Denoising (db10)	Before Denoising	After Denoising (Designed Wavelet)	After Denoising (db10)
3.6	48.06 (25.26)	48.83 (26.41)	48.65 (25.80)	-0.388 (0.08)	-0.386 (0.08)	-0.39 (0.078)	51.60 (27.24)	120.47 (66)	115.20 (68.72)
4.65	3.34 (2.77)	4.07 (2.59)	4.08 (2.548)	-0.345 (0.086)	-0.297 (0.061)	-0.3 (0.061)	3.97 (3.70)	10.82 (6.66)	10.31 (6.05)
7.35	0.53 (0.50)	0.56 (0.476)	0.44 (0.502)	-0.22 (0.153)	-0.19 (0.136)	-0.16 (0.129)	-5.71 (7.00)	-0.78 (5.70)	-3.03 (6.01)
9.45	0.12 (0.152)	0.14 (0.155)	0.07 (0.107)	-0.05 (0.296)	0.04 (0.138)	-0.055 (0.187)	-13.96 (8.49)	-7.93 (5.84)	-10.47 (5.18)
13.2	0.008 (0.013)	0.0003 (0.003)	0.0001 (0.004)	0.13 (0.485)	0.185 (0.245)	0.131 (0.214)	-22.96 (5.64)	-20.92 (5.72)	-22.22 (3.61)
14.85	0.021 (0.032)	0.014 (0.023)	0.006 (0.008)	0.175 (0.466)	0.277 (0.277)	0.145 (0.285)	-20.58 (6.26)	-19.93 (7.56)	-20.37 (4.94)
16.95	0.0016 (0.008)	0.0005 (0.002)	0.001 (0.004)	0.05 (0.738)	0.147 (0.185)	0.146 (0.235)	-23.11 (3.62)	-24.80 (4.34)	-23.54 (4.84)
18.9	0.00003 (0.007)	0.0003 (0.003)	0.004 (0.005)	-0.08 (0.87)	0.223 (0.243)	0.162 (0.261)	-26.15 (5.13)	-22.92 (4.01)	-19.3 (4)
20.25	0.001 (0.005)	0.001 (0.002)	0.002 (0.002)	-0.142 (0.837)	0.0034 (0.292)	0.151 (0.402)	-23.39 (1.74)	-22.52 (3.95)	-24.93 (4.37)
22.65	0.002 (0.005)	0.003 (0.001)	0.002 (0.002)	-0.064 (0.891)	0.018 (0.28)	0.052 (0.360)	-24.64 (4.05)	-21.65 (2.12)	-23.88 (3.42)
24.15	0.0001 (0.004)	0.002 (0.003)	0.001 (0.004)	-0.064 (0.857)	0.122 (0.511)	0.01 (0.573)	-24.33 (1.53)	-22.51 (3.73)	-21.76 (2.20)

Figure (8.3) shows mean and standard deviations of extracted physical parameters m_0, m_1 and SNR over all range bins (over ten sets) of data. Here standard deviation is plotted around the mean value vertically. However, as it is expected there is no much improvement in standard deviations in m_0 as shown in figures (8.3a) but m_1 is improved substantially after denoising and designed wavelet results smaller standard deviations compared to standard wavelet db10 as shown in Fig (8.3b). Further, it can be observed that SNR is improved after denoising as shown in (8.3c).

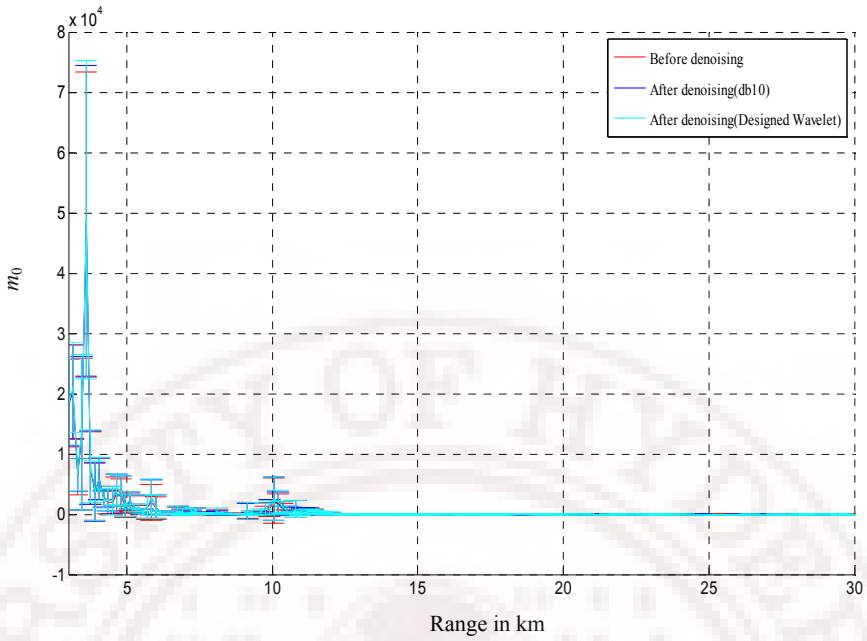
x 10^4
Before denoising
After denoising(db10)
After denoising(Designed Wavelet)
m_0
Range in km

(8.3a)

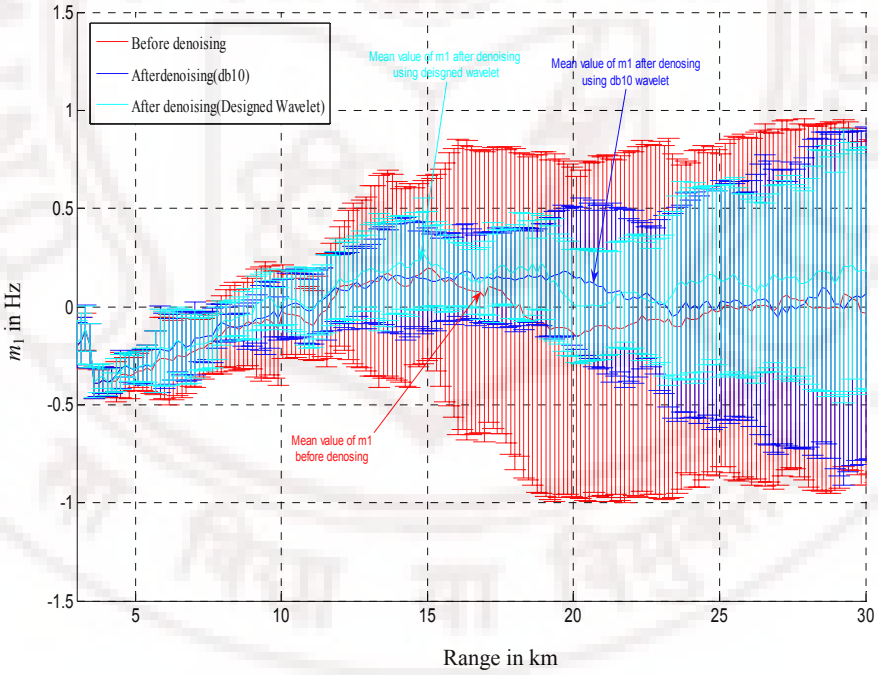
Before denoising
Afterdenoising(db10)
After denoising(Designed Wavelet)
Mean value of m1 after denoising using designed wavelet
Mean value of m1 after denosing using db10 wavelet
Mean value of m1 before denosing
m_1 in Hz
Range in km

(8.3b)

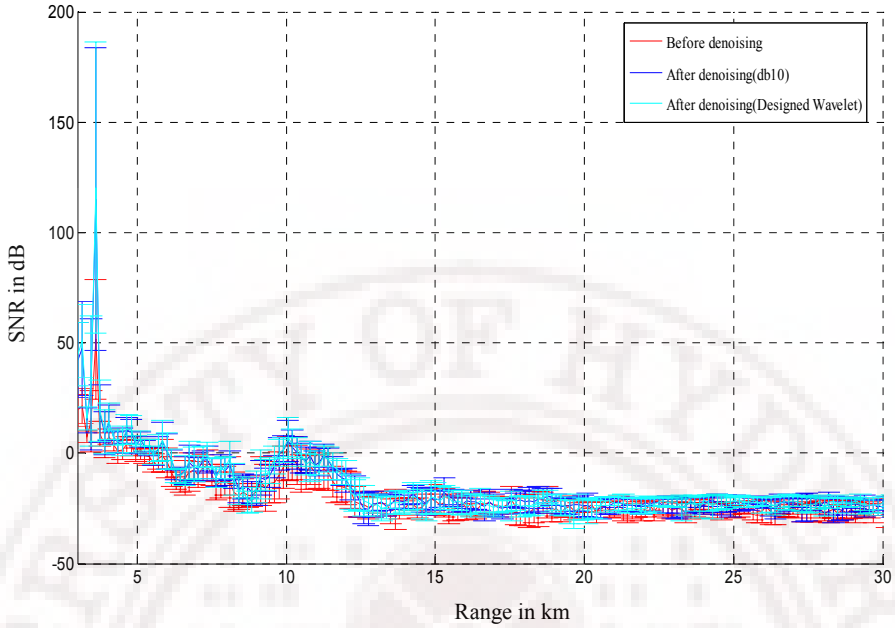

(8.3c)

Figure 8. 3: Mean and standard deviations computed over ten sets of experimental profiles in 10^0 East beam direction, collected in a short span under steady weather conditions (a) Zeroth moment m_0 (b) First moment m_1 and (c) SNR. Here length of error bar (vertical lines) indicates amount of deviation from average value.

The individual plots of standard deviations of derived parameter m_0, m_1 and SNR, computed over ten sets of experimental profiles in 10^0 East direction as explained above are shown in Fig (8.4). As seen in Fig (8.4b), standard deviations in m_1 after wavelet analysis are smaller and designed wavelet gives better standard deviations than standard db10 wavelet. Further, this improvement is much more in higher altitudes compared to lower altitudes.

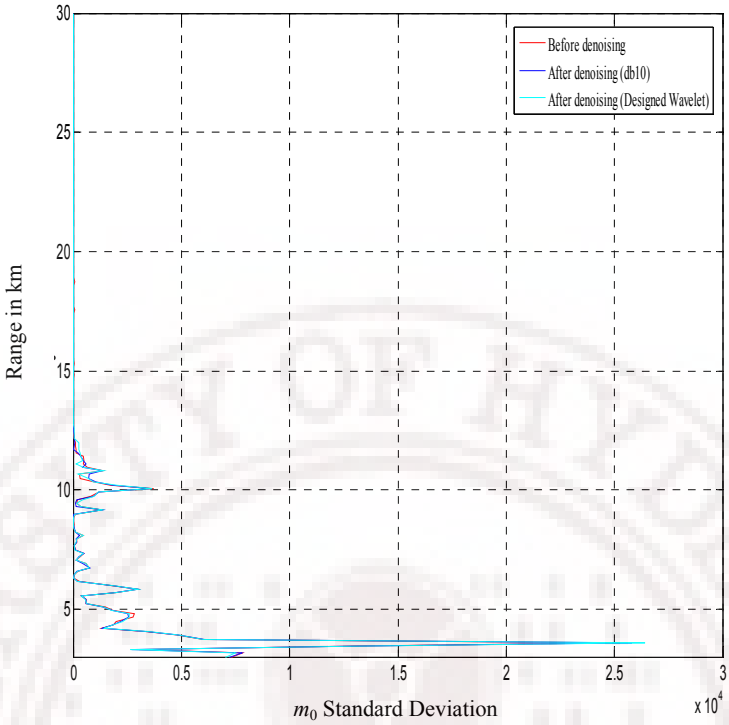
Before denoising
After denoising (db10)
After denoising (Designed Wavelet)
Range in km
m_0 Standard Deviation
x 10^4

(8.4a)

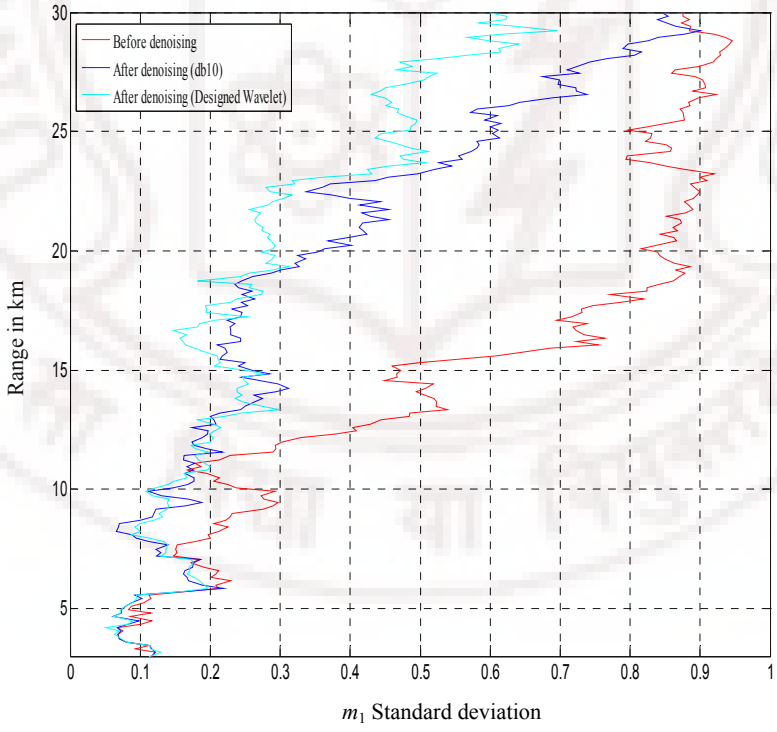
Before denoising
After denoising (db10)
After denoising (Designed Wavelet)
Range in km
m_1 Standard deviation

(8.4b)

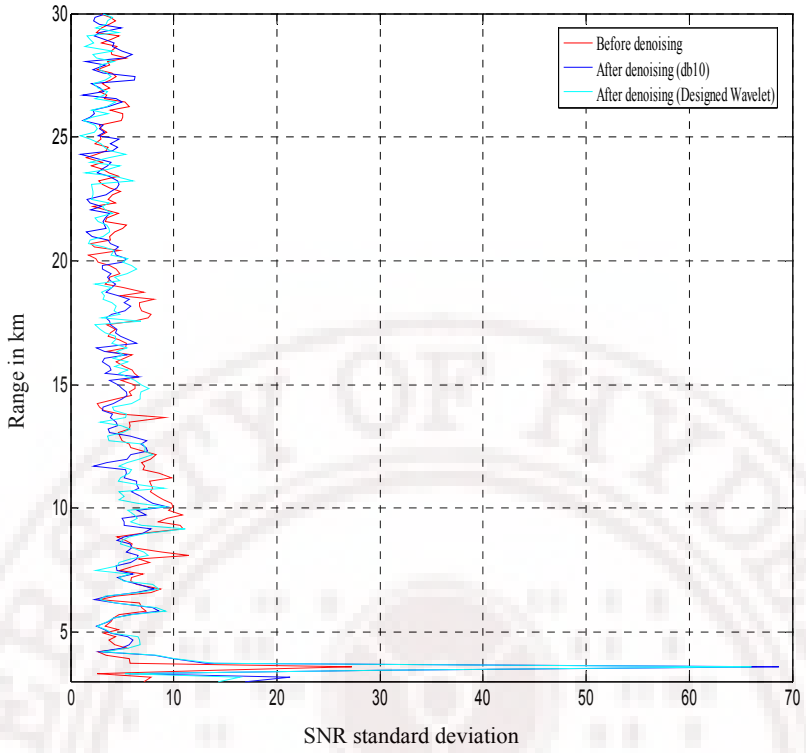

(8.4c)

Figure 8. 4: Standard deviations computed over ten sets of experimental profiles in 100 East beam direction, collected in a short span under steady weather conditions (a) Zeroth moment m_0 (b) First moment m_1 and (c) SNR

8.3 Conclusion

These studies show that the wavelet analysis based denoising of MST radar data improves the detectable range of Doppler echoes. These studies also show that the wavelet designed to suite clear air echoes specifically performs better than the available standard wavelets. While the standard wavelet (db10) based denoising improves the ability to detect Doppler echoes reliably by about 40% (improvement in the range), employing the wavelet designed in this work provides almost 80% improvement. This clearly demonstrates the suitability of the designed wavelet to the clear air echo signals of the MST radar. Besides, wavelet denoising improves SNR and hence the accuracy in estimated physical parameters such as in m_0, m_1 and m_2 as evidenced by the decrease in the mean square deviations in the large sets of data collected under steady weather conditions. Further, the wavelet designed in this work provides smaller deviations compared to the standard wavelet (Daubechies db10).

Chapter 9

Conclusions

9.1 Summary of research work

The aim of this thesis to use wavelet transform based signal processing to improve the range, over which the signals can be reliably detected, of an atmospheric radar such as Mesosphere-Stratosphere-Troposphere (MST) radar. The MST radar echo is extremely weak because it is a result of scattered energy of an RF pulse fired from the ground, and the scattering occurs due to variation in RF refractive index of neutral atmosphere due to the variations in the density with altitude. It is estimated that the signal strength drops typically by about 2 dB per km [Anandan et al., 2005] and the signal is obscured by the noise beyond a range when the SNR drops below -10 dB. The range up to which discernable signal can be observed in MST radar data is limited to typically 12-14 km, when only standard signal averaging and filtering techniques are used. Certain adaptive techniques were proposed to trace the signals from noisy data at higher ranges (up to 16-22 km). Similarly higher order spectral estimation technique was used to account for non-Gaussian nature of the Doppler echoes. All these methods have yielded reliable detection of the Doppler echoes to a maximum range of about 22 km under favorable conditions. The work reported here deals with application of discrete time wavelet transform for denoising and analysis of MST radar data with a view to increase the height coverage and improve the accuracy of the parameters extracted from the spectra. The Experimental data used in this work was collected using the MST radar facility at the National Atmospheric research laboratory at Gadanki, India (13.5^0N, 79^0E).

The advantages of wavelet transforms such as providing time-frequency representation and freedom to choose basis function (with in certain constraints) are exploited in wavelet analysis of MST radar data in this work. When chosen basis function resembles the functional form of the signal of interest, then wavelet transform provides the sparsest representation of the signal, wherein the entire energy in the signal is with in

few wavelet coefficients, facilitating good signal to noise separation. Therefore first step in this work was to design a wavelet suitable to clear-air echoes of MST radar. As the spectrum of the MST radar clear-air Doppler echo is predominantly of Gaussian in nature in the off-vertical direction, it was assumed that the wavelet basis function is a shifted Gaussian in frequency domain. The corresponding MRA filter coefficients were computed by rewriting the recursion relations of the low pass filter coefficients in terms of trigonometric functions of Sine and Cosine represented by parametric angles broadly following the algorithm used by Soon and Huat [Soon and Huat, 2002]. Then these parametric angle values were obtained by LEVENBERG-MARQUARDT optimization method. It was found that 8 filter coefficients adequately represent chosen wavelet. Then high pass filter coefficients were calculated using the recursion relation between low pass and high pass filter coefficients. Frequency response of these filter coefficients were found to be as desired i.e. say, as in the case of a standard wavelet like Daubechies wavelet (db10). It was verified, by performing forward and inverse transform operations on MST radar signal, that the designed wavelet reconstructed back the signal without any observable artifacts.

Then it is necessary to find out the required levels of decomposition for the designed wavelet for MST radar data before applying denoising technique. It was found that three-level wavelet decomposition is sufficient in the present case. Then proper thresholding method and threshold values were selected in order to get best level of denoising. Different standard threshold selection techniques such as an Adaptive threshold, Universal threshold, a Heuristic threshold and Minimax (minimum of maximum) threshold selection method were examined and hard and soft thresholding techniques were considered. These techniques were tested by denoising both reasonably strong and reasonably weak signals. After extensive study it was found that the Adaptive threshold selection technique provided suitable thresholds, the threshold values are slightly adjusted manually in order to have single set of thresholds for all the ranges.

It was also found that the soft thresholding results in better SNR values, compared to hard thresholding in the case of strong signals whereas hard thresholding is better in the case of weak signals. The signals at lower altitudes can be even tracked without denoising techniques and our main concern is about weak signals at higher altitudes. Hence hard thresholding technique is chosen for MST radar data. It was also observed that designed wavelet results better SNR improvement compared to standard wavelet db10.

The denoising methods developed for MST radar data were first tested on simulated data as the details of the signal are known in simulated data. The Doppler echo in these simulated spectra was chosen to have Gaussian distribution with width typical of observed Doppler echoes, with a chosen shift. Random Gaussian noise was added to this spectrum to obtain a noisy signal by using standard noise generator. The peak value for the Doppler echo was chosen to be unit for the lowest range bin. Then the data for higher range bins were generated by reducing the Doppler echo strength by 2 dB per every kilometer keeping the noise power constant as in the case of a realistic MST radar data. Different experimental situations were simulated by varying the Doppler shifts in a chosen fashion. The situation of different data collections under conditions where the wind parameters are not expected to vary, where only random noise values vary (with the same noise power) were replicated by generating the profiles for different seed values of the noise generator. Wavelet based denoising technique is applied on all these profiles to verify denoising performance.

Adaptive tracking methods were employed earlier to track the MST radar signals in the higher range bins, where the signal strength becomes comparable or even less than the noise level based on the knowledge of the position and other details of the Doppler echoes at lower bins. An Adaptive Tracking Method (ATM) is developed in this work on the same lines of one of the earlier algorithms with suitable modifications. This adaptive tracking algorithm combined with wavelet denoising using the wavelets designed here was used in this work for the processing of the MST radar data.

The methodology developed in this work for the wavelet denoising of the MST radar data was first tested using the simulated data, generated as described the above, as the details of the signal are known in simulated data. Different types of variations in the Doppler shifts were considered. The analysis of the data using the procedure as described the above resulted in an increase in the range, on the average, by about 60%. That is, when the data were denoised using the wavelet designed in this work and the Doppler echo was tracked using the ATM described the above, the range up to which the signal was correctly detected was typically about 60% higher compared to tracking the raw signal itself. Further if the denoising is performed using the next best suited wavelet, *viz*., Daubechies wavelet and then the same adaptive tracking method was applied, the improvement in the range compared to raw signal was only about 30%. This demonstrates that the wavelet based denoising provides considerable improvement in the range over which the Doppler echo signals can be reliably detected and perhaps the

designed wavelet is better suited compared to the best suited standard wavelet to the clear air echo signals of the MST radar.

Subsequently the combination of wavelet transform based denoising technique and ATM was employed on the experimental data. The correctness of the detected Doppler echoes using developed algorithms was ascertained by comparing the East and West beams, and North and South beams as the profiles of the Doppler echoes in the opposite directions should show mirror symmetry within the normal ranges. The results show that the detected echoes show mirror symmetry to much higher ranges when they were denoised using the designed wavelets compared to the Daubechies wavelet or the raw data. These studies show that the wavelet designed in this work improves the ability to detect Doppler echoes reliably by about 80% (improvement in the range); where as Daubechies wavelet provides only 40% improvement. This clearly demonstrates the suitability of the designed wavelet to the clear air echo signals of the MST radar.

These studies show that the wavelet based denoising technique not only improves the range over which the Doppler echoes are reliably detected; it also improves the accuracy of the parameters derived from such data. This is first demonstrated on simulated data. As mentioned about several sets (about 10) of simulated data with different seed values (keeping all other parameters constant) were considered equivalent to the data collected by repeating the experiment under identical experimental conditions. The Doppler echoes of all these profiles are identified by ATM. The first three moments corresponding to the Doppler spectra (m_0, m_1 and m_2) were computed for some chosen range gates. Then mean and standard deviations of these parameters over all the sets of data (about 10) were computed. Similar computations were performed after denoising these signals using the designed wavelet and standard db10 wavelet. These results were compared with the raw data. It was found that the wavelet based denoising technique, besides increasing the detectable range, improves the accuracy of estimated parameters even at lower altitudes where correct Doppler echo were detected without denoising. Similar computations were made on experimental data as well by collecting 10 sets of the MST radar data with a time span of about half an hour on a day when the weather was steady. It was assumed that the weather conditions, such as wind velocities and directions did not change within this short period. The data was denoised using the designed wavelet and Doppler echoes were detected using the adaptive tracking method ATM for each of these sets of the data. The first three moments (m_0, m_1 and m_2) of the Doppler echoes of each range in each of these profiles were computed for those detected echoes.

Now the data for a given range in all these sets were averaged and corresponding standard deviations were computed. These results were compared with the raw data. The results show that wavelet analysis improved SNR and also standard deviation of measured parameters after denoising. However there is a nominal improvement in standard deviations in m_0 and SNR as it is expected since m_0 depends on shape of the Doppler echo, but m_1 is improved substantially after denoising and designed wavelet results smaller standard deviations compared to Daubechies wavelet.

9.2 Possible Extensions of the Work

The ability of wavelet transform based analysis of MST radar data is not limited to improving detectable range and improve accuracy in estimated parameters. As the wavelet analysis provides good time frequency representation of a given signal wavelet analysis can be used to detect specific signatures like meteor or lightning signals, detect wind disturbances (localized and transient gravity waves). Similarly, the wavelet used here is specifically designed for clear air echoes and hence it gives sparse representation only for clear air echoes, wavelet based analysis can be potentially be used to separate precipitation echoes from clear air echoes. Thus this work, which points to the applicability of wavelet based signal processing and analysis could be extended to the above areas. Another possible extension of this work is implementation of the above wavelet based signal-processing procedures on DSP processor based hardware or FPGA for online computation, which will vastly improve the speed of computations there by permitting different types of online analysis of the data.

Appendix A

Levenberg-Marquardt algorithm Matlab code

waveletfitfn2para.m

```
% ***************************** waveletfitfn2para*****************************
% A driver program to use lmfit.m fitting program.  Specify names of the X and Y data, error in
% Y vectors (S), if there are more than one functions (funcsel ('y'/'n')), number of functions (nfunc,
% maximum three), if there are any frozen parameters (fropt), frozen %parameter index vector (Froz), if  %
the parameters are to % be saved on the disc (savopt  ('y'/'n')),

% ************************************************************************

clear;clc;close all;
totalwidth=7;
Npoints=256;
dt=totalwidth/Npoints;
t1=0:dt:totalwidth/2-dt;
t2=totalwidth/2+dt:dt:totalwidth;
t=[t1,t2];
phi=fphical(t);
Ydati=[real(phi),imag(phi)];
Xdati=[t,t];
yerr = 1;
S = Ydati*0.0001;
funsel = 'Y';
nfunc = 2;
% Funam = 'RecWaveletreal';
P = [pi/4,pi/4];
Fact = [1,1,1];
fropt ='n';
Froz = [1,2,3];
savopt = 'n';
lmfit

% To generate freqencies spaced uniformly on a logarithemic scale.

CalWavelet = RecWaveletreal(Xdati(1:Npoints),Parafi);
 plot(Xdati(1:Npoints),Ydati(1:Npoints));
 hold on;plot(Xdati(1:Npoints),Ydati(1:Npoints),'.');
 plot(Xdati(1:Npoints),CalWavelet,'-r');plot(Xdati(1:Npoints),CalWavelet,'.k')
 title(['LEVENBERG-MARQUARDT FIT of real part       ',Datid]);
 xlabel('Time (S)');
 ylabel('Amplitude');

 CalWavelet = RecWaveletimag(Xdati(1:Npoints),Parafi);
 figure;plot(Xdati(1:Npoints),Ydati(Npoints+1:2*Npoints));
 hold on;
 plot(Xdati(1:Npoints),CalWavelet,'-r');plot(Xdati(1:Npoints),CalWavelet,'.k')
 title(['LEVENBERG-MARQUARDT FIT of real part       ',Datid]);
```

```
 xlabel('Time (S)');
 ylabel('Amplitude');


a=Parafi(1);b=Parafi(2);
c=pi/4-a-b;
h(1)=cos(a)*cos(b)*cos(c);
h(2)=sin(a)*cos(b)*cos(c);
h(3)=-cos(a)*sin(b)*sin(c);
h(4)=-sin(a)*sin(b)*sin(c);
h(5)=-sin(a)*sin(b)*cos(c);
h(6)=cos(a)*sin(b)*cos(c);
h(7)=-sin(a)*cos(b)*sin(c);
h(8)=cos(a)*cos(b)*sin(c);

N=length(h);
figure;filterfreqresp(h,N);
```

lmfit.m

```
% ************************** LMFIT **************************
% LMFIT is an interactive driver program for the general purpose routine mrqm which does least-squares
% fitting of parameters in functions with nonlinear parameter dependence using Levenberg-Marquardt
% method.  The iterative fitting procedure is terminated when the joint condition (absolute change in chi- %
square < 0.1) & (relative change in chi-square < 0.00 is satisfied in two successive iteration steps. The  %
fitting function(s) must be specified in a function file, which, upon calling Y=fnamce(X,P), supplies a    %
vector Y of function values for a vector of independent variable values and a vector P of parameter        %
values. It is convenient to write a separate script file containing the input vector. When several such    %
script files are used in one MATLAB session, the workspace must be cleared before running a new file. %
The numerical output of LMFIT may (optionally) be saved on disk in a text file which can be accessed %
from within MATLAB (don't double-click the icon-ope from the File menu) or with a word processing %
editor. In the current version of LMFIT, graphs are not saved. All vectors passed between LMFIT and  %
MATLAB functions are column vectors.

% ************************************************************************

disp('')
disp('***** NONLINEAR LEAST-SQUARES FIT BY LEVENBERG-MARQUARDT METHOD
*******')
% Acquire input date and convert row vectors to column vectors

Xdat = trscol(Xdati);
ndx = length(Xdat);
Ydat = trscol(Ydati);
ndy = length(Ydat);

if yerr == 1
   Ysig = trscol(S);
elseif yerr == 2
      ysig = S;
      Ysig = ysig*ones(ndy,1);
elseif yerr == 3
      yspr = SR;
      Ysig = yspr*Ydat;
elseif yerr == 4
      Ysig = ones(ndy,1);
end
if exist('ctd') == 0
if ndx > 49
```

```
  dspdat = input('DISPLAY X-Y DATA TABLE ?      Y/N : ','s');
% dspdat=inputfunc(dispdata);
  if dspdat == 'Y', dspdat = 'Y'; end
else
  dspdat = 'Y';
end

if funsel == 'Y', funsel = 'Y'; end

if funsel == 'Y'

  if nfunc > 3
    disp('SORRY: Maximum 3 fitting functions')
  end
fun1 = input('FILE NAME FOR FUNCTION 1     =','s');
fun2 = input('FILE NAME FOR FUNCTION 2     =','s');

% fun1 =inputfunc(funcreal);
% fun2 =inputfunc(funcimag);

if length(fun1) ~= length(fun2)
  disp('SORRY: All file names must be of same length')
  fun1 = input('FILE NAME FOR FUNCTION 1   =','s');
  fun2 = input('FILE NAME FOR FUNCTION 2   =','s');
%    fun1 =inputfunc(funcreal);
%    fun2 =inputfunc(funcimag);
end
  Funam = [fun1;fun2];
  Fnprt = [fun1,', ',fun2];
  Nf1 = input('DATA INDEX VECTOR FOR FUNC 1 = ');
  Nf2 = input('DATA INDEX VECOTR FOR FUNC 2 = ');
%    Nf1 =inputfunc(funcrealindx);
%    Nf1 =inputfunc(funcrealindx);
%
  if nfunc == 3
    fun3 = input('FILE NAME FOR FUNCTIN 3      =','s');
    if length(fun1) ~= length(fun3)
      disp('SORRY: All file names must be of same length')
      fun3 = input('FILE NAME FOR FUNCTIN 3      =','s');
    end
    Funam = [Funam;fun3];
    Fnprt = [Fnprt,', ',fun3];
    Nf3 = input ('DATA INDEX VECTOR FOR FUNC 3   = ');
  end
  Fidx(Nf1) = ones(size(Nf1));
  Fidx(Nf2) = 2*ones(size(Nf2));
  if nfunc == 3
    Fidx(Nf3) = 3*ones(Nf3);
  end
  Fidx = trscol(Fidx);
  if length(Fidx) ~= ndx
    error('INPUT ERROR: Function index vectors do not match X vector')
  end
else
  Fnprt = Funam;
  Fidx = ones(ndx,1);
end
end
Para = trscol(P);
nptot = length(Para);
```

```
List = (1:nptot)';

if fropt == 'y', fropt = 'Y'; end
if fropt == 'Y'
  Froz = trscol(Froz);
  List(Froz) = [];
  Chek = [List;Froz];
  if length(Chek) ~= nptot
    disp('INPUT ERROR: Improper list of frozen parameter indices')
    Froz = trscol(input('FROZEN PARAMETER INDEX VECTOR  = '));
    List(Froz) = [];
    Chek = [List;Froz];
    if length(Chek) ~= nptot
      error('INPUT ERROR: Improper list of frozen parameter indices')
    end
  end
end
npfit = length(List);
nfree = ndx - npfit;
if nfree < 0
  error('ERROR:Number of fitting parameters exceeds number of data points!')
end
Pnz = find(Para(List));
if length(Pnz) < npfit
  disp('WARNING: Function derivative at par = 0 computed with dpar = 0.01')
end
if exist('ctd') == 0
if savopt == 'y", savopt = 'Y'; end
if savopt == 'Y'
  prtfil = input('NAME OF OUTPUT FILE     = ','s');
end
end

% Diplay input data

if savopt == 'Y'
  diastr = ['diary ',prtfil];
  eval(diastr)
end
Tc = fix(clock);
if Tc(4) < 10, ts4= '0'; else, ts4 = ''; end
if Tc(5) < 10, ts5= '0'; else, ts5 = ''; end
if Tc(6) < 10, ts6= '0'; else, ts6 = ''; end
Tid = [ts4,int2str(Tc(4)),':',ts5,int2str(Tc(5)),':',ts6,int2str(Tc(6))];
Datid = [date,'     ',Tid];
fprintf('\n\n')
disp(Datid)
aste = '*************************************************************';
dash1 = '----------------------------------------';
dash2 = '--------------------------------------------------';
dash3 = '------------------------------------------------------------';
dash4a = '------------------------------------------------------------';
dash4b = '----------------------';
dash4 = [dash4a dash4b];
head = 'NONLINEAR LEAST-SQUARES FIT BY LEVENBERG-MARQUARDT METHOD\n';
fitfun = ['Fitting function routine(s): ',Fnprt];
datpar = '%g parameters fitted to %g data points\n';
disp(aste)
fprintf(head)
disp(fitfun)
```

```
fprintf(datpar,npfit,ndx)
disp(aste)
disp('')
if dspdat == 'Y'
if yerr == 4
  dathead = ['    X-DATA      Y-DATA         X-DATA         Y-DATA'];
else
  dathead = ['   X-DATA     Y-DATA    Y-SIGMA    X-DATA   Y-DATA   Y-SIGMA'];
end
if rem(ndx,2)
  Xdat = [Xdat;NaN];
  Ydat = [Ydat;NaN];
  if yerr ~= 4, Ysig = [Ysig;NaN]; end
  ndx = ndx + 1;
end
Xr = reshape(Xdat,ndx/2,2);
Yr = reshape(Ydat,ndx/2,2);
if yerr ~= 4
  Ysr = reshape(Ysig,ndx/2,2);
  Tab = [Xr(:,1) Yr(:,1) Ysr(:,1) Xr(:,2) Yr(:,2) Ysr(:,2)];
else
  Tab = [Xr(:,1) Yr(:,1) Xr(:,2) Yr(:,2)];
end
if rem(ndy,2)
  Xdat(ndx) = []; Ydat(ndx) = [];
  if yerr ~= 4, Ysig(ndx) = [];end
  ndx = ndx -1;
end
disp(dathead)
if yerr ~= 4
  disp(dash3)
else
  disp(dash2)
end
disp(Tab)
if yerr ~= 4
  disp(dash3)
else
  disp(dash2)
end
disp('')
end
ithead = ['   ITERATION      LAMBDA      CHI2RED'];
disp(ithead)
disp(dash1)
Parain = Para;

% Initialize mrqmin and make the first iteration

iter = 0;
lam = -1;
Alfa = [];
[lam,chisq,oldchi,Para,List,Alfa,Beta,chisq0] = mrqmin(Funam,lam,Xdat,Ydat,...
                                                    Ysig,Para,List,Alfa,Fidx);
chired0 = chisq0/nfree;
lam0 = -1;
Iter = [iter lam0 chired0];
fprintf('   %6g  %14.1e  %12.4f\n', iter,lam0,chired0);
Resu = [Iter';Parain];
iter = iter + 1;
```

```
lam0 = 0.001;
chired0 = chisq/nfree;
Iter = [iter lam0 chired0];
fprintf('   %6g  %14.1e  %12.4f\n', iter,lam0,chired0);
Resu = [Resu [Iter';Para]];
test = 0;
marker = 0;

% Call mrqmin until chi-square has converged and display reduced chi-square
% after each iteration

while 1
  iter = iter + 1;
  prechi = oldchi;
  [lam,chisq,oldchi,Para,List,Alfa,Beta] = mrqmin(Funam,lam,Xdat,Ydat,Ysig,...
                                                  Para,List,Alfa,Fidx,Beta,oldchi);
  if chisq > prechi
    test = 0;
    marker = marker + 1;
    if lam >= 1e3,
      error('Check your input parameters and start again');
    end
  elseif (prechi/chisq - 1 < 0.001) & (prechi - chisq < 0.1)
    test = test + 1;
  end
  chired = oldchi/nfree;
  Iter = [iter lam  chired];
  fprintf('   %6g  %14.1e  %12.4f\n', iter,   lam,   chired)
  Resu = [Resu [Iter';Para]];
  if test == 2, break, end
end

disp(dash1)
disp('')
Parafi = Para';
chisqfi = chisq;

% Display iteration diary

diahd1 = '------------------------------- PARAMETER PATH ';
diahd2 = '---------------------------------';
diahead = [diahd1 diahd2];
disp(diahead)
disp('')
it = iter;
if it > 20
  it = 20;
  disp('Only the first 20 iterations are displayed')
end
Res1 = Resu;
It1 = '       0';
for k = 1:min(it,6)
   It1 = [It1,sprintf('%10.0f',k)];
end
if iter > 6
  Res1 = Resu(:,1:7);
  Res2 = Resu(:,8:it+1);
  It2 = '       7';
  for k = 8:min(it,13)
     It2 = [It2,sprintf('%10.0f',k)];
```

```
  end
end
if iter > 13
  Res2 = Resu(:,8:14);
  Res3 = Resu(:,15:it+1);
  It3 = '      14';
  for k = 15:min(it,20)
     It3 = [It3,sprintf('%10.0f',k)];
  end
end
fprintf('ITERATION'), disp(It1)
for k = 1:nptot
   Para1 = '',
   for n = 0:min(it,6)
           Para1 = [Para1,sprintf('%10.4f',Res1(3+k,1+n))];
   end
   fprintf('PARAM(%g)  ',k), disp(Para1)
end
disp(dash4)
if iter > 6
  fprintf('ITERATION'), disp(It2)
  for k = 1:nptot
    Para2 = '';
    for n = 7:min(it,13)
           Para2 = [Para2,sprintf('%10.4f',Res2(3+k,n-6))];
    end
   fprintf('PARAM(%g)  ',k), disp(Para2)
  end
  disp(dash4)
end
if iter > 13
  fprintf('ITERATION'), disp(It3)
  for k = 1:nptot
    Para3 = '';
    for n = 14:min(it,20)
           Para3 = [Para3,sprintf('%10.4f',Res3(3+k,n-13))];
    end
   fprintf('PARAM(%g)  ',k), disp(Para3)
  end
  disp(dash4)
end
disp('')

% Call mrqmin with lambda = 0 and display final parameters with uncertainties
% and the covariance matrix

lam = 0;
[lam,chisq,oldchi,Para,List,Alfa,Beta,Cova]=mrqmin(Funam,lam,Xdat,Ydat,...
                                        Ysig,Para,List,Alfa,Fidx,Beta,oldchi);
if yerr == 4
  yvarc = chisqfi/nfree;
  ysigc = sqrt(yvarc);
  Cova = yvarc*Cova;
  Ysig = ysigc*ones(ndx,1);
else
  Yfit = funcs(Xdat,Fidx,Funam,Parafi);
  Ydif = Ydat - Yfit;
  yvarc = Ydif'*Ydif/nfree;
  ysigc = sqrt(yvarc);
end
```

```
Sigma = (sqrt(diag(Cova)))';
Par1 = '';
for n = 1:min(nptot,6)
  Par1 = [Par1,sprintf('%10.4f',Parafi(n))];
end
Sig1 = Sigma;
if nptot > 6
  Par2 = '';
  for n = 7:min(nptot,12)
  Par2 = [Par2,sprintf('%10.4f',Parafi(n))];
end
  Sig1 = Sigma(1:6);
  Sig2 = Sigma(7:n);
end
if nptot > 12
  disp('Only the first 12 parameters are displayed')
end
fprintf('FINAL PARAMETERS'), disp(Par1)
fprintf('UNCERTAINTIES   '), disp(Sig1)
if nptot > 6
  fprintf('FINAL PARAMETERS'), disp(Par2)
  fprintf('UNCERTAINTIES   '), disp(Sig2)
end
disp('')
covhd1 = '-----------------------RELATIVE COVARIANCE MATRIX ';
covhd2 = '----------------------';
covhead = [covhd1,covhd2];
disp(covhead)
disp('')
Covred = Cova/max(diag(Cova));
if nptot > 8
Covplt = Covred(1:8,1:8);
else
  Covplt = Covred;
end
disp(Covplt)
if nptot > 8
  disp('Only the first 8 parameters are displayed')
end
disp(dash4)
disp('')

% Compute chi-square probability (goodness-of-fit)

if yerr ~= 4
  chiprb = gammainc(nfree/2,chisqfi/2);
  fprintf('Credibility of given model (1 -high, 0 -low) = %10.4f\n',1-chiprb)
end
fprintf('Computed standard deviation for all Y data = %10.4f\n\n\n',ysigc)
if savopt == 'Y', diary off, end
cont = n;
if cont == 'y', cont = 'Y'; end
if cont ~= 'Y', clear ctd, return, end
fprintf('\n\n\n')
ctd = 1;
lmfit
```

fphical.m

```
% A function to compute mother wavelet values for every time instant
```

```
function [phi]=fphical(t)
sig=0.12;
shift=0.4;
phi=(exp(-2*(pi^2)*(sig^2)*((t-3.5).^2))).*(exp(j*2*pi*shift*(t-3.5)));
```

covsrt.m

```
function Cova = covsrt(Covf,List,nptot,npfit)

% This MATLAB code was written based on the FORTRAN code in Press et al,
% Numerical Recipes, p 515, where detailed information can be found.

if npfit == nptot, Cova = Covf; return, end

Cova = zeros(nptot,nptot);
for i = 1:npfit
   for j =1:npfit
      Cova(List(i),List(j)) = Covf(i,j);
   end
end
```

funcs.m

```
function [Y,Dyda] = funcs(X,Fidx,Funam,Para)

% Function and derivative (w.r.t parameters) evaluation routine used by
% MATLAB functions LMFIT and mrqcof.

% Compute function vector

I1 = find(Fidx == 1);
if isempty(I1) == 0
  Y(I1) = feval(Funam(1,:),X(I1),Para);
end
I2 = find(Fidx == 2);
if isempty(I2) == 0
  Y(I2) = feval(Funam(2,:),X(I2),Para);
end
I3 = find(Fidx == 3);
if isempty(I3) == 0
  Y(I3) = feval(Funam(3,:),X(I3),Para);
end
Y = trscol(Y);
if nargout < 2, return, end

% Compute derivative matrix using central finite-difference approximation

Dp = 0.01*Para;
Pzero = find(Para == 0);
if isempty(Pzero) == 0
          Pz = length(Pzero);
  Dp(Pzero) = 0.01*ones(Pz,1);
end
nptot = length(Para);
for k = 1:nptot
   Parm = Para; Parp = Para;
   Parm(k) = Para(k) - Dp(k)/2;
   Parp(k) = Para(k) + Dp(k)/2;
```

```
   if isempty(I1) == 0
          Ym1 = feval(Funam(1,:),X(I1),Parm);
          Yp1 = feval(Funam(1,:),X(I1),Parp);
      Dyda(I1,k) = (Yp1 -Ym1)./Dp(k);
   end
   if isempty(I2) == 0
          Ym2 = feval(Funam(2,:),X(I2),Parm);
          Yp2 = feval(Funam(2,:),X(I2),Parp);
      Dyda(I2,k) = (Yp2 -Ym2)./Dp(k);
   end
  if isempty(I3) == 0
          Ym3 = feval(Funam(3,:),X(I3),Parm);
          Yp3 = feval(Funam(3,:),X(I3),Parp);
      Dyda(I3,k) = (Yp3 -Ym3)./Dp(k);
   end
end
```

mrqcof.m

```
function [chisq,Alfa,Beta] = mrqcof(Funam,Xdat,Ydat,Ysig,Para,List,Fidx)

% This MATLAB code was written based on the FORTRAN code in Press, et al,
% Numerical Recipes, p 527, where detailed information can be found.

% Compute model function vector and matrix of derivatives w.r.t all
% parameters at all experimental X values

[Yfit,Dyda] = funcs(Xdat,Fidx,Funam,Para);

% Compute linearized curvature matrix Alfa and vector Beta

Sig2 = 1./(Ysig.^2);
Ydif = Ydat - Yfit;
Dyda = Dyda(:,List);
npfit = length(List);
Alfa = zeros(npfit);
for k = 1:npfit
   DydaSk = Dyda(:,k).*Sig2;
   for n = 1:npfit
          Alfa(k,n) = DydaSk'*Dyda(:,n);
   end
end
Beta = Dyda'*(Ydif.*Sig2);

% Compute chi-square

Term = Ydif./Ysig;
chisq = Term'*Term;
```

mrqmin.m

```
function [lam,chisq,oldchi,Para,List,Alfa,Beta,Cova] = mrqmin(Funam,lam,...
          Xdat,Ydat,Ysig,Para,List,Alfa,Fidx,Beta,oldchi)

% Levenberg-Marquardt algorithm, varying the parameters to reduce chi-square
% The variables Beta and oldchi must not be altered by the calling routine.
% All vectors passed between mrqmin and other functions are column vectors.
% This MATLAB code is based on the FORTRAN code in Pres et al, Numerical
```

```
% Recipes, p 526, where detailed information can be found.

nptot = length(Para);
npfit = length(List);

% Initialization

if lam < 0
  lam = 0.001;
  [chisq,Alfa,Beta] = mrqcof(Funam,Xdat,Ydat,Ysig,Para,List,Fidx);
  oldchi = chisq;
  Cova = chisq;
  Ptry = Para;
end

% Compute covariance matrix when chi-square has covnerged

if lam == 0
  Covf = inv(Alfa);
  Cova = covsrt(Covf,List,nptot,npfit);

end

% Augment diagonal elements of linearized curvature matrix

Alfp = Alfa + diag(lam*diag(Alfa));
Pstp = Beta;

% Solve matrix equation by Guassian elimination

Pstp = Alfp\Pstp;

% Increment fitting parameters

Ptry = Para;
Ptry(List) = Para(List) + Pstp;

% Compute chi-square and curvature matrix with new parameters

[chisq,Alfp,Pstp] = mrqcof(Funam,Xdat,Ydat,Ysig,Ptry,List,Fidx);

% Test chi-square to decide change in lamda

if chisq < oldchi
  lam = lam/10;
  oldchi = chisq;
  Alfa = Alfp;
  Beta = Pstp;
  Para(List) = Ptry(List);
else
  lam = 10*lam;
end
```

trscol.m

```
function C = trscol(M)

% Transpose matrix M if it has more column than rows
% In particular, transform row vectors into column vectors.  *900725*
```

```
[r,c] = size(M);
if r < c
  C = M';
else
  C = M;
End
```

RecWaveletreal.m

```
 % computes real part of the wavelet based on recursion relation

function [RWReal]= fRecWaveletreal (xdat,para)
a=para(1);b=para(2);

c=pi/4-a-b;
h(1)=cos(a)*cos(b)*cos(c);
h(2)=sin(a)*cos(b)*cos(c);
h(3)=-cos(a)*sin(b)*sin(c);
h(4)=-sin(a)*sin(b)*sin(c);
h(5)=-sin(a)*sin(b)*cos(c);
h(6)=cos(a)*sin(b)*cos(c);
h(7)=-sin(a)*cos(b)*sin(c);
h(8)=cos(a)*cos(b)*sin(c);

%-----y' calculation using recursion relation------%
for G=1:length(xdat)
   phiCAL=0;
   for n=1:8
      SS=real(fphical(2*xdat(G)-n+1));
      phiCAL=phiCAL+((sqrt(2)*h(n)*SS));
   end
   RWReal (G)=(phiCAL);
end
```

ImagWaveletimag.m

```
% computes Imaginary part of the wavelet based on recursion relation

function [RWImag]= fImagWaveletreal (xdat,para)
a=para(1);b=para(2);

c=pi/4-a-b;
h(1)=cos(a)*cos(b)*cos(c);
h(2)=sin(a)*cos(b)*cos(c);
h(3)=-cos(a)*sin(b)*sin(c);
h(4)=-sin(a)*sin(b)*sin(c);
h(5)=-sin(a)*sin(b)*cos(c);
h(6)=cos(a)*sin(b)*cos(c);
h(7)=-sin(a)*cos(b)*sin(c);
h(8)=cos(a)*cos(b)*sin(c);

%-----y' calculation using recursion relation------%
for G=1:length(xdat)
   phiCAL=0;
   for n=1:8
      SS=imag(fphical(2*xdat(G)-n+1));
      phiCAL=phiCAL+((sqrt(2)*h(n)*SS));
   end
```

```
   RWImag(G)=(phiCAL);
end
```

filterarrange.m

```
% A function which computes high pass analysis filter coefficients  and synthesis low pass and high pass
% filter coefficients  from Low pass analysis filter coefficients

function [Hi_D, Lo_R, Hi_R]=filterarrange(Lo_D)

K=length(Lo_D);
for i=1:K
     Hi_D(i)=((-1)^(i)) * (Lo_D(K-i+1));
     Lo_R(i)=(Lo_D(K-i+1));
end
for i=1:K
   Hi_R(i)=(Hi_D(K-i+1));
end
```

filterfreqresp.m

```
% A function which plots MRA filter frequency response.

function[]= filterfreqresp(h0,N)
h0
for K=1:N
   g0(K)=((-1)^(K-1)).*(h0(N-(K-1)));
end
g0
[H0,w0] = freqz(h0);
plot(w0,(abs(H0)/max(abs(H0)))*sqrt(2),'k');hold on;

[H1,w1] = freqz(g0);
plot(w1,(abs(H1)/max(abs(H1)))*sqrt(2),'-.k');
grid on;

% hdb10=wfilters('db10');
%
% N=length(hdb10);
% for K=1:N
%     g0db10(K)=((-1)^(K-1)).*(hdb10(N-(K-1)));
% end
%
% [H0db10,w0db10] = freqz(hdb10);
% plot(w0db10,(abs(H0db10)/max(abs(H0db10)))*sqrt(2),'k');hold on;
%
% [H1db10,w1db10] = freqz(g0db10);
% plot(w1db10,(abs(H1db10)/max(abs(H1db10)))*sqrt(2),'-.k');
legend('Lowpass','Highpass','db10',1);xlabel('frequency in rad/sec');ylabel('Amplitude');
% grid on;
```

Bibliography

[Aldroubi93] Aldroubi A and Unser M, "Families of multiresolution and wavelet spaces with optimal properties," *Numer. Func. Anal. Optim*., **14,** 417-446, 1993.

[Anandan01] Anandan V K, Ramachandra Reddy G and Rao P B, "Spectral analysis of atmospheric radar signal using higher order spectral estimation technique, *IEEE Trans. Geosci. Remote Sensing*"**, 39,** 1890-1895, 2001.

[Anandan05] Anandan V K, Balamuralidhar P, Rao P B, Jain A R. and Pan C J, **"**An Adaptive Moments Estimation Technique Applied to MST Echoes", *J. Atmos. Oceanic Technol.*, **22**, 396-408, 2005.

[Balsley80] Balsley B B and Gage K S, "The MST Radar Technique: Potential for Middle Atmospheric Studies", *Pure. & Appl. Geophys*., **118**, 452-493, 1980.

[Basseville92] Basseville M, Benveniste A, Chou K, Golden S, Nikoukhah R and Willsky A, "Modeling and estimation of multiresolution stochastic processes", *IEEE Trans. Inform. Theory*, **38**(3), 766-784, 1992.

[Battan73] Battan L J, *Radar Observation of the Atmosphere*, The University of Chicago Press, Chicago, 1973.

[Bijaoui96] Bijaoui A, Slezak E, Rue F and Léger E, "Wavelets and the study of the Distant Universe", *Proc. IEEE,* **84**(4)*,* 670-679, 1996.

[Boisse99] Boisse J –C, Klaus V and Aubagnac J –P, "A wavelet transform technique for removing airplane echoes from ST radar signals", *J. Atmos. Oceanic Techol.*, **16**, 334-346, 1999.

[Brailean95] Brailean J C and Aggelos Katsaggelos K, "Simultaneous recursive displacement estimation and restoration of noisy-blurred image sequences", *IEEE Trans. Image Processing*, **4**(9), 1236-1251, 1995.

[Brigham88] Brigham E O, *The fast Fourier transform and its application*, Prentice Hall, New Jersey, 1988.

[Burrus98] Burrus C S, Gopinath R A and Guo H, *Introduction to Wavelets and Wavelet Transforms: A Primer*, Prentice Hall, 1998.

[Burt83] Burt P and Adelson E, "The laplacian pyramid as a compact image code", *IEEE Trans. Comm.*, **31**(5), 532-540, 1983.

[Chang00] Chang S G, Bin Y, and Vetterli M, "spatially adaptive wavelet thresholding with context modeling for image denoising", *IEEE Trans. Image Proc.*, **9**(9), 1532-1546, 2000.

[Chen94] Chen S and Donoho D, "Basis pursuit", *Proc. IEEE 28th Annu. Asilomar Conf. Signals, Syst.*, Comput., 1994.

[Chui92] Chui C, *Wavelets*, Academic Press, 1992.

[Clothiaux94] Clothiaux E E, Rene R S, Thomson D W, Ackerman T P and Williams S R, "A first-guess feature based algorithm for estimating wind speed in clear-air Doppler radar spectra", *J Atmos Oceanic Technol*, **11,** 888-908,1994.

[Cohen96] Cohen A and Kovacevic J, "Wavelets: the mathematical background", *Proc. IEEE*, **84,** 514–522, 1996.

[Dai-fei00] Dai-fei G, Wei-hong Z, Zhen-ming G and Jian-qiang Z, "A study of Wavelet thresholding de-noising", *IEEE Proc. Of ICSP*, 329-332, 2000.

[Daubechies88]Daubechies I, "Orthogonal bases of compactly supported wavelets", *Commun. Pure Appl. Math.*, **31**, 909-996, 1988.

[Daubechies92] Daubechies I, *Ten Lectures on Wavelets*, Philadelphia: SIAM, 1992.

[Donoho94a] Donoho D L and Johnstone I M, "Ideal spatial adaptation by wavelet shrinkage", *Biometrika*, **81**, 425–455, 1994.

[Donoho94b] Donoho D L and Johnstone I M, "Threshold Selection for Wavelet Shrinkage of Noisy Data", *IEEE Proc. of the 16th Annual International Conference on Engineering Advances: New Opportunities for Biomedical Engineers,* 3-6 Nov., **1**, A24 -A25, 1994**.**

[Donoho95a] Donoho D L, "Denoising via soft thresholding", *IEEE Trans. Inform. Theory,* **41**(3), 613-627, 1995.

[Donoho95b] Donoho D L and Johnstone I M, "Adapting to unknown smoothness via wavelet shrinkage", *J. Amer. Stat. Assoc.*, **90**(432), 1200–1224, 1995.

[Donoho98] Donoho D L and Johnstone I M "Minimax Estimation via Wavelet Shrinkage", *Ann. Statist*., **26**(3)**,** 879-921, 1998.

[Doviak84] Doviak R J and Zrnic D S, *Doppler radar and Weather Observations,* Academic Press, London 1984.

[Ehara94] Ehara N, Sasase I and Mori S, "Weak radar signal detection based on wavelet transform", *Electronics and Communications in Japan*, Part 3, **77**, 105–114, 1994.

[Elsehely99] Elsehely E and Sobhy M I, "Detection of radar target pulse in the presence of noise and jamming signal using the multi-scale wavelet transform", *IEEE International Symposium on Circuits and System,* **3**, 536-539, 1999.

[Elsehely00] Elsehely E and Sobhy M I, "Reduction of interference in microwave automotive radars", *IEEE Microwave Theory and Techniques Society*, 1419-1422, 2000.

[Evans69] Evans J V, "Theory and practice of ionosphere study by Thomson scatter radar", *Proc. IEEE,* **57**, 496-530, 1969.

[Fischler81] Fischler M A and Boltes R C, Random sample consensus: "A paradigm for model fitting with application to image analysis and automated cartography", *Cummun Assoc Comput Mach*, **24**, 381 -395, 1981.

[Fliege94] Fliege F J, *Multirate Digital Signal Processing: Multirate Systems Filter Banks, and Wavelets,* Wiley & Sons, New York 1994.

[Gage80] Gage K S and Balsley B B, "On the scattering and reflection mechanisms contributing to clear air radar echoes from the troposphere, stratosphere, and mesosphere", *Radio Sci.,* **15**, 243-257, 1980.

[Goodrich02] Goodrich R K, Morse C S, Cornman L B and Cohn S A, "A horizontal wind and wind confidence algorithm for Doppler wind profilers", *J Atmos Oceanic Technol*, **19**, 257-273, 2002.

[Gopinath92] Gopinath R A and Burrus C S, Wavelet transforms and filter banks, In Charles K Chui editor, *Wavelets: A Tutorial in Theory and Applications*, 603-655, Academic Press, CA, 1992. Volume 2 in the series: Wavelet Analysis and its Applications.

[Gopinath94] Gopinath R A, Odegard J E and Burrus C S, "Optimal wavelet representation of signals and wavelet sampling theorem", *IEEE Trans. Circuits Syst*. II, **41**, 262-277, 1994.

[Graps95] Graps A, "An introduction to wavelets", IEEE *Computational Science and Engineering*, **2**(2), 1995.

[Guohuo03] Guohuo W and Siliang W, "Denoising radar signals using complex wavelet", *International symposium on signal processing* ", **1**, 341-344, 2003.

[Harper78] Harper R M, "Preliminary Measurements of the Ion component of the Incoherent scatter spectrum in the 60-90km Region over Arecibo", *Geophys. Res. Lett.*, **5**, 784-786, 1978.

[Jain95] Jain A R and Narayana Rao D, *Lecture Notes*, Second winter school on Indian MST radar, 1995.

[Jiang01] Jiang X and Zhang J, "Wide-band signal detection based on time-scale domain two-dimensional correlation", *MTS/IEEE Conference and Exhibition*, **3**, 1660-1663, 2001.

[John02] John R Minkoff, "*Signal Processing Fundamentals and Applications for Communications and Sensing Systems*", Artech House Publishers, 2002.

[Jordon97] Jordon J R, Lataitis R J and Carter D A, "Removing ground and intermittent clutter contamination from wind profiler signals using wavelet transforms", *J Atmos Oceanic Techol*, **14**, 1280-1297,1997.

[Kelley99] Kelley C, "*Iterative methods for Optimization*", SIAM publications, Philadelphia, 1999.

[Lehmann01] Lehmann V and Teschke G, "Wavelet based methods for improved wind profiler signal processing", *Annales Geophysicae,* **19**, 825-836**,** 2001.

[Liu01] Liu R, Liu X, Suo J and Wang X, "The radar clutter processor with wavelet floating threshold", *Proc. of CIE International Conference on Radar*, 1001-1005, 2001.

[Mallat89] Mallat S, "A theory for multiresolution signal decomposition: The wavelet Representation", IEEE *Trans. Pattern Recog. And Mach. Intellig.*, **11**(7), 674-693, 1989.

[Mallat92] Mallat S, Hwang W L, "Singularity Detection and Processing with Wavelets", IEEE *Trans. Inform. Theory*, **38** (2), 617–643, 1992.

[Mallat93] Mallat S and Zhang Z, "Matching pursuit with time-frequency dictionaries", *IEEE Trans. Signal Processing*, **41**, 3397-3415, 1993.

[Mallat96] Mallat S, "Wavelets for Vision", *Proc. IEEE*, **84**(4), 604–614, 1996.

[Mallat98] Mallat S, *A Wavelet Tour of Signal Processing*, Academic Press, 1998.

[Marcellin00] Marcellin M W, Gormish M J, Bilgin A and Boliek M P, "An Overview of JPEG 2000", *Proc. Data Compression Conf.*, 523-541, 2000.

[Marr82] Marr D, *Vision*, W H Freeman and Co., New York, 1982.

[Masen04] Masen K, Nielsen H and Tingleff O, "*Methods for non-linear Least Squares problems*", Technical University of Denmark, 2004, Lecture notes.

[Matlab04] Matlab help, Wavelet Toolbox, Matlab version 7.0, 2004

[May89] May P T and Strauch R G, "An examination of wind profiler signal processing algorithms", *J Atmos Oceanic Technol.*, **6,** 731-735, 1989.

[May98] May P T and Strauch R G," Reducing the effect of ground clutter on wind profiler velocity measurements", *J Atmos Oceanic Technol.*, **15,** 579-586, 1998.

[Merritt95] Merritt D A, "A statistical averaging method for wind profiler Doppler spectra", *J. Atmos. Oceanic Technol.*, **12**, 985-995, 1995.

[Meyer93] Meyer Y, *Wavelets: Algorithms and Applications*, Society for Industrial and Applied Mathematics, 1993.

[Morse02] Morse C S, Goodrich R K and Cornman L B, "The NIMA method for improved moment estimation from Doppler spectra", *J Atmos Oceanic Technol*, **19,** 274-295, 2002.

[Nielsen96] Nielsen N H and Wickerhauser M V, "Wavelets and time frequency analysis", *Proc. IEEE*, **84**(4), 523–541, 1996.

[Nocedal 99] Nocedal J and Wright S, "*Numerical optimization*", Springer, New York, 1999.

[Peng96] Peng Y N, Tian L S and Zhang X P, "Wavelet detectors for wide-band radar signals", *CIE International Conference of Radar*, 289-292, 1996.

[Polikar97] Polikar R, Greer M H, Udpa L and Keinert F, "Multiresolution Wavelet Analysis of ERPs for the Detection of Alzheimer's Disease, Proceedings", *19th Intl. Conf. IEEE/ EMBS*, 1301-1304, 1997.

[Proakis96] Proakis J G and Manolakis D G, *Digital Signal Processing: Principles, Algorithms, and Applications*, (3rd edition), Prentice-Hall, 1996.

[Rabbani02] Rabbani M and Joshi R, "An overview of the JPEG2000 still image compression standard", *signal processing: Image Communication*, **17**, 3-48, 2002

[Rao98] Rao R and Bopadikar A, *Wavelet Transforms, Introduction to theory and applications*, Addison Wesley, 1998.

[Rötteger90] Rötteger J, and Larsen M F, *UHF/VHF Radar techniques for atmospheric research and wind profiler applications, in Radar in Meteorology*, edited by D. Atlas, Chap. 21a, 235-281, American Meteorological Society, Boston, Mass., 1990.

[Saidi03] Saidi H, "Radar target detection using time-frequency transform", Master thesis, Isfahan University of technology, 2003.

[Sato89] Sato T, "Radar principles, in Hand book for MAP", edited by Fukao S, *SCOSTER Secr., Urbana, III.*, **30,** 19-53, 1989.

[Shapiro93] Shapiro J M, "Embedded image coding using zero trees of wavelet coefficients", *IEEE Image Proc.*, **41**(2), 3445-3462, 1993.

[Shimomai96] Shimomai T, Yamanaka M D and Fukao S, "Application of wavelet analysis to wind disturbances observed with MST radar techniques", *J Atmos. Terr. Phys.*, **58,** 683-696, 1996.

[Soon-Huat02] Soon-Auat Ong "Signal-Adapted Wavelets for Doppler Radar System" *Seventh International Conference on Control, Automation, Robotics and Vision (LCARCV)*, 19-23, 2002.

[Strang94] Strang G, "Wavelets", *American Scientist,* **82**, 250–255, 1994.

[Strang95] Strang G, and Strela V, "Short wavelets and matrix dilation equations", *IEEE Trans. Signal Proc.*, **43** 108–115, 1995.

[Strang96] Strang G and Nguyen T, *Wavelets and Filter Banks*, Wellesley-Cambridge Press, Wellesley, Massachusetts, 1996.

[Sweldens96] Sweldens W, "The lifting scheme: A custom design construction of biorthogonal wavelets", *J. Appl. Comput. Anal.*, **3**(2), 186-200, 1996.

[Tewfik92] Tewfik A H, Sinha D and Jorgensen P, "On the optimal choice of a wavelet for signal representation", *IEEE Trans. Inform. Theory*, **38,** 747-765, 1992.

[Vaidyanathan88] Vaidyanathan P P and Hoang P-Q, "Lattice structures for optimal design and robust implementation of two-channel perfect reconstruction filter banks", *IEEE Trans. Acous. Speech Signal Proc.*, **36**(1), 81-94, 1988.

[Vaidyanathan92] Vaidyanathan P P, *Multirate systems and Filter Banks,* Prentice-Hall, NJ, 1992.

[Vidakovic94] Vidakovic B, "Nonlinear wavelet shrinkage with bayes rules and bayes factors", *J. American Statistical Association*, **93**,173–179, 1994.

[Vetterli95] Vetterli M and Kovaˇcevi´c J, *Wavelets and Subband Coding,* Prentice-Hall, 1995.

[Weaver91] Weaver J, Xu Y, Healy D and Driscoll J, "Filtering MR images in the wavelet transform domain", *Magn. Reson. Med*, **21** (2), 288-295, 1991.

[Wilfong93] Wilfong T L, Smith S A and Creasey R L,"High temporal resolution velocity estimates from a wind profiler", *J Spacecraft and Rackets*, **30,** 348-354**,** 1993.

[Woodman74] Woodman R F, and Guillen A, "Radar observations of winds and turbulence in the stratosphere and mesosphere", *J. Atmos. Sci.*, **31**, 493-505, 1974.

[Woodman80] Woodman R F, Kugel R P and Rottger, "A coherent integrator- decode processor for the SOUCY-VHF-Radar", *Radio Sci.*, **15**, 233-242, 1980.

[Woodman85] Woodman R F, "Spectral moments estimation in MST Radars", *Radio Sci.*, **20,** 1185-1195, 1985.

[Woods86] Woods J and O'Neil S, "Subband coding of images", *IEEE Trans. Acous. Speech Signal Proc.*, **35**(5), 1278-1288, 1986.

Publications

1. **Sreedevi K**, Venu K, Rao P B, Sarma T V C and Narayana Rao D "Range and Accuracy Improvements of MST Radar using Wavelet denoising", *MST-11*, Tirupathi, 2006.
2. **Sreedevi K**, Venu K, Rao P B, Sarma T V C and Narayana Rao D, "Wavelet Transform based Signal Processing of MST radar data" *National Space Science Symposium* (*NSSS*), Visakhapatnam, 2006.
3. **Sreedevi K**, Venu K, Rao P B "MST Radar Signal Processing Employing Wavelet Transforms", *MST RADAR VIII Users Workshop*, Tirupathi, 2006.